SLOTTED PHOTONIC CRYSTAL BIOSENSORS

Mark Gerard Scullion

A Thesis Submitted for the Degree of PhD
at the
University of St Andrews

2013

Slotted Photonic Crystal Biosensors

Mark Gerard Scullion

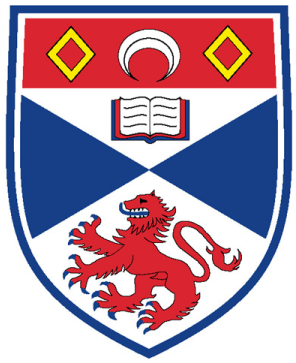

University
of
St Andrews

Thesis submitted for the degree of Doctor of Philosophy at the University of St Andrews

December 2012

Declarations

I, Mark Gerard Scullion, hereby certify that this thesis, which is approximately **40,000** words in length, has been written by me, that it is the record of work carried out by me and that it has not been submitted in any previous application for a higher degree.

I was admitted as a research student in July 2009 and as a candidate for the degree of Doctor of Philosophy in July 2009; the higher study for which this is a record was carried out in the University of St Andrews between 2009 and 2012.

Date:…….. Signature of Candidate:…….....

I hereby certify that the candidate has fulfilled the conditions of the Resolution and Regulations appropriate for the degree of Doctor of Philosophy in the University of St Andrews and that the candidate is qualified to submit this thesis in application for that degree.

Date:…… Signature of Supervisor:……

In submitting this thesis to the University of St Andrews I understand that I am giving permission for it to be made available for use in accordance with the regulations of the University Library for the time being in force, subject to any copyright vested in the work not being affected thereby. I also understand that the title and the abstract will be published, and that a copy of the work may be made and supplied to any bona fide library or research worker, that my thesis will be electronically accessible for personal or research use unless exempt by award of an embargo as requested below, and that the library has the right to migrate my thesis into new electronic forms as required to ensure continued access to my thesis. I have obtained any third-party copyright permissions that may be required in order to allow such access and migration, or have requested the appropriate embargo below.

The following is an agreed request by the candidate and supervisor regarding the electronic publication of this thesis:

Access to printed copy and electronic publication of thesis through the University of St Andrews.

Date……..

Signature of Candidate:……. Signature of Supervisor……..

Acknowledgements

To be able to achieve the results within this thesis, I owe thanks to many wonderful people who have helped me throughout my life. I would first like to thank Prof Thomas F. Krauss for giving me the opportunity to work within his research group, and for his continued patience, support and guidance over the course of the project. His strong enthusiasm for research has inspired me greatly. I also have to say a big thank you to Dr Andrea Di Falco, who trained me on nearly all of the fabrication, and also provided much support and guidance over the 3 and a half years. I have learned a lot from you both.

To all the members of the Microphotonics group past and present. Not only have you been great colleagues, providing me with support, a pleasurable working environment and much useful advice, you have also been great friends. I would particularly like to thank Dr William Whelan-Curtin for useful fabrication tips, Dr Praveen Ashok and Dr Rob Marchington for the initial training, and many useful discussions on, microfluidics, Dr Christopher Reardon for the general running of the group and dry humour, and to the unsung heroes of the group Mr Steve Balfour, Mr Callum Smith and Mr George Robb who kept the cleanroom running. I would also like to say a special thank you to members of the group who have made my time at St Andrews unforgettable, in particular: Abdul Shakoor, Annett Klemm, Dr Armando Ricciardi, Emiliano Rezende Martins, Dr Isabella Rey, Kapil Debnath, Dr Karl Welna, Dr Marcel Spurny, Dr Marcello Ferrera, Dr Paolo Cardile, Dr Tim James as well as members or other groups such as Dr Sebastian Kosemier and Raphael Adler. A big thank you also goes to the collaborators who provided many fascinating discussions, samples and tours: Dr Simon Powis (exosomes), Dr Bernie McConnell (marine biology) and Dr Ailsa Hall (marine biology). Their passion and knowledge gave me strong motivation in my own research. To Prof Kishan Dholakia for use of his lab for preparing microfluidic channels. Also to Dr Donatella Cassettari for her interest and support in the role of my second supervisor, and to Prof. Carlos A. Barrios, and Prof. Kishan Dholakia for agreeing to examine my work.

I would like to thank EPSRC for funding my work.

I would also like to mention three people who made my undergraduate studies a joy and gave me friends for life: Michael Ling, Colin Parry and Alexei Saliev. To my high school teacher, Mr Patrick Cleary who really inspired me to study physics, and whose lessons I will never forget.

To my mother, Marianne, who spent so much time with me as a child and my father, Gerard, who works so hard for his family, you have given me the platform for all of my achievements. I love and respect you more than you can imagine. Also, my wonderful sister, Laura, with whom I have many happy childhood memories, and all the grandparents, aunts and uncles who have contributed to raising me up.

Finally, I would like to thank my wife, Zhan (Vivian), for being the sunshine in my life. I believe that your love and support have helped me reach higher than I could by myself, and look forward to continuing the journey of life with you.

To all of you fantastic people: THANK YOU!!!

Publications Resulting from this Work

M. G. Scullion, T. F. Krauss, and A. Di Falco, “Slotted Photonic Crystal Sensors,” Submitted for Publication, December (2012).

A. Di Falco, M. Massari, **M. G. Scullion**, S. A. Schulz, F. Romanato, and T. F. Krauss, “Propagation Losses of Slotted Photonic Crystal Waveguides”, IEEE Photonics Journal, **4**, 1536-1541 (2012).

M.G. Scullion, T.F. Krauss and A. Di Falco, “Slotted Photonic Crystals for Biosensing Applications”, Proc. of SPIE, **8425**, Photonic Crystal Materials and Devices X, 842507 (2012).

M.G. Scullion, A. Di Falco and T.F. Krauss, "Slotted Photonic Crystal Cavities with Integrated Microfluidics for Biosensing Applications", Biosensors and Bioelectronics, **27**, 101-105 (2011).

T.D. James, **M.G. Scullion**, P.C. Ashok, A. Di Falco, K. Dholakia and T.F. Krauss, "Valve Controlled Fluorescence Detection System for Remote Sensing Applications", Microfluidics and Nanofluidics, **11**, 529-536 (2011).

M.G. Scullion, T.F. Krauss and A. Di Falco, "High Efficiency Interface for Coupling into Slotted Photonic Crystal Waveguides", IEEE Photonics Journal, **3**, 203-208 (2011).

News Articles

Mark Scullion, Thomas Krauss and Andrea Di Falco, “Integrated optics provide a convenient platform for efficient biosensors,” SPIE Newsroom, Sensing and Measurement, DOI: 10.1117/2.1201205.004251, May (2012).

Awards

Best Student Oral Presentation, **Mark Scullion**, “Losses in Slotted Photonic Crystal Waveguides,” EOS Topical Meeting on Silicon Photonics, EOSAM, Aberdeen (2012).

Conferences

M.G. Scullion, A. Di Falco, M. Massari, S. A. Schulz, F. Romanato and T.F. Krauss, “Losses in Slotted Photonic Crystal Waveguides”, EOSAM, Aberdeen, UK (2012). Talk.

M.G. Scullion, A. Di Falco and T.F. Krauss, "Slotted Photonic Crystals for Sensing Applications", Group IV Photonics, London, UK (2011). Poster.

M.G. Scullion, A. Di Falco and T.F. Krauss, "Slotted PhC Waveguides with Low Insertion Losses for Slow Light Sensing Applications", PECS, Granada, Spain (2010). Poster.

M.G. Scullion, A. Di Falco, P.C. Ashok and T.F. Krauss, "Slotted Photonic Crystal Sensors", Photonics4Life, St Andrews, UK (2010). Poster.

U.P. Dharanipathy, A. Di Falco, **M.G. Scullion**, P.C. Ashok, R.F. Marchington and T.F. Krauss, "An Integrated Slotted Photonic Crystal Array", Blue Photonics, Aberdeen, UK (2009). Attendee.

Abstract

Optical biosensors are increasingly being considered for lab-on-a-chip applications due to their benefits such as small size, biocompatibility, passive behaviour and lack of the need for fluorescent labels. The light guiding mechanisms used by many of them result in poor overlap of the optical field with the target molecules, reducing the maximum sensitivity achievable. This thesis presents a new platform for optical biosensors, namely slotted photonic crystals, which engender higher sensitivities due to their ability to confine, spatially and temporally, the peak of optical mode within the analyte itself. Loss measurements showed values comparable to standard photonic crystals, confirming their ability to be used in real devices. A novel resonant coupler was designed, simulated, and experimentally tested, and was found to perform better than other solutions within the literature. Combining with cavities, microfluidics and biological functionalization allowed proof-of-principle demonstrations of protein binding to be carried out. High sensitivities were observed in smaller structures than most competing devices in the literature. Initial tests with cellular material for real applications was also performed, and shown to be of promise. In addition, groundwork to make an integrated device that includes the spectrometer function was also carried out showing that slotted photonic crystals themselves can be used for on-chip wavelength specific filtering and spectroscopy, whilst gas-free microvalves for automation were also developed. This body of work presents slotted photonic crystals as a realistic platform for complete on-chip biosensing; addressing key design, performance and application issues, whilst also opening up exciting new ideas for future study.

“How far that little candle throws his beams! So shines a good deed in a weary world.”

William Shakespeare, *The Merchant of Venice*

Contents

Chapter 1

Introduction

1.1 Introduction to Sensors

1.1.1 Why We Need Sensors

Humans rely on natural sensors such as the eyes, ears, tongue, skin and nose to interact with and detect changes in their surrounding environment, and to react to potential dangers early. These sensors depend on specialized types of cells, such as neuron or epithelial cells, which convert some external stimulus, be it light, sound, chemical or other, into a change in the potential energy of the cell's membrane [1]. Despite the incredible abilities of these receptors, danger can often elude them, making man-made sensors necessary in many situations. In addition, sensors can provide a way to quantify a change in a physical quantity, which can be useful in everyday life.

The very word 'sensor' is something we associate with the high-tech inventions of the modern world, but sensors have found use throughout human history. Early inventions such as the water clock, weigh scales and the compass allowed our ancient ancestors to measure the passage of time, the relative mass of an object and to navigate over long distances, respectively. These simple but very powerful devices are now taken for granted, but it would also be wrong to assume that the ancients were limited by their technology. Incredibly, as early as 132 A. D. the Chinese had a pendulum-based device capable of detecting the direction of an earthquake hundreds of miles away [2], whilst in ancient Alexandria, automatic doors that responded to fire were already being developed [2]. Over time, technological advances, most notably in the electronics industry, have allowed a huge expansion in the capabilities of the sensors we have today. Just imagine a trip to the airport. The car you use to get there can measure speed and distance. Automatic doors open at the entrance. Your ticket and passport are scanned. On passing through security, x-rays, metal detectors, thermal scanners and other devices check passengers' belongings for weapons and illegal substances, and bodies for flu-like symptoms. The water you buy in the departure lounge has been tested at source for toxins and minerals. The plane you take can measure altitude, position, pitch, temperature, speed, pressure and a multitude of other quantities which are needed to keep you safe. But sensors are not just needed here. They can be found in warzones to detect and control explosives and other weapons, in marine environments to identify toxins and pollutants, in satellites to detect changes in the environment (e.g. global warming) both here and on other planets, and perhaps most importantly in hospitals for detecting pathogens, diseases, tumours, fractures and other life threatening conditions. Sensors have found use almost everywhere in the modern world.

Many different types of sensor exist, most of which are optimised for one particular role, and which rely on changes in a physical quantity which we can measure. A sensor in its simplest form can be defined as a device which translates some change in a physical quantity into a number (or output state) which can be read by the user, allowing them to detect the change. Sensors can be classified in a number of different ways, but comparison between them, most notably their performance, can often be confusing and misleading. As a basic starting point, they can be sorted in terms of their **transduction** mechanism, being how they convert the change in some physical property into some quantity that can be measured. Some of the most common transduction mechanisms rely on a change in **electrical** (conductivity, capacitance, phase or induction), **optical** (phase, intensity or spectral component), **chemical** (reaction

products, pH or reaction speed), **acoustic and mechanical** (intensity, phase or wavelength) or **thermal** (temperature, thermal conductivity, thermal expansion) properties. In some cases there can even be an overlap between these different mechanisms. In general, many sensors in the past have relied on electrical transduction mechanisms due to the maturity of the electronics industry, and the subsequent cheap components and fabrication techniques available. Recent advances in optics and photonics technology have started to address the imbalance, by introducing many sensors based on optical transduction. In some situations optical sensors can offer certain advantages over their electrical counterparts, for example, optical sensors are immune to electromagnetic interference, they can be combined with many types of biological material and can have well defined spectral features that can be engineered in a device as a point of reference, and also many media have unique optical absorption and scattering spectra that can act as a 'fingerprint' to help identify them. As the **slotted photonic crystal** sensors presented within this thesis are based on optical transduction (see Fig 1.1), the remainder of this brief introduction will focus primarily on this mechanism. Medical and biological applications (biosensors) will also feature predominately in the following pages as they are the main thrust of this thesis.

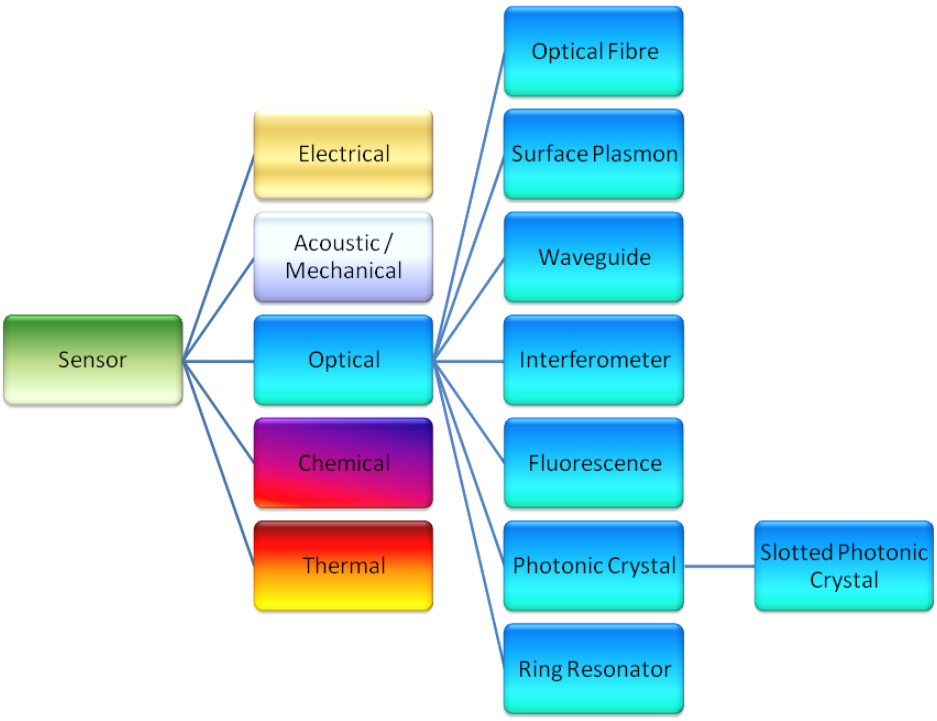

Figure 1.1: Diagram showing different sensor transduction mechanisms, with emphasis on small optics-based devices. The slotted photonic crystals presented in this thesis are an example of an optical sensor.

1.1.2 Biophotonics

Optics and biology have enjoyed a long history together. On publishing his book *Micrographia* [3] in 1665, British scientist Robert Hooke, better known for his work on elasticity and the spring constant, caused a sensation as he sketched the results of his observations of plants, insects, materials and man-made objects obtained using microscopes and magnifying glasses, revealing a miniature world:

> *"…by the help of Microscopes, there is nothing so small, as to escape our inquiry; hence there is a new visible World discovered to the understanding … and in every little particle of its matter; we now behold almost as great a variety of Creatures, as we were able before to reckon up in the whole Universe itself* [3]"

In this work he also first coined the term 'cell', and anticipates the need for and use of devices to enhance our natural senses whilst also realising the potential of optics in medical applications:

> *"The next care to be taken, in respect of the Senses, is a supplying of their infirmities with Instruments …And as Glasses have highly promoted our seeing, so 'tis not improbable, but that there may be found many Mechanical Inventions to improve our other Senses, of hearing, smelling, tasting, touching…*
>
> *… the roughness and smoothness of a Body is made much more sensible by the help of a Microscope, then by the most tender and delicate Hand, Perhaps, a Physitian might, by several other tangible proprieties, discover the constitution of a Body as well as by the Pulse* [3]"

Since Hooke, optical instruments such as the microscope have been vital tools for the biologist. Photonics, being the generation and manipulation of photons (and of which optics is a subset), has expanded the abilities of the modern scientist beyond just observation to include the identification, treatment and manipulation of biological material with light. This rapidly expanding field is known as **biophotonics**. Under this umbrella term can be found a plethora of different applications for photonics technology such as: optical tweezers [4] which utilise laser beams to move cells at will, Raman spectroscopy [5] which measures changes in light scattered from a substance to identify its composition, optical coherence tomography (OCT) [6] which uses light waves in a manner similar to that of ultrasound to image through tissues, photodynamic therapy [7] which treats skin cancer with light-activated drugs, fluorescence based techniques such as fluorescence resonance energy transfer (FRET) [8] which can measure distances on the molecular scale, photoporation [9] in which holes are punched into cells by lasers in order to inject DNA, and optical biosensors [10] which measure small quantities of a biological material.

1.1.3 Lab-on-a-Chip

Small optical biosensors form a substantial part of the growing field of **'lab-on-a-chip'**. This phrase epitomises the main goal of much biosensor research, being the ability to shrink down many of the analytical capabilities of a major research lab into a small disposable chip. In one scenario we can imagine a small chip into which a single drop of blood is placed. This drop is then rapidly screened by a multitude of different sensor elements on the device for many different diseases or other important factors. The full breakdown of the sample is then read-out to the user, who can react accordingly (for example, a doctor). If the device could be made cheap, simple to use and disposable, then it would be suitable for rapid, high throughput testing rather than labour intensive laboratory tests, which require much experience, time and training. In essence, the goal is to make devices that are similar to the home pregnancy tests available today: cheap and simple to use, and a clear result that can be obtained and read by a non-specialist.

Several challenges are evident in this field to make this a reality, but many technologies offer potential solutions to the problem. A growing presence in this area is that of integrated optics, which combines several micro- or nano-photonic components on the same chip, using fabrication techniques borrowed from the electronic industry. This combination of components on a single chip is therefore very similar in goal to that of lab-on-a-chip. The small size of each component means that hundreds of devices be fabricated on said chip, offering multi-functionality and multiplexing capabilities. Many micro-photonic devices have been proposed as optical biosensors, including the slotted photonic crystals presented here. Whilst micro-photonic devices, by definition, are very small, many of them require bulky external equipment, such as sources and spectrometers, to function fully as a sensor. A key challenge would be to integrate all of these functions on-chip (lab-on-a-chip), rather than the current reality of chip-in-a-lab. Another issue is getting the target molecules to the sensing region of the device. In most cases this is limited by diffusion, which can be problematic in very low sample concentrations. Andreas Manz and co-workers pioneered the field of Micro Total Analysis Systems (**MicroTAS**) [11], another name for lab-on-a-chip, combining electrical and optical components with small capillaries that can be used to control different liquid samples. Groups such as his, Stephen Quake's [12], George Whitesides' [13] and others have further developed these **microfluidic** (see Chapter 5) circuits, allowing a variety of micro-scale chemistry and biology experiments on-chip. The merging of optics and microfluidics is known as **optofluidics**, and provides potential for improving the performance of optical sensors.

Some desktop sized devices containing photonic chips and microfluidic circuits have been developed commercially such as the surface plasmon based Biacore [14] and the ring resonator based Genalyte [15]. Whilst these devices are very sensitive, they are housed with very bulky and expensive instrumentation and are thus not truly lab-on-a-chip. Performing all functions on chip engenders stability, good alignment and compactness, thus the environmental requirements may not be as challenging as the above machines. Many sensors have been presented in the literature as alternative solutions, though many challenges remain. The current state of photonic biosensors and their challenges will be addressed more fully in Chapter 2.

1.2 Slotted Photonic Crystals

A new player in the field of optical biosensors is that of the slotted photonic crystal (Fig 1.2), the subject of the present thesis. These devices, which are fabricated in silicon-on-insulator substrates using lithographic techniques, combine two photonic structures, namely the slot waveguide and photonic crystal to squeeze light down into small volumes of air. This strong confinement of light to air is the key advantage of this architecture, as it promotes strong light-matter interactions with a substance of interest. As shall be seen throughout this thesis, the small footprint of this device, as small as a few microns, not only presents opportunities for dense arrays of sensing elements in lab-on-a-chip applications, but also provides potential for some unique and interesting experiments with biological material. The work presented in this thesis builds upon much of the early work [16-18] of Dr Andrea Di Falco and colleagues in the Microphotonics group of St. Andrews (led by Prof. Thomas F. Krauss) in the area of slotted photonic crystals, who demonstrated the chemical sensing, and slow light abilities of these devices and developed one of the main cavity designs used within this work.

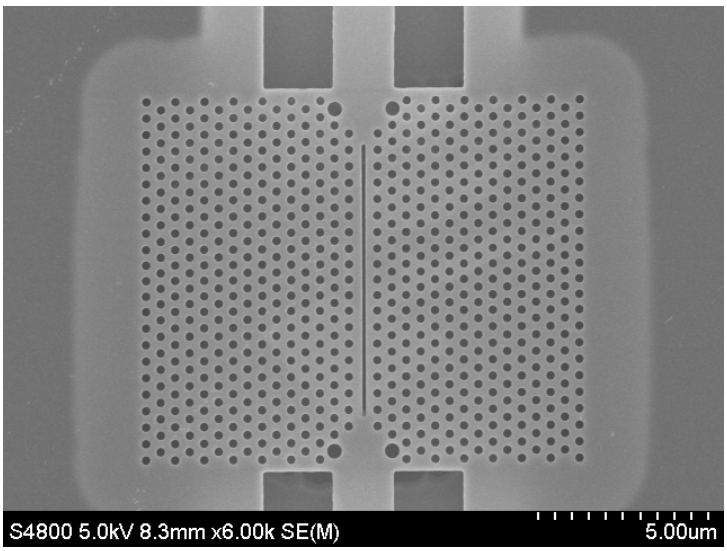

Figure 1.2: SEM image of slotted photonic crystal cavity fabricated in silicon-on-insulator substrate.

1.3 Goals of this Thesis

Using the unique optical properties of slotted photonic crystals, this thesis aims to realise cheap, compact and disposable sensors capable of specifically detecting biomolecules of interest in real-time with high sensitivity. In addition, this thesis aims to highlight the benefits of this solution over others by demonstrating their use in real biological problems of importance. A vision of these goals is expressed in the device shown in Fig 1.3. The interdisciplinary nature of this research means that much effort was taken to collaborate with biologists and other potential end-users of the device.

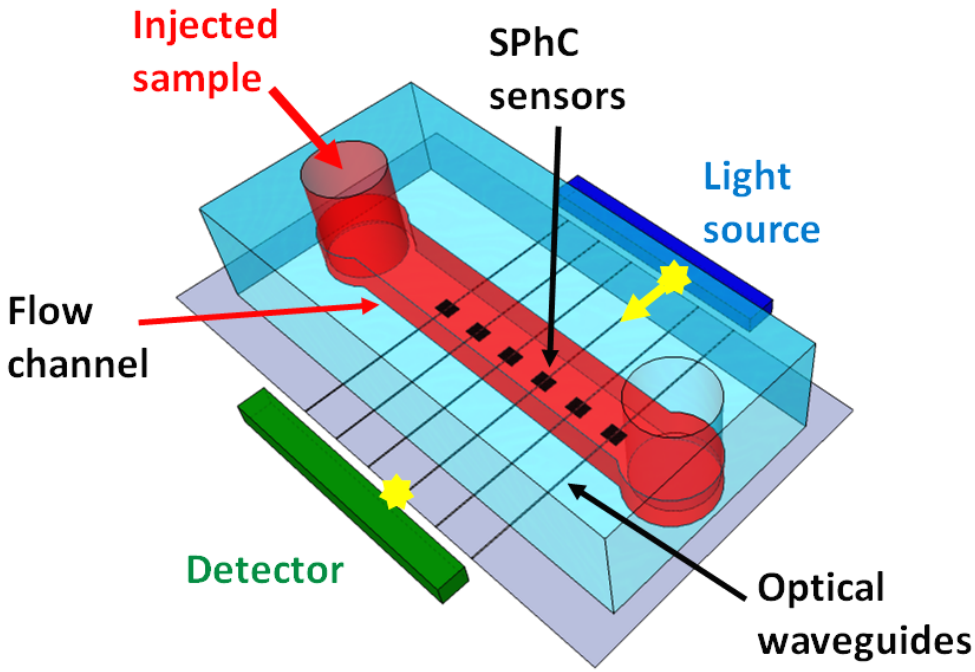

Figure 1.3: Conceptual design of future slotted photonic crystal sensor device. An injected sample (e.g. blood) flows through a microchannel over a large number of sensors optimised for different biomolecules of interest. Light is sent from an integrated light source, through an optical waveguide and into the sensor. Light emerging from the back of the device is collected by an integrated detector.

A number of challenges and goals associated with this vision are listed below, along with a short summary for each:

Improve coupling of light into slotted photonic crystal devices. The unique dispersive properties of slotted photonic crystals create additional problems associated with efficiently coupling light into them. A suitable method for improving the coupling efficiency is therefore required.

Functionalize with bio-recognition elements. In order to specifically detect a substance, suitable receptors have to be found that can be chemically attached to the silicon surface on which the sensors are fabricated. The chemicals used present additional challenges due to their effects on the sensor materials, and also the biological receptors used.

Integrate device with microfluidic channels. Microfluidic channels are required to direct samples to the sensors, minimise sample volumes and prevent evaporation. Microfluidics also has potential in remote sensing applications.

Demonstrate specific detection of bio-molecules. These devices must be able to detect biomolecules in real-time with high sensitivity**.** Ideally the chemistry used should be adaptable to different receptors, so as to open up a wide range of applications.

Packaging. Ideally the sources and detectors required for device operation should be integrated with the sensor chip to provide a fully working device. The full device should be as small, cheap and user friendly as possible in view of potential commercial and research grade devices.

Solve real biological problems of interest. Another major goal is to demonstrate that these sensors can provide unique ways of exploring fundamental biological problems. Can they tell us something new that other types of tests cannot?

1.4 Layout of this Thesis

This thesis is structured into a number of chapters, each looking at achieving some of the goals listed in the previous section. Note that a reference list is provided at the end of each chapter for ease of reading. A brief synopsis of the following chapters is here presented:

Chapter 2 looks in more detail at the operational principles of optical biosensors, such as specific sensing with antibodies, and compares different devices in the literature using useful figures-of-merit.

Chapter 3 introduces the physics behind slotted photonic crystals, and details the main fabrication and optical characterization techniques.

Chapter 4 looks at improving coupling into slotted photonic crystals. A solution based on resonant defects is presented, with results from theoretical and experimental investigations. Propagation losses are also considered.

Chapter 5 looks at integrating microfluidic structures with the sensors. Key concepts in microfluidics are introduced along with results of creating microchannels and microvalves.

Chapter 6 presents the results of investigations into functionalizing the device with appropriate antibodies, and using said device to detect biological material. Initial proof-of-principle results with the popular biotin-avaidin system are shown.

Chapter 7 shows the results from other projects designed to solve real biological problems that were carried out with the help of collaborators such as the detection of cellular material and harmful algae, along with appropriate background material. Investigations into on-chip spectrometer functions are also performed.

Chapter 8 provides a general discussion, before a **conclusions** section at the end.

References – Chapter 1

[1] Campbell, N. A., Reece, J. B., Urry, L. A., Cain, M. L., Wasserman, S. A., Minorsky, P. V. and Jackson, R. B., [Campbell Biology, 9th Edition], Pearson, San Francisco, Chpt. 5, 11, 43-45 (2008).

[2] James, P. and Thorpe, N., [Ancient Inventions], Ballantine Books, New York, Chpt. 3 (1994).

[3] Hooke, R., [Micrographia: or Some Physiological Descriptions of Minute Bodies Made by Magnifying Glasses with Observations and Inquiries Thereupon, 1st Edition], J. Martyn and J. Allestry, London (1665).

[4] Stevenson, D. J., Gunn-Moore, F. and Dholakia, K., "Light forces the pace: optical manipulation for biophotonics," J. Biomed. Opt. 15, 041503 (2010).

[5] Tuma, R., "Raman spectroscopy of proteins: from peptides to large assemblies," J. Raman Spec., 36, 307-319 (2005).

[6] Fercher, A. F., Drexler, W., Hitzenberger, C. K. and Lasser, T., "Optical coherence tomography – principles and applications," Rep. Progress Phys. 66, 239-303 (2003).

[7] Dolmans, D. E. J. G. J., Fukumura, D. and Jain, R. K., "Photodynamic therapy for cancer," Nature Rev. Cancer 3, 380-387 (2003).

[8] Li, I. T., Pham, E. and Truong, K., “Protein biosensors based on the principle of fluorescence resonance energy transfer for monitoring cellular dynamics,” Biotech. Lett. 28, 1971-1982 (2006).

[9] Tsukakoshi, M., Kurata, S., Nomiya, Y., Ikawa, Y. and Kasuya, T., “A novel method of DNA transfection by laser microbeam cell surgery,” Appl. Phys. B 35, 135-140 (1984).

[10] Fan, X., White, I. M., Shopova, S. I., Zhu, H., Suter, J. D. and Sun, Y., “Sensitive optical biosensors for unlabelled targets: A review,” Analy. Chem. Act. 620, 8-26 (2008).

[11] Manz, A., Graber, N., and Widmer, H. M., “Miniaturized total chemical analysis systems: A novel concept for chemical sensing,” Sen. Act. B 1, 244-248 (1990).

[12] Melin, J. and Quake, S. R., “Microfluidic large-scale integration: The evolution of design rules for biological automation,” Annu. Rev. Biophys. Biomol. Struct. 36, 213-231 (2007).

[13] Weibel, D. B., Di Luzio, W. R., and Whitesides, G. M., “Microfabrication meets microbiology,” Nature Rev. Microbiology 5, 209-218 (2007).

[14] http://www.biacore.com, last visited on 18/04/2012.

[15] http://www.genalyte.com/, last visited on 17/05/2012.

[16] Di Falco, A., O’Faolain, L. and Krauss, T. F., “Photonic crystal slotted slab waveguides,” Phot. Nano. Fun. Appl. 6, 38-41 (2008).

[17] Di Falco, A., O’Faolain, L. and Krauss, T. F., “Dispersion control and slow light in slotted photonic crystal waveguides,” Appl. Phys. Lett. 92, 083501 (2008).

[18] Di Falco, A., O’Faolain, L. and Krauss, T. F., “Chemical sensing in slotted photonic crystal heterostructure cavities,” Appl. Phys. Lett. 94, 063503 (2009).

Chapter 2

Optical Biosensors: Principles, Uses and Comparison

2.1 Optical Biosensor Basics

2.1.1 Principle of Operation and Figures-of-Merit

Optical sensors function by observing changes in some property of light as it passes through the substance of interest. Many optical sensors rely on a spectral feature, usually a sharp peak or dip, which is formed due to some resonance within the structure, one example being a cavity. In its simplest form, a cavity can be viewed as two mirrors separated by a distance *s* (see Fig. 2.1), and filled with a medium such as air or water. Only certain wavelengths of light can be supported in this system due to the nodes created by the mirrors. Light bouncing backwards and forwards between the two mirrors interacts with the medium hundreds or thousands of times, the limiting factor being the losses both at the mirrors and within the cavity medium itself. If this medium were to increase in refractive index, say due to the presence of some dissolved particles, then the *optical* path length between the mirrors increases, leading to a corresponding increase in the resonant wavelength of the system.

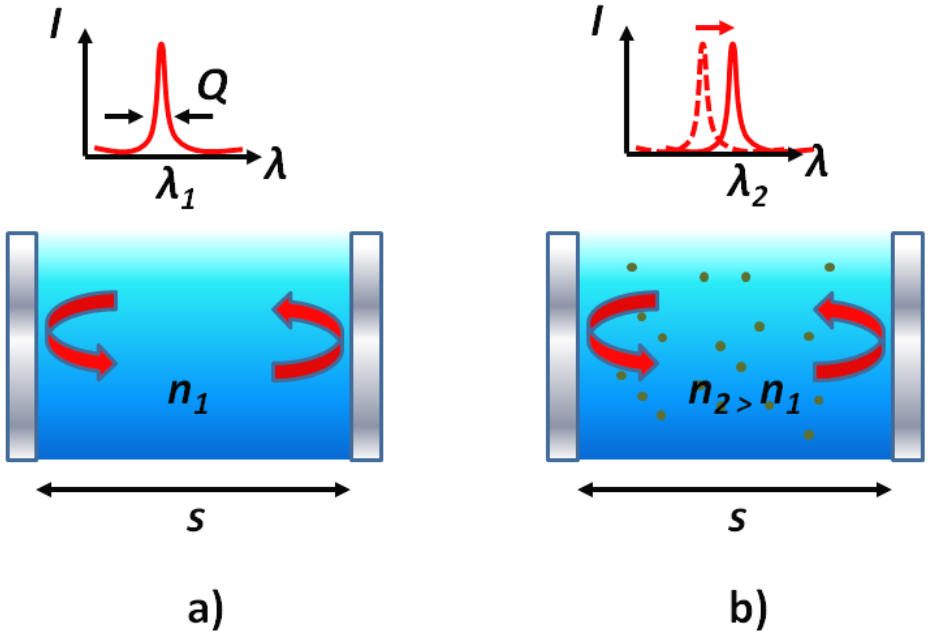

Figure 2.1: (a) Simple optical cavity formed by two mirrors separated by *s*. (b) An increase in refractive index *n* leads to an increase in the optical path length *ns* between the two mirrors. This alters the resonant wavelength λ of the cavity allowing the refractive index change to be detected.

Sensitive refractive index measurements can therefore be made by tracking the peak wavelength of a resonance. The sensitivity of detecting such a wavelength change $\Delta\lambda$ due to a refractive index change Δn can be defined by the approximation [1]:

$$\Delta\lambda = \eta\Delta n\frac{\lambda}{n_{eff}} \tag{2.1}$$

When the refractive index change is assumed to be small, and where η is the overlap of the optical mode with the sample, and n_{eff} is the effective refractive index of the mode. The sensitivity is often quoted in units of nanometre per refractive index unit (nm/RIU). Higher sensitivities can be achieved by increasing η, the overlap of the optical mode of the sample, though many integrated optical sensors tend to utilise the evanescent tail of a guided mode rather than its peak due to the restrictions of total internal reflection. As already stated, the number of times light can travel between the mirrors in a resonant cavity is limited by the losses of the system (both mirror and propagation). For better sensitivity, a high number of passes is desired so as to maximise the interaction with the medium. How well light is confined within the cavity is described by its quality factor Q, which relates the energy stored to the energy lost per optical cycle. Higher quality factor cavities have a narrower spread in resonant wavelength as expressed in the following approximate relation:

$$Q = \frac{\lambda}{\Delta\lambda} \tag{2.2}$$

Where $\Delta\lambda$ is taken to be the full-width-at-half maximum (FWHM). When using the peak (or dip) of a cavity as a point of reference for refractive index measurements, it helps to have a narrower linewidth so as to resolve smaller shifts. In addition, the resolution is also limited by the detector resolution and sources of noise such as thermal effects. A useful figure-of-merit when comparing sensors is therefore the detection limit, defined as [1]:

$$\text{Detection Limit} = \text{Resolution/Sensitivity} \tag{2.3}$$

The detection limit specifies the smallest changes in refractive index that can be resolved by the sensor. The best optical sensors can reach values of 10^{-6} RIU [2]. Although refractive index sensors can be very sensitive, they are not very specific. Many biological tests involve complex blends of different substances, and thus an additional layer of complexity must be added to the refractive index sensor to allow it to specifically detect a given substance, and make it a biosensor. This specificity can be achieved by taking advantage of bio-recognition elements such as antibodies.

2.1.2 DNA, RNA and Proteins

Three of the most important bio-molecules for life are **DNA**, **RNA** and **proteins**, which work together in partnership [3]. DNA (deoxyribonucleic acids) and RNA (ribonucleic acids) are formed from nucleic acid bases, and are used to store, encode and transfer genetic information inside a cell. In the case of DNA, the bases adenine (A), thymine (T), guanine (G) and cytosine (C) are used, whereas in RNA, (A), (G), (C) and another base known as uracil (U) are used. One interesting property of DNA is that at each joint between its two constituent strands only certain combinations of base pairs can be used. If one strand has (A) at a certain point, then the corresponding part on the second strand must be (T). Similarly, (C) only bonds to (G). This selective base pairing means that the genetic information contained in the sequence can be extracted from a single strand of the helix, a property that can be exploited in techniques such as **polymerase chain reaction** (PCR). In PCR, DNA is replicated by breaking it down into two single strands by high temperature, and then cooling to allow the complementary pairs to be re-built on each strand. Each temperature cycle allows the amount of DNA present at that point to be doubled.

In the case of a cell, DNA is replicated in another way. Encoded DNA stored within the nucleus can be read and copied to a template (transcribed), from which new proteins are then synthesized (translated), by a partnership between different forms of RNA and structures known as ribosomes [3]. The proteins created in this process consist of combinations of folded chains of amino acids, and their main role is to trigger or help facilitate biological functions. The importance of these processes for life mean that DNA, RNA and proteins are of intense study in many fields of biology such as proteomics, the study of protein function and expression, and genomics, the study of gene function and expression. To specifically detect these substances, which are commonly found amongst biological material, we can exploit their biological and chemical properties, most notably how they bind to each other. First consider the detection of proteins, which will be the main focus of this thesis.

2.1.3 Protein Detection using Antibodies

The immune and hormonal systems of the human body rely on proteins imbedded within the membrane of a cell which act as receptors for molecules of a certain shape. Any substance which induces a response from T and B cells, types of white blood cell known as lymphocytes, by binding to one of their receptors is known as an **antigen** [3]. Each receptor anchored on the surface of a B cell is composed of a Y-shaped protein, with antigen binding sites at the end of each branch (as shown in Fig 2.2). These binding sites have constant and variable regions of amino acids. It is the large differences in the variable region between different receptors that give them their specificity [3]. Binding sites display a ‘lock-and-key’ mechanism, thus only a particular antigen (for example a protein) has the correct geometry to bind to a given receptor. Geometry is so important in fact, that even the correct protein cannot bind if it has mis-folded or denatured due to excessive heating [3]. Taking the door analogy further, activated receptors can form a gateway into the cell through the membrane for a particular substance.

When an antigen binds a B cell receptor it triggers cell division, the new ‘effector’ cells formed by this division producing soluble forms of the receptor that was activated [3]. These secreted receptor proteins are known as **antibodies**, and bind to antigens flagging them up as needing to be destroyed, or stopping them from functioning properly. The immune system uses this mechanism to quickly build stocks of the correct antibody needed to fight invaders, and strongly relies on specific binding to target only invading substances (such as pathogens) and not itself.

This shape dependant binding is often exploited in many biological tests, and can be used to make optical sensors specific to one substance.

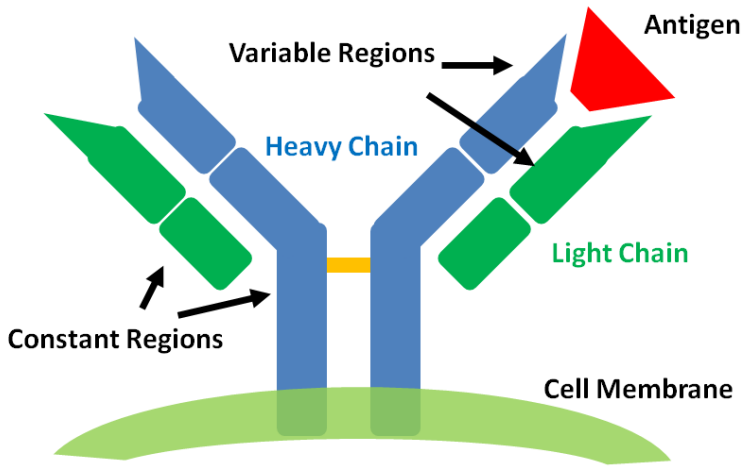

Figure 2.2: Structure of antigen receptor. In the soluble form secreted by effector cells these are known as antibodies. Only antigens of correct geometry can bind to receptor.

Antibodies can be attached to a surface using chemicals. This process is known as **functionalization**, and any surface coated with functional groups such that bio-recognition elements can be attached is said to be **functionalized** (see Section 2.1.6). These surface coated antibodies act as specific capture agents (as shown in Fig 2.3), thus creating a sort of artificial B cell: protein binding to these surface receptors induces a response from the sensor (rather than a cell). When a sample is flown across a functionalized sensor, in addition to a bulk refractive index change, there will also be a *surface* refractive index change due to the antigen-antibody binding. In this case the response curve of the device is shaped by the diffusion of target molecules within the sample. As they diffuse in solution, some of the target molecules will be captured by the functionalized surface receptors, until some saturation level is reached. Higher concentrations of target molecules induce sharper diffusion curves, with higher plateaus. The concentration of binding antigens can therefore be estimated from the shape of this curve. Other antigens cannot bind to a particular antibody as they lack the correct geometry, and thus do not induce the diffusion limited surface refractive index change. This way sensor response can be attributed to one antigen type alone and is not confused by the presence of multiple antigens in a single solution. **Optical biosensors** are distinguished from **optical refractive index sensors** by this mechanism, and in this case it is the binding dynamics and the density of surface bound material we measure rather than just a bulk refractive index change.

Many different **figures-of-merit** are used to assess the performance of biosensors. Often, the minimum detected (or interpolated) **concentration** (in terms of parts per billion, μM, particles/L or g/L), **bound mass** (in terms of pg), **number of molecules or cells**, or **surface density** (in terms of pg/mm^2) are quoted for a device which can lead to confusion when comparing different designs. It is probably best to at least quote the minimum concentration detected, as this can be readily checked and controlled, unlike other quantities which rely on assumptions. This concentration performance will, however, vary between different antibody-antigen pairs [2], and

is not in fact what the sensor physically measures (it measures surface density of bound material). Expressing concentration in μM gives an idea of the number of detected molecules per litre, but makes molecules of different mass hard to compare with this number alone; whilst on the other hand using g/L lets you compare different mass concentrations, but not different number of molecules without additional information. Comparing biosensors is therefore not trivial, and the more figures-of-merit that can be supplied the better.

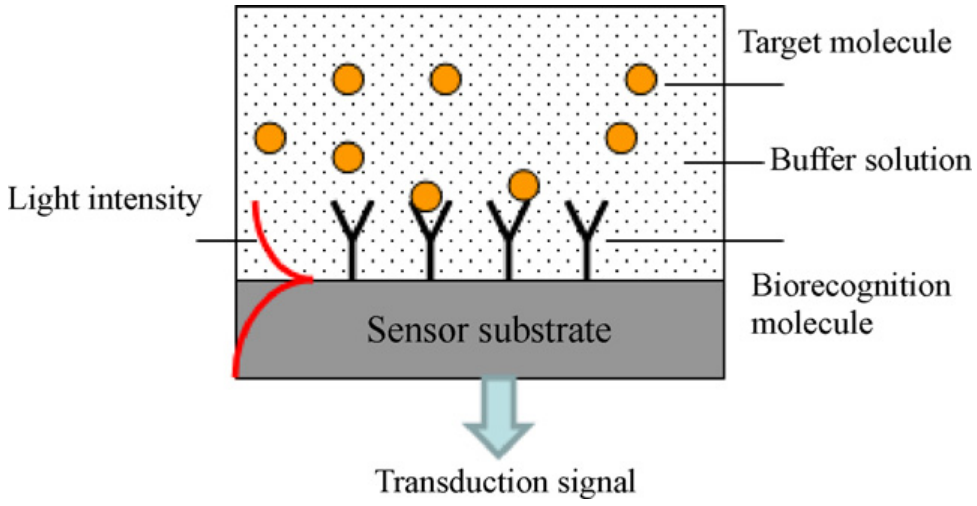

Figure 2.3: Basic principle of operation of label-free optical biosensors (reproduced with permission of Elsevier from [2], Copyright 2008). Binding of target molecules to biorecognition elements on sensor surface results in altered optical properties.

2.1.4 Fluorescent Labelling versus Label-Free

The main differences between available optical biosensors are the generation mechanism of the spectral feature(s), how sensitive it is to changes in refractive index, and whether the device uses a fluorescent tag or not. The generation mechanism of the spectral feature will be covered shortly, but first consider fluorescent tags. Fluorescent dye molecules, such as Cy-3 and Cy-5 [4], can be readily attached to bio-molecules of interest using chemistry. Optical biosensors are therefore commonly referred to as **labelled**, or **label-free** depending on whether such tags are used. These tags act as beacons, allowing the amount and path of the labelled material to be tracked. For example, a protein of interest can be labelled with a fluorescent tag and flown across a surface coated with appropriate antibodies. If the proteins have the correct geometry they can bind to the antibodies on the surface. By measuring the amount of fluorescence remaining, after a subsequent flush of the surface with blank medium, allows an estimate of the amount of immobilized proteins to be made [5]. This is the basic principle behind **immunoassays**. Alternatively the protein can be tagged with an enzyme that facilitates a visible colour change on binding in what is known as an **enzyme-linked immunosorbent assay (ELISA)**, or radioactive isotopes or silver particle based tags can also be used. In (often) more complicated form, several antibodies or antigens may be used, forming sandwich assays as shown in Fig 2.4 a). Assays are sometimes carried out with the antigens immobilized on the

surface to capture antibodies rather than the other way round, and/or can be carried out in competitive form where the presence of the target prevents binding on the surface causing a reduction in signal.

Immunoassays are a common tool for identifying antibodies and antigens and can be very sensitive, but also very laborious. The surface containing the capture antibody or antigen is spilt up into tens or hundreds of different wells on the same 'plate' (e.g. a 96-well plate), each of which is optimised for a different molecule. To fully carry out the test for each well requires multiple chemical, dilution and washing steps, as well as skill, training and knowledge for the user. Complicated fluorescent labelling steps greatly reduce the speed of this process. Such labels also suffer from processes such as fluorescence quenching [4], and their presence can interfere with biological processes (sometimes the tag is even larger than the substance it is attached to) giving false or unnatural results. Tags can also only be used in the lab (in vitro), and not on material that would potentially be injected into human beings (in vivo) in a clinical setting due to their toxic nature. Another disadvantage is the inability to measure the binding dynamics in sandwich assays. Although the final concentration or mass of bound material can be determined, it is not known how long this took to accrue or the shape of the binding curve (which can also tell us about the concentration), thus an important piece of information is lost during the test. It is for these reasons that label-free biosensors are the subject of intense interest, and are what are considered within this thesis.

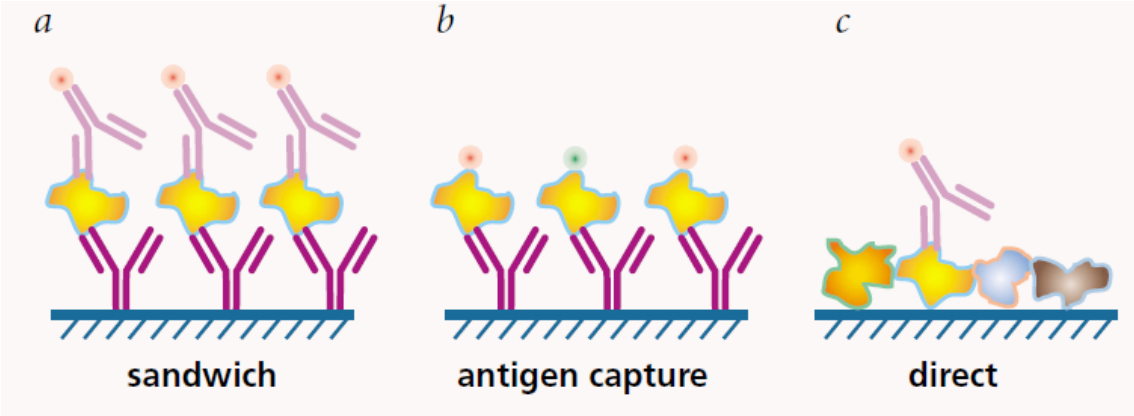

Figure 2.4: Immunoassay strategies (reproduced with permission of Nature Publishing Group from [5], Copyright 2002). (a) Sandwich form. This requires 2 antibodies. One set acts as capture agent for target protein. Secondary antibody with label flown later to detect binding. (b) In capture form the protein is labelled. (c) In direct form the protein is immobilized and a labelled antibody flown over the sample.

2.1.5 Microarrays

In addition to antibodies, other types of bio-recognition elements can be used to target other biologically interesting substances. Often fragments of DNA or RNA are used. As already seen in Section 2.1.2, a single strand of DNA can only bind correctly to its complement due to specific base pairing. In one example known as **DNA microarrays**, thousands of single-stranded DNA fragments, each corresponding to different genes, can be attached to a surface [3, 6]. A sample DNA fragment is then labelled with a fluorescent marker and flown over the surface of the chip. By observing which DNA spots display fluorescence, the binding of complementary sequences can be detected. Thousands of genetic tests can therefore be carried

out at once on this chip. The DNA fragments can be deposited on surfaces in spots as small as 5 - 150 μm using inkjet printing techniques, flow cells or photolithographic techniques [6].

It would be extremely valuable for developing drugs and diagnosing disease if such a scheme could be extended to proteins, allowing thousands of them to be tested at once on a **protein microarray**; even better if it could be done label-free. This is due to the fact that the proteins, and not the genes, are the real targets of drugs [5]. Proteins are used to facilitate and trigger many biological functions based on their shape, a process with which drugs, disease and pathogens interfere (be it beneficially or detrimentally). Compared to DNA, proteins are far more complex and delicate structures. The shape of the protein is so important, that their functionality can easily be lost should the shape change, for example due to denaturing [3]. The functionalization chemistry is therefore more challenging for proteins as they are less resilient to harsh conditions such as high temperatures. DNA can be rapidly copied using high temperature processes such as polymerase chain reaction (PCR), but there is no equivalent for proteins. Despite these challenges, protein chips are expected to experience rapid growth due to the advantages they offer [5].

2.1.6 Functionalization Techniques

Many ways exist to immobilize bio-recognition elements on a surface. The main focus here will be on antibodies for detecting proteins, but other bio-recognition elements such as the DNA probes mentioned above, lectins, neuroreceptors and enzymes can be used [5]. Some of the main challenges are finding suitable antibodies for the application, chemicals that don't harm the antibodies, and methods to pattern them on a surface. Chemicals are typically used to functionalize surfaces such as glass, silicon and silicon nitride, by adding -OH, -NH_2, -COOH or -SH groups to the surface [6]. Several techniques are shown in Fig 2.5. A common chemical used to functionalize glass and silicon with -NH_2 functional groups is aminopropyltriethoxysilane (APTES), which will be used for the devices presented within this thesis (see Chap 6). The process of using this chemical to functionalize surfaces is known as **aminosilanization** (Fig 2.5 a)). These amino groups can be further activated using substances such as glutaraldehyde.

Often antibodies can be combined with the **avidin-biotin** system [7, 8], which acts as a linker. This system (more of which will be discussed in Chap 6) of binding between the vitamin biotin and the protein avidin (or in other form streptavidin) has the strongest affinity known in nature. Proteins can also be conjugated to biotin; such proteins are said to be **biotinylated** (Fig 2.5b)). These proteins can then be captured by an avidin (or streptavidin) coated surface. Antibodies can also be attached to polystyrene microbeads that have undergone aminosilanization or streptavidin coating. If these beads have iron cores, then they can be manipulated by magnets, allowing bound proteins to be removed from a solution [9].

In the case of gold surfaces, thiol chemistry can be used, one example being the **self assembled monolayer (SAM)** [10]. SAMs rely on the different hydrophobic properties of a surfactant to form a monolayer of functional groups on a surface. The molecules of the surfactant consist of a hydrophilic head that has an affinity for a substrate, and a functional hydrophobic tail which does not [10]. These properties ensure that the head molecule attaches to the surface, whilst the functional tail, onto which antibodies and other proteins can be attached, faces away (see Fig 2.5d)).

To prevent **non-specific binding** of material to parts of a surface that have a functional group but no antibody attached, blocking agents can be used, which bind to these un-reacted functional groups after functionalization, making them in-active. **Bovine serum albumin (BSA)** in solution is commonly used. Care must be taken however as blocking agents can also cause problems, most notably in the case of very small proteins which can be masked by BSA, requiring that other agents such as glycene be used [6]. BSA can be used in functionalizing surfaces, by coating it on a glass slide [11] (Fig 2.5 c)). BSA can also be combined with the avidin-biotin system. Immobilized BSA is conjugated with biotin, as is the target protein, whilst (strept)avidin is used as a linker between the two.

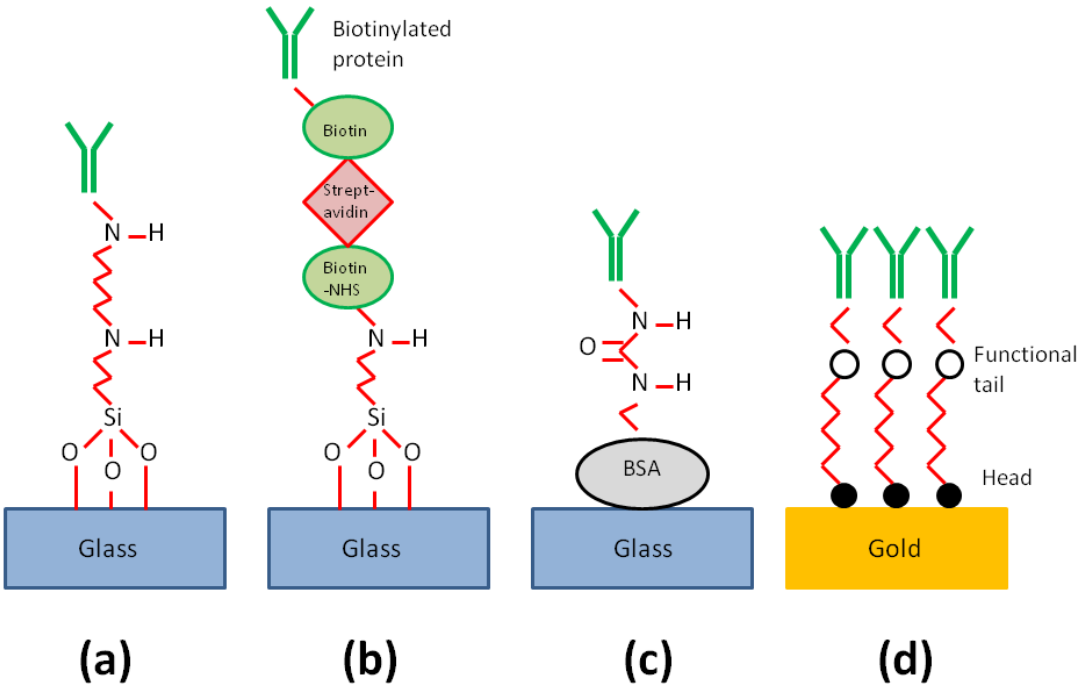

Figure 2.5: Common surface immobilization techniques ([6], [8], [9], [11]) for glass and gold. Glass surfaces can often be substituted for oxidized silicon. (a) Antibody immobilized on aminosilanized glass. (b) (Stept)avidin-biotin can be used as linker to biotinylated molecules. (c) BSA-NHS (N, N'-succinimidyl carbonate) immobilization on glass slide. (d) Immobilization on gold using self assembled monolayers (SAMs) of molecules with hydrophilic head and hydrophobic tail.

2.1.7 Surface Patterning of Biomolecules

Many strategies exist for patterning surfaces with a variety of antibodies via these functionalization schemes. This is necessary if we want high densities of independent sensors optimized to detect different biomolecules of interest (e.g. lab-on-a-chip). In one technique, **ink-jet printing** is used to deposit small spots of capture proteins, such as in ref [12] where a piezoelectric non-contact printer capable of dispensing 350 pL drops on top of ring resonators was used (see Fig 2.6 a)). Another way is to use **microfluidic flow cells** (see Chap 5) with different channels for each sensor on the surface [13, 14]. This way each sensor can be functionalized simultaneously with different antibodies, without cross contamination. In **dip-pen nanolithography** [15], perhaps the highest resolution method available, the tip of an

atomic force microscope (AFM) can be used to directly write antibodies on to a surface. It does this by first dipping the pen (the AFM tip) into the ink (biomolecules) and then writing (scanning) across the surface. **Lithographic** techniques based on UV or electron beam lithography (see Chap 3) can also be used [16], where windows are opened in a photoresist covered substrate.

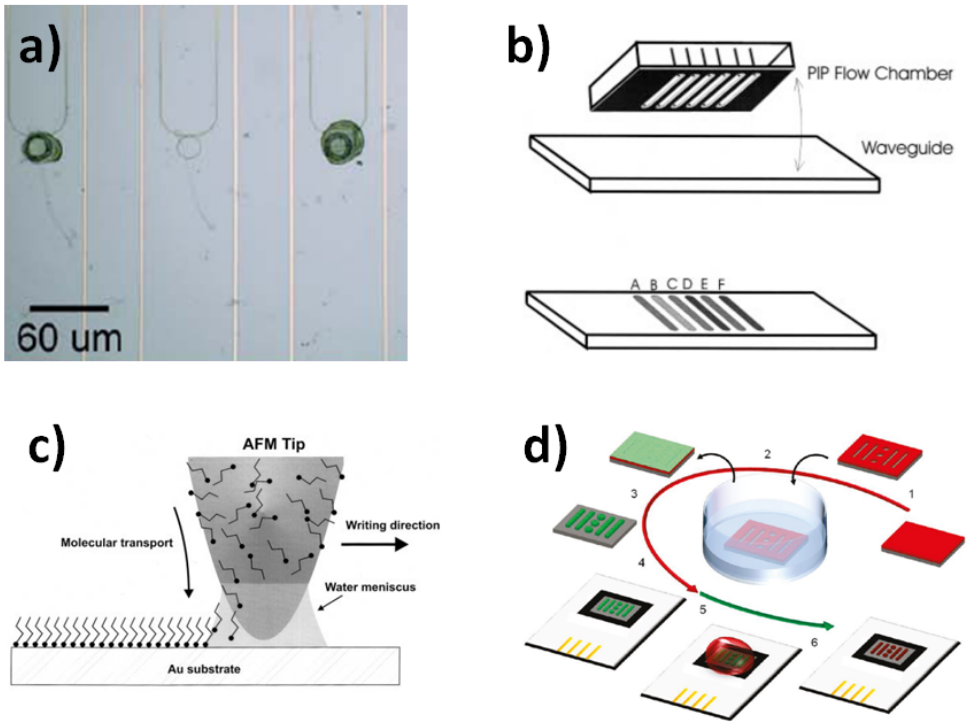

Figure 2.6: Common biomolecule patterning techniques. a) Ink-jet functionalization of individual ring resonators (reproduced with permission of The Royal Society of Chemistry from [12], Copyright 2011). b) Flow cell patterning (reproduced with permission of Springer from [13], Copyright 1999). c) Dip-pen nanolithography patterning (reproduced with permission of the American Association for the Advancement of Science from [15], Copyright 1999). d) Photolithographic patterning of surface (reproduced with permission of ACS Publications from [16], Copyright 2010).

2.2 Label-Free Optical Biosensor Technologies

Many different optical phenomena can be exploited in biosensors. Label-free biosensors mostly rely on generating and tracking a sharp spectral feature which shifts with antigen binding to the surface of the device. As of 2010, the market for label-free biosensors is believed to be worth $ 234M, with growth to $ 310M expected by 2015 [17]. The 'gold standard' label-free optical biosensors are the surface plasmon resonance (SPR) based devices sold commercially by **Biacore** [18], which have 54 % of the current market share [17]. One of most popular of these devices, the Biacore 3000 (Fig 2.7), which is housed in a temperature controlled environment, is capable of detecting small molecules in concentrations below 1nM, using samples as small as 5 µL, inside 4 different flow cells which can be optimised for different antibodies [19]. Although the sensor area is on the order of square millimetres, the surrounding equipment result in a large machine that weighs 50 kg [19] and could only be of real use within a lab. The goal of much

research in biosensor technologies is to produce a cheaper, more compact and higher throughput device that can compete with the performance of the Biacore without being restricted to high-end labs.

Figure 2.7: Biacore 3000 surface plasmon optical biosensor (reproduced from [18], image courtesy of GE Healthcare).

A number of competing optics based sensors exist, many of which will be discussed below. A relatively new entry to this field is that of integrated optics, in which several micro- or nano-photonic devices can be fabricated together on the same small chip using semiconductor processing technology borrowed from the electronics industry. The main advantage of doing this is economies of scale. Integrated optical sensors can be made very small, on the scale of tens or hundreds of microns, and be fabricated very cheaply, giving potential for dense arrays of sensor elements all optimised to detect something different, and therefore approaching the vision of a machine that could be incorporated with a label-free protein microarray (see Section 2.1.5). This is a significant advantage over the Biacore as it would allow very high throughput and minimize sample volumes, both of which are strongly desired in many costly biological tests. A mini review of the operation principle and performance of these integrated and other small optical sensors is presented below, along with surface plasmon devices, to give a flavour of the vast amount of work going on within this field at present. Please note that the following review is biased towards photonic crystal sensors as the focus of this thesis.

2.2.1 Surface Plasmon Resonance

At a particular angle of incidence on a dielectric/metal interface, light can induce a bound electromagnetic mode on the metal's surface, provided the k-vector of this mode is matched to that of the incident light. This phenomenon is known as surface plasmon resonance (SPR). Light is typically coupled into this mode using a prism, with the presence of the mode causing a dip in monochromatic light reflected off the metal interface at a particular angle. Metals such as gold are used as these can be functionalized relatively easily using techniques such as SAMs (as

discussed in Section 2.1.6). Biacore [18, 19] and most other surface plasmon based devices [20] track changes in the angle of the reflection dip that result from specific binding of bio-molecules to the metal surface. Alternatively, grating couplers or an optical waveguide layer can be used to couple to these modes [20].

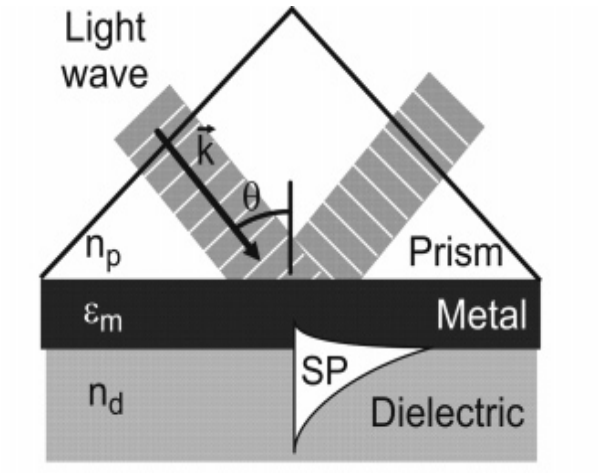

Figure 2.8: Basic operation of prism-coupled SPR (reproduced with permission of American Chemical Society from [20], Copyright 2008). Binding of material to the gold film is detected from shifts in the angle of a reflection minimum that results from coupling to the plasmon mode on the metal surface.

SPR has been used to detect a variety of substances such as: salmonella (at a lowest limit of $2.5x10^5$ cells/mL) [21], the toxin domoic acid (10 nM limit) [22], human growth hormone antibodies (2.47 nM limit) [23], antibodies associated with diabetes (0.5 μM limit) [24] and the toxin ricin (200 ng/mL limit) [25], amongst the hundreds reported in literature. Some authors utilise a broadband light source at fixed angle and measure changes in wavelength, rather than angle, such as one device [26] which was used to measure toxins in milk at concentrations as low as 5 ng/mL. In another form known as localized surface plasmon resonance (LSPR), the plasmon mode is bound to the surface of metal nanostructures, such as in [27] where gold nanorods are used to detect binding of antibodies (1 nM limit). Whilst surface plasmon biosensors are amongst the most sensitive available, they typically have low throughput. Although the recent Biacore 4000 machine has the ability to run 4800 interactions in a period of 24 hours, only 20 different target spots (i.e. 20 different assays) can be addressed [18], which is an improvement over the 4 of Biacore 3000, but a long way off the desired hundreds or thousands in protein microarrays.

2.2.2 Ring Resonator

Another popular platform in recent years for optical biosensors is the ring resonator. Ring resonators consist of an optical waveguide in ring geometry, placed closely to a standard channel waveguide. Light passing through the channel waveguide can couple into the ring at wavelengths that are exact integers of the optical path length of the ring. This coupling produces a dip in the transmission spectrum of the channel waveguide at resonant wavelengths. As usually several wavelengths can be supported in ring, a 'comb' of resonant dips is observed. A second channel waveguide can also be used as a 'drop' channel, through which this resonance can out-couple (see Fig 2.9), producing a peak in transmission. By tracking changes in these sharp spectral features, binding of bio-molecules to a functionalised ring can be detected.

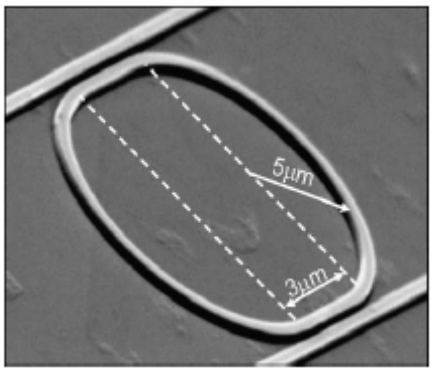

Figure 2.9: Ring resonator optical biosensor (reproduced with permission of the Optical Society of America from [28], Copyright 2007). A given wavelength of light couples from a channel waveguide into a ring waveguide on resonance. The resonant wavelength out-couples via a second channel waveguide.

Several groups have reported sensors based on this: The University of Ghent [28] report detection of avidin binding to biotin coated rings at levels as low as 10 ng/mL, as do a group from Caltech [29] (6.8 ng/mL limit), whilst [30] detect its other form, streptavidin, also using biotin coated rings (60 fM limit). At present, ring resonators are perhaps the most developed alternative platform to surface plasmon resonance for label-free optical biosensing. The main advantage over their SPR counterparts is the much smaller footprint of the device, which gives greater potential for microarrays. One device under commercial development is that of Genalyte [17, 31] which has up to 128 micro-ring resonators on one chip, each of which can be individually addressed. Patterning of antibodies takes place via the flow cell technique of Section 2.1.7. Concentrations of a few tens of pM can be detected in this device, which is based on that shown in Ref [30].

The main advantage of ring resonators over surface plasmon based devices is that they can have similar levels of sensitivity in a more compact structure. The big disadvantage compared to other resonant cavity approaches (e.g. photonic crystals) is that ring resonators have low free spectral range, which limits the number that can be multiplexed together on the same chip with different resonant frequencies. This problem can be overcome by physically moving the spot from the excitation light source between different waveguides (such as the case of Genalyte),

but this requires extra equipment and engineering. As will be shown in the next section, ring resonators have also been incorporated with slot waveguides.

2.2.3 Slot Waveguide

Slot waveguides [32] will be covered in greater detail in the next chapter. These devices confine light strongly to a ~100-200 nm scale air slot inserted into high index media. This architecture allows for increased light interactions with biomolecules, as the majority of the modal field interacts with the analyte, rather than just the tail as in the standard waveguide geometry (Fig. 2.9). Currently, many slot waveguide biosensors are based on ring resonators. In one such case from Spain by C. A. Barrios and co-workers [33, 34] a slot ring resonator is fabricated in silicon nitride and functionalized to detect BSA, the lowest limit being 0.042 μg/mL. A similar device from a collaboration of researchers [35] featuring an array of slot ring resonators has been combined with microfluidics, splitters, a photodiode array and grating couplers, and has shown detection of anti-BSA binding (0.125 μg/mL limit). A smaller biotin coated SOI slot ring from Ghent [36] that was used to detect avidin at 100 μg/mL concentration was shown to induce a larger wavelength response when compared to the above mentioned devices.

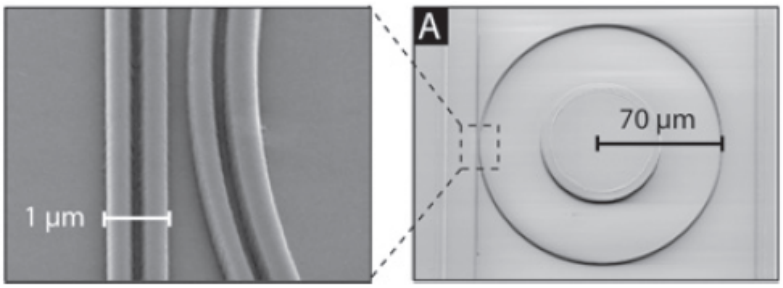

Figure 2.10: Slot waveguide ring resonator (reproduced with permission of The Royal Society of Chemistry from [35], Copyright 2010). Light is strongly confined to a narrow air slot in the waveguide.

Slot waveguides have also been used to demonstrate optical guiding of sub-100 nm particles along the slot [37]. Whilst this is not strictly 'trapping', trapping of sub-100 nm dielectric particles may be possible using slot cavities (e.g. slotted photonic crystals). This is difficult to achieve with more conventional optical traps due to the low polarisability of dielectrics; though slots provide a strong intensity gradient that could compensate for this. In addition, slot waveguides have been used as sensitive refractive index sensors. In one case refractive index changes as small as 10^{-4} RIU due to the presence of acetylene gas was demonstrated by Lipson's group at Cornell by incorporating a gas flow cell onto the chip [38]. As will been seen in later sections (and in Chapt 3), slots can also be combined with photonic crystals.

2.2.4 Photonic Crystal

Photonic crystals have also found use as biosensors. As these will be covered in more detail in the next chapter, it suffices here to say that these devices use periodic lattices of dielectric media to guide and slow down light. Their transmission spectrum contains a photonic bandgap in which almost all of the light is reflected for a wavelength range determined by the period of the lattice. This and other features which can be engineered in the spectrum can be used as a reference for sensing purposes. One group in Valencia report detection of single-stranded DNA as low as 19.8 nM by tracking spectral features near the band edge of a photonic crystal waveguide [39]. Another group at DTU, Denmark, has used a photonic crystal waveguide to demonstrate detection of 10 μg/mL (0.15 μM) BSA by measuring shifts in the cut-off wavelength [40].

One of the main advantages of photonic crystals is their ability to control the dispersion of light. By introducing defects into the lattice, high quality factor cavities can be created of size comparable to a single wavelength. The small size of the cavity is a big advantage over the larger cavities of ring resonators as it gives larger free spectral range, allowing many more devices of different resonance to be multiplexed. Slow light behaviour can also be engineered in photonic crystals by altering the dispersion curve of the device through deformations in the lattice. This allows high group indices to be achieved, resulting in enhanced light-matter interaction. In both cases, cavity and slow light, the amount of time the light interacts with the sample is increased leading to better sensitivity. Another advantage is the narrow linewidth of a cavity, which gives a useful point of reference and allows smaller wavelength shifts to be detected (see Section 2.1.1).

Some devices have used cavities in this way. In two cases, a single hole defect cavity in a 2-D photonic crystal has been used to detect BSA (2% concentration limit) [41, 42] and anti-biotin (20 pM limit) [43]. These cavities are coupled in-line, but side coupling is also used such as in

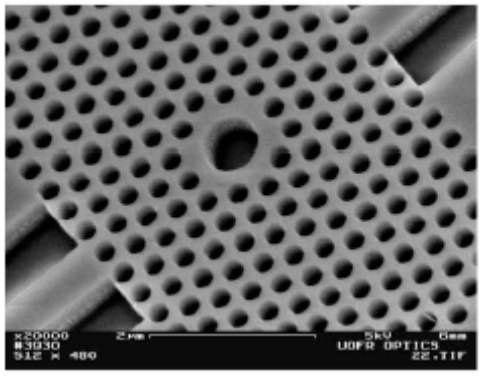

Figure 2.11: Photonic crystal biosensor based on defect hole cavity (reproduced with permission of the Optical Society of America from [42], Copyright 2007).

[44] where an L3 type cavity (three missing holes) and other designs has shown detection of BSA concentrations below 1 μM, whilst [45] also use a variety of designs including a combination of hole and L3 defects to detect 3-APTES monolayers. 1-D photonic crystals are also used. In one such case, arrays of 1-D photonic crystals with cavities are used to demonstrate detection of anti-streptavidin (1 μg/mL limit) [46]. In this device, each cavity of

unique resonance is excited by a single channel waveguide in a side-coupled design, allowing the response of multiple cavities to be obtained at once. Using the flow cell approach, each resonator is functionalized with a different antibody, giving potential for multiplexing. Other 1-D photonic crystal biosensors include [47] (3 μg/mL limit) and [48] (1 nM limit). 1-D photonic crystals can also be constructed from porous silicon, which is used in many different biosensor platforms [49] due to its large surface area. In one such device [50], protease concentrations as low as 14 μM could be detected by the human eye (7 μM with a sensor) due to colour changes in the photonic crystal as a result of infiltration into the pores.

Photonic crystal structures can also support guided resonances [51], in which light is coupled to a short lived guided mode in the device. Such modes are leaky as they exist above the light line and can therefore couple out of the slab. Instead of coupling to the photonic crystal in-plane, this coupling can be performed through the slab itself. These resonances can result in sharp features in the transmission or reflection spectrum of the device which can be used for sensing. One group in Illinois [52] exploit such a resonance in a sub-wavelength grating to measure the surface attachment of cells. As the local refractive index changes on the grating due to cell attachment, this results in changes in the position of the spectral feature. This and later iterations of the device [53, 54] have been used to image the attachment of cells to a surface in detail, which is useful in ascertaining the viability of a cell. Light is scanned over a range of angles through the grating (and an objective) and onto a CCD camera. From these images, the spectral profile at each point on the cell can be determined with a resolution of 0.61 μm^2. The device has been incorporated into a 96-well plate and is being developed commercially by SRU Biosystems [55]. Another similar device which works by scanning the wavelength has also recently been demonstrated for detecting nanoparticles [56].

2.2.5 Slotted Photonic Crystal

Although they can be thought of as a sub-section of photonic crystals, slotted photonic crystal biosensors are considered here separately, as they constitute many of the devices presented within this thesis. Slotted photonic crystals [57, 58] combine the strong spatial confinement of light by slot waveguides, with the strong temporal confinement of photonic crystals (e.g. cavity, slow light) to make a highly sensitive system (see Chap 3). Many early forays into sensing with such structures have shown that they make excellent refractive index or chemical sensors. Sensitivities of up to 1500 nm/RIU have been reported, with detection limit 7.8×10^{-6} RIU, by Di Falco and colleagues at the University of St Andrews [59]. It should be noted that this sensitivity is higher than the theoretical sensitivity of 500 nm/RIU due to variations in wetting properties with dissolved concentration. Other groups have shown detection of gases using these devices, in one case using cavities to detect a variety of gases (510 nm/RIU) [60], or by using slow light effects to enhance absorption of light by methane (100 ppm limit) [61]. The same slow light device is also used to measure xylene in water (86 μg/L limit) [62]. A group at COBRA, Eindhoven have used a cavity created by two deflected photonic crystal nanobeams fabricated in InGaAsP to demonstrate detection of sugar/water solutions with up to 900 nm/RIU sensitivity [63]. Interestingly, this device is coated with a single layer of quantum dots, which allows the refractive index shift to be detected using measurements of the photoluminescence spectrum from top.

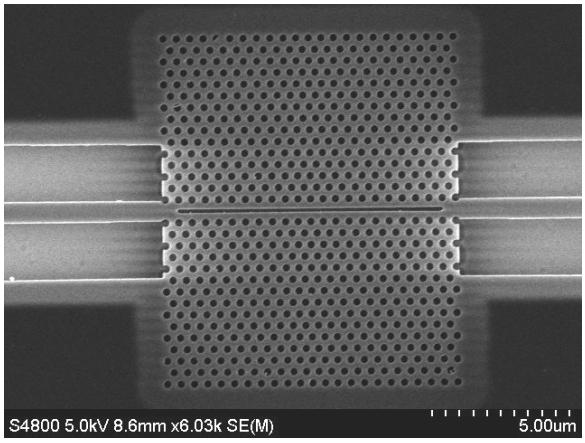

Figure 2.12: SEM image of slotted photonic crystal with channel waveguides for coupling light in and out of the structure. Light is strongly confined to the air slot region in the centre of the crystal.

Other than the devices fabricated and tested within this thesis, there are few true biosensors (as opposed to purely refractive index sensors) based on slotted photonic crystals, though several designs have been considered theoretically [64-66]. One device [67] that has been demonstrated experimentally by Toshihiko Baba and co-workers in Japan uses a glutaraldehyde coated slotted photonic crystal nanolaser fabricated in GaInAsP/InP to detect BSA with very high sensitivity (255 fM limit), by observing changes in the laser spectrum. Whilst BSA has a high affinity for glutaraldehyde, this reaction is non-specific, and in this particular case the affinity was calculated to be four orders of magnitude higher than normal. The authors suggest this could be as a result of optical trapping within the cavity. In another device from the University of Rochester, single latex spheres, 100 nm in diameter, are detected using a slotted microcavity photonic crystal [68]. The main advantage over ring-resonators is that slotted photonic crystals sense with the peak of the optical mode, rather than the evanescent tail, which leads to bigger shifts in wavelength from biomolecule binding. Slotted photonic crystals are also more compact structures, and have larger free spectral range than ring resonators, which allows potential for 100s of sensors to multiplexed on the same chip with different frequencies.

2.2.6 Interferometer

Interferometers use interference to recover information about the optical path of light waves. In a Mach-Zehnder architecture, light is split into two arms and then later re-combined. If one arm only is functionalized, usually through the use of a window in an isolation layer, surface binding results in differences in phase between the two arms. In one example, an integrated Mach-Zehnder was fabricated in a glass substrate by ion exchange, and was used to detect streptavidin (100 μg/mL) [69]. In another, human serum albumin antigen was detected (7.7 μM) [70]. Mach-Zehnder structures have also been combined with slot waveguides (306 nm/RIU) [71] and surface plasmons (37 μg/mL BSA detected) [72]. Other interferometer designs have also been used, such as the Young – type interferometer, whereby one group at the University of Twente was able to detect HSV-1 virus with exceptional sensitivity (850 particles/mL) [73]. Although interferometers can be sensitive, they require that the arms be very long to induce a large enough phase change. Spiral or other folded up arms can be used,

but the overall footprint of the device is typically larger than the other solutions mentioned above.

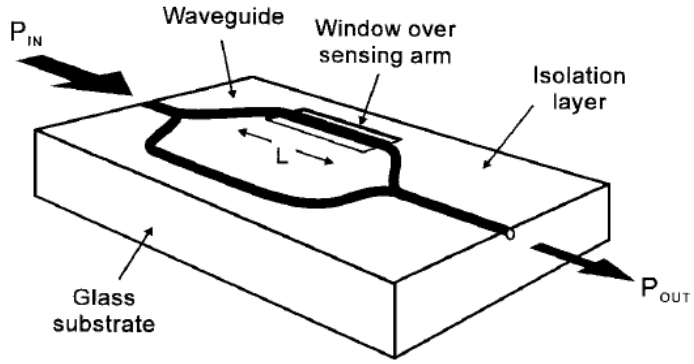

Figure 2.13: Integrated Mach-Zehnder interferometer biosensor (reproduced with permission of IEEE from [69], Copyright 1998). One arm is functionalized through a window in an isolation layer. Surface binding causes a phase difference between the arms.

2.2.7 Other

Many other optical sensors exist based on optical fibres, Raman spectroscopy, photonic wires, microtoroids and microspheres, but it is impossible to comment on every device available. A couple of devices are briefly mentioned here due to the novel nature of their material platform. The first of these [74] consists of optical waveguides fabricated in agarose gel (a material commonly used in gel electrophoresis for separating out DNA strands) using Polydimethylsiloxane (PDMS) stamps (see Chapt 5). The main advantage of doing this is that live cells and DNA strands can be embedded within the gel, thus ensuring they interact with the peak of the waveguide mode. In the other [75], optical elements such as gratings and lenses are fabricated in silk using PDMS moulds. Silk gratings were combined with red blood cells and enzymes as a test for biocompatibility. For more information about what other optical biosensors have been presented in the literature please see some recent review papers on the subject [2, 76].

2.2.8 Comparison of Small Optical Biosensors

Table 2.1 below shows a comparison between many of the different devices mentioned above, highlighting their size, sensing area, target substance, detection limit, and to aid comparison, sensor response for a given concentration (where information is available or applicable). The relevant numbers from the slotted photonic crystal cavity device presented in Chapter 6 are also included here for ease of comparison (highlighted in blue).

Table 2.1: Comparison of selected small optical biosensors.

Reference	Type of Device	Target Substance	Estimated Sensing Surface Area (μm²)	Minimum Conc. Measured	Δλ for 10 μg/ml Conc. (nm)
		Surface Plasmon Resonance			
Biacore 3000 [18, 19]	Surface plasmon resonance	Multiple	1-16x10^6	<1 nM	N/A
Kausaite-Minkstimiene et al. [23]	Surface plasmon resonance	Human growth hormone antibodies	-	2.47 nM	N/A
Stevens et al. [22]	Surface plasmon resonance	Domoic acid toxin	6x10^5	10 nM	N/A
Lee et al. [24]	Surface plasmon resonance	Diabetes anti-GAD antibodies	-	0.5 μM	N/A
Homola et al. [26]	Surface plasmon resonance	Staphylococcal enterotoxin B in milk	-	5 ng/mL	-
Feltis et al. [25]	Surface plasmon resonance	Ricin	-	200 ng/mL	N/A
Barlen et al. [21]	Surface plasmon resonance	Salmonella	-	2.5x10^5 cells/mL	N/A
Mayer et al. [27]	Localized surface plasmon resonance	Antibodies	-	1 nM	-
		Ring Resonator			
Iqbal et al. [30] / Genalyte [17, 31]	Ring resonator	Streptavidin	84.8	60 fM	<0.1
Ksendzov and Lin [29]	Ring resonator	Avidin	2.4x10^4	6.8 ng/mL (0.1 nM)	-
De Vos et al. [28]	Ring resonator	Avidin	21.8	10 ng/mL (0.15 nM)	0.55
		Slot Waveguide			
Barrios et al. [33] / Banuls et al. [34]	Slot ring resonator	BSA	> 250	0.042 μg/mL	2.5
Carlborg et al. [35]	Slot ring resonator	Anti-BSA	> 250	0.125 μg/mL	1.2
Claes et al. [36]	Slot ring resonator	Avidin	> 13	100 μg/mL (1.5 μM)	-

Photonic Crystal					
Zlatanovic et al. [42]	2-D Photonic crystal cavity	Anti-biotin	0.272	20 pM	-
Toccafondo et al. [39]	2-D Photonic crystal waveguide	s-DNA	> 100	19.8 nM	< 0.2
Skivesen et al. [40]	2-D Photonic crystal waveguide	BSA	> 100	10 µg/ mL (150 nM)	0.2
Dorfner et al. [44]	2-D Photonic crystal cavity	BSA	8.15	< 1 µM	-
Lee and Fauchet [41,42]	2-D Photonic crystal cavity	BSA	50	2%	-
Kang et al. [45]	2-D Photonic crystal cavity	3-APTES	-	-	-
Guo et al. [48]	1-D Photonic crystal	Biotin-20T	-	1 nM	0.5
Orosco et al. [50]	1-D Porous silicon photonic crystal	Protease	-	7 µM	-
Mandal et al. [46]	1-D Photonic crystal cavity	Anti-streptavidin	8.36	1 µg/mL	0.25
Konopsky and Alieva [47]	1-D Photonic crystal	Biotin	-	3 µg/mL	-
Slotted Photonic Crystal					
Device in this thesis (Chapter 6)	**Slotted photonic crystal cavity**	**Avidin**	**< 2.2**	**1 µg/mL (15 nM)**	**1.5**
Lee et al. [68]	Slotted microcavity photonic crystal	Latex spheres	< 2	-	-
Kita et al. [67]	Slotted photonic crystal nanolaser	BSA	< 1	255 fM	-
Lai et al. [62]	Slow light slotted photonic crystal	Xylene in water	-	86 µg/mL	N/A
Interferometer					
Prieto et al. [70]	Mach-Zehnder interferometer	Human serum albumin	$< 1x10^{5}$	7.7 µM	N/A
Luff et al. [69]	Mach-Zehnder interferometer	Streptavidin	$4.4x10^{4}$	100 µg/mL	N/A

Wu et al. [72]	SPR Mach-Zehnder	BSA	-	37 µg/mL	N/A
Ymeti et al. [73]	Young interferometer	HSV-1 virus	-	850 particles/mL	N/A

As can evidently be seen in Table 2.1 above, surface plasmons have found use in detecting a variety of substances that are useful to know in many real world applications. Also evident is that the main integrated optics-based competitors have mainly demonstrated proof-of-principle by detecting substances such as streptavidin or BSA. Whilst these substances can be conjugated to a vast library of different antibodies [7], in general, most of these devices have yet to find application in a real world problem of importance (one notable exception is Genalyte). As stated in the introduction, real application is one of the major goals of this present work. This lack of application is to be expected, however, due to the relative infancy of many of the integrated optics based devices when compared to the commercial history of surface plasmon based devices. Despite this problem, it can also been seen from this table that many integrated optical sensors can have sensitivities similar to that of the surface plasmon devices, despite being generally much smaller in size. This small size gives greater potential for high throughput and multiplexing, which are desirable for minimizing costs. Table 2.1 shows that all of these devices are capable of detecting biomolecules with high sensitivity. Slot based devices, however, have a major advantage versus their non-slotted counterparts. Slot waveguide based ring resonators have much larger wavelength shifts than standard ring resonators. Similarly, slotted photonic crystals have much larger wavelength shifts than photonic crystals. In both cases this results from the strong optical field – analyte overlap of the slot waveguide effect. Bigger wavelength shifts for a given concentration reduce the performance requirements of any potential on-chip spectrometer; a necessary component for true lab-on-a-chip devices. Slotted photonic crystals have a much smaller sensing area than slot waveguide ring resonators. The smaller cavity size of the slotted photonic crystal also gives much larger free spectral range. I therefore believe slotted photonic crystals to be the most suitable for multiplexing given the smaller footprint and greater bandwidth they offer for multiple sensing elements. There may also be some room for improving experimental performance through better environmental control.

2.3 Barriers to Entry

From the wide variety of applications, sensitivity and commercial success, surface plasmon resonance can be viewed as the technology to beat in terms of label-free biosensing. For any technology to replace the existing standard it must meet at least one of the following requirements:

Perform better: in the case of biosensing, having better sensitivity or limit of detection, and/or be easier to operate.

Cost less: For biosensors, not only the cost of the device, but also the cost per test in terms of materials and labour.

Do something new: can the biosensor investigate some problem that other devices cannot?

One of the main barriers for taking full advantage of the integrated optics approach is the sources and detectors available. Although the sensor chips can be very small, they often require a bulky spectrometer to function fully, and are thus more 'chip-in-a-lab' than 'lab-on-a-chip'. This point is often brushed over and is one of the key limiting factors of many devices in the literature. Some form of on-chip spectrometer is required (see Chapter 7). Multiplexing at the same time can also be tricky. Either the source has to be split and the detector arrayed (e.g. [35]), which can be lossy, or each sensor has to be rapidly addressed individually as in the case of Genalyte [31]. Sensors based on silicon also suffer from a lack of integrated light sources due to the indirect bandgap of silicon, though solutions such as flip-chip bonding can be used to attach sources constructed in other material platforms. A further barrier comes from the fact that the machines sold by Biacore benefit from a research and commercial history stretching back more than 20 years, and posses the majority of the current market. Much of the cost for Biacore and Genalyte comes from the great lengths they go to stabilising the sample environment, minimising noise (such as temperature fluctuations) from unwanted sources. Whilst 'lab-on-a-chip' devices based will also have to take environmental conditions into consideration, the integrated optics approach is perhaps more stable and requires less engineering as all the elements are on the same chip, thus variables can be cancelled out more easily using a reference.

More generally the fragile and expensive nature of antibodies limits the vision of protein microarrays below their DNA counterparts. Whilst DNA can be copied rapidly in PCR, proteins are more vulnerable to harsh conditions. The use of surface based sensors also means that detection is based on diffusion and sedimentation, which limits both performance and speed. Antigens in solution may never see the capture antibody on the surface of the device within a reasonable timescale. Many of the sensors presented above also rely on having prepared solutions involving steps such as centrifugation and dilution rather than work with unaltered samples (e.g. a drop of blood), and are thus not user-friendly to the non-specialist. Different proteins can also have different solubility or functionaliztion chemistry, limiting the number of different receptor types on a single chip. Despite all of these problems, it is conceivable that integrated optical sensors will feature in future commercial biosensors due to the advantages of size, mass producibility and sensitivity they offer. With improving technology and design most of the desired goals of a compact, multiplexed device can conceivably be realized. Whilst there is also some room for improved performance, in future it will ultimately be the biology and chemistry that impose limits rather than the devices themselves [17].

2.4 Micro-Opto-Electro-Mechanical Systems

Optical biosensors are not just limited to observing shifts in a resonance due to refractive index changes. Micro-Opto-Electro-Mechanical Systems (MOEMS) are micron scale devices which utilise the interplay between optical, electrical and mechanical phenomena. One popular sensing method is to measure a microcantilever as it undergoes biomolecule binding using optical techniques. The cantilever can either be static, where a bend is detected due to stresses induced by biomolecule binding, or continuously oscillated, where a change in frequency is detected due to increased mass. For example, Timurdogan *et al* [77] report on the detection of hepatitis viruses using electromagnetically actuated cantilevers with embedded diffraction gratings on their tips. A limit of detection of 0.1 ng/mL was achieved. In another scheme from Koev *et al* [78], a cantilever doubles as an optical waveguide, butt coupled to another fixed waveguide. Bending of the cantilever due to biomolecule binding alters the amount of light coupled between the two waveguides, with a limit of detection of 10 μM for homocysteine

being demonstrated. It is also interesting to note, given the topic of this thesis, that slot waveguides have been proposed as micro cantilever biosensors. In a paper by Barrios [79], a vertical slot waveguide formed between discs of Si_3N_4 and Si, and supported by a SiO_2 spacer was considered theoretically, and shown to behave as a very sensitive cantilever when compared to the literature. A full review of different cantilever biosensors can be found in Ref [80].

2.5 Electronic Biosensors

Given the cross-over in technology platforms and their more prevalent history, it is best, as an aside, to consider very briefly biosensors based on electronic transduction in addition to their optical counterparts. As mentioned earlier, electronics is a more mature technology than photonics, and as such benefits from mass producibility, standards, wide availability, repeatability and low costs. Many existing biosensors are therefore based on electronics. Although optical sensors have made inroads into the market it is best to utilize a technology because it has the most advantages to offer, rather than because it is new. Electronic biosensors therefore still have a major role to play in many applications. Like the optical biosensors explored above, electronic sensors need to exploit some physical quantity in order to function. In the case of optics we look to intensity, phase or spectral component, in the case of electronics it is capacitance, inductance, phase or conductance. Electrical nanowires (see Refs [81, 82] for reviews) are interesting to compare with the optical sensors mentioned above, as they share similar material platforms and surface chemistry. Binding of biological material causes accumulation or depletion of charge carriers, causing changes in electrical properties that can be detected with high sensitivity. For example, Dengue fever virus has been detected with silicon nanowires capable of 10 fM limit of detection [83]; whilst a 64x64 array of microelectrodes, 21 μm spacing, has been used to study neuronal networks [84]. Also interesting is the ability to locally functionalize using electrical methods. Functional groups created on carbon nanotubes can be converted from nitro groups to amine groups by applying a potential [85]. This allows only certain areas to be functionalized, and this or other schemes could perhaps be adapted to help functionalize optical sensors (e.g. doping the silicon). It is even conceivable that some performance enhancements will come from devices the exploit both optical and electronic transduction simultaneously.

References – Chapter 2

[1] White, I. M. and Fan, X., "On the performance quantification of resonant refractive index sensors," Opt. Exp. 16, 1020-1028 (2008).

[2] Fan, X., White, I. M., Shopova, S. I., Zhu, H., Suter, J. D. and Sun, Y., "Sensitive optical biosensors for unlabelled targets: A review," Analy. Chem. Act. 620, 8-26 (2008).

[3] Campbell, N. A., Reece, J. B., Urry, L. A., Cain, M. L., Wasserman, S. A., Minorsky, P. V. and Jackson, R. B., [Campbell Biology, 9th Edition], Pearson, San Francisco, Chpt. 5, 11, 43, 44, 45 (2008).

[4] Gruber, H. J., Hahn, C. D., Kada, G., Reiner, C. K., Harms, G. S., Ahrer, W., Dax, T. G. and Knaus, H. -G., "Anomalous fluorescence enhancement of Cy3 and Cy3.5 versus anomalous fluorescence loss of Cy5 and Cy7 upon covalent linking to IgC and noncovalent binding to avidin," Bioconjugate Chem. 11, 696-704 (2000).

[5] MacBeath, G., "Protein microarrays and proteomics," Nature Gen. 32, 526-532 (2002).

[6] Prasad, P. N., [Introduction to biophotonics], Wiley Interscience, Hoboken, N.J., Chpts 9, 10 (2003).

[7] Wilchek, M., Bayer, E. A. and Livnah, O., "Essentials of biorecognition: The (strept)avidin-biotin system as a model for protein-protein and protein-ligand interaction," Immun. Lett. 103, 27-32 (2006).

[8] Lapin, N. A. and Chabal, Y. J., "Infrared characterization of biotinylated silicon oxide surfaces, surface stability, and specific attachment of streptavidin," J. Phys. Chem. B. 113, 8776-8783 (2009).

[9] Bange, A., Halsall, B. and Heineman, W. R., "Microfluidic immunosensor systems," Biosens. Bioelect. 20, 2488-2503 (2005).

[10] Schreiber, F., "Structure and growth of self-assembling monolayers," Progress Surface Sci. 65, 151-256 (2000).

[11] Rasnik, I., McKinney, S. A. and Taekjip, H. A., "Surfaces and orientations: Much to FRET about?," Accounts Chem. Res. 38, 542-548 (2005).

[12] Kirk, J. T., Fridley, G. E., Chamberlain, J. W., Christensen, E. D., Hochberg, M. and Ratner, D. M., "Multiplexed inkjet functionalization of silicon photonic biosensors," Lab Chip 11, 1372-1377 (2011).

[13] Feldstein, M. J., Golden, J. P., Rowe, C. A., MacCraith, B. D. and Ligler, F. S., "Array biosensor: Optical and fluidics system," J. Biomed. Microdevices 1, 139-153 (1999).

[14] Mandal, S., Goddard, J. M. and Erickson, D., "A multiplexed optofluidic biomolecular sensor for low mass detection," Lab Chip 9, 2924-2932 (2009).

[15] Piner, R. D., Zhu, J., Xu, F., Hong, S. and Mirkin, C. A., " "Dip-pen" nanolithography," Science 283, 661-663 (1999).

[16] Suarez, G., Keegan, N., Spoors, J. A., Ortiz, P., Jackson, R. J., Hedley, J., Borrise, X. and McNeil, C. J., "Biomolecule patterning on analytical devices: a microfabrication-compatible approach," Langmuir 26, 6071-6077 (2010).

[17] Gunn, C. (Genalyte), "Biosensors from an industrial angle," Invited talk, Silicon Photonics Summer School, St Andrews, U.K. (2011).

[18] http://www.biacore.com, last visited on 18/04/2012.

[19] Biacore 3000 Product Information sheet, available from ref [18].

[20] Homola, J., “Surface plasmon resonance sensors for detection of chemical and biological species,” Chem. Rev. 108, 462-493 (2008).

[21] Barlen, B., Mazumdar, S. D., Lezrich, O., Kampfer, P. and Keusgen, M., “Detection of salmonella by surface plasmon resonance,” Sensors 7, 1427-1446 (2007).

[22] Stevens, R. C., Soelberg, S. D., Eberhart, B. -T. L., Spencer, S., Wekell, J. C., Chinowsky, T. M., Trainer, V. L. and Furlong, C. E., “Detection of the toxin domoic acid from clam extracts using a portable surface plasmon resonance biosensor,” Harmful Algae 6, 166-174 (2007).

[23] Kausaite-Minkstimiene, A., Ramanaviciene, A. and Ramanavicius, A., “Surface plasmon resonance biosensor for direct detection of antibodies against human growth hormone,” Analyst 134, 2051-2057 (2009).

[24] Lee, J. W., Sim, S J,, Cho, S. M. and Lee, J., “Characterization of a self-assembled monolayer of thiol on a gold surface and the fabrication of a biosensor chip based on surface plasmon resonance for detecting anti-GAD antibody,” Biosens. Bioelect. 20, 1422-1427 (2005).

[25] Feltis, B. N., Sexton, B. A., Glenn, F. L., Best, M. J., Wilkins, M. and Davis, T. J., “A hand-held surface plasmon resonance biosensor for the detection of ricin and other biological agents,” Biosens. Bioelect. 23, 1131-1136 (2008).

[26] Homola, J., Dostalek, J., Chen, S., Rasooly, A., Jiang, S. and Yee, S. S., “Spectral surface plasmon resonance biosensor for detection of staphylococcal enterotoxin B in milk,” International J. Food Microbiology 75, 61-69 (2002).

[27] Mayer, K. M., Lee, S., Liao, H., Rostro, B. C., Fuentes, A., Scully, P. T., Nehl, C. L. and Hafner, J. H., “A label-free immunoassay based upon localized surface plasmon resonance of gold nanorods,” ACS Nano 2, 687-692 (2008).

[28] De Vos, K., Bartolozzi, I., Schacht, E., Bienstman, P., Baets, R., “Silicon-on-insulator resonator for sensitive and label-free biosensing,” Opt. Exp. 15, 7610-7615 (2007).

[29] Ksendzov, A. and Lin, Y., “Integrated optics ring-resonator sensors for protein detection,” Opt. Lett. 30, 3344-3346 (2005).

[30] Iqbal, M., Gleeson, M. A., Spaugh, B., Tybor, F., Gunn, W. G., Hochberg, M., Baehr-Jones, T., Bailey, R. C. and Gunn, L. C., “Label-free biosensor arrays based on silicon ring resonators and high-speed optical scanning instrumentation,” IEEE J. Selected Topics in Quantum Electrodyn. 16, 654-661 (2010).

[31] http://www.genalyte.com/, last visited on 17/05/2012.

[32] Almeida, V. R., Xu, Q., Barrios, C. A. and Lipson, M., “Guiding and confining light in void nanostructure,” Opt. Lett. 29, 1209-1211 (2004).

[33] Barrios, C. A., Gylfason, K. B., Sanchez, B., Griol, A., Sohlstrom, H., Holgado, M. and Casquel, R., “Slot-waveguide biochemical sensor,” Opt. Lett. 32, 3080-3082 (2007).

[34] Banuls, M. -J., Gonzalez-Pedro, V., Barrios, C. A., Puchades, R. and Maquieira, A., "Selective chemical modification of silicon nitride/silicon oxide nanostructures to develop label-free biosensors," Biosens. Bioelect. 25, 1460-1466 (2010).

[35] Carlborg, C. F., Gylfason, K. B., Kazmierczak, A., Dortu, F., Banuls Polo, M. J., Maquieira Catala, A., Kresbach, G. M., Sohlstrom, H., Moh, T., Vivien, L., Popplewell, J., Ronan, G., Barrios, C. A., Stemme, G. and van der Wijngaart, W., "A packaged optical slot-waveguide ring resonator sensor array for multiplex label-free assays in lab-on-chips," Lab Chip 10, 257-396 (2010).

[36] Claes, T., Molera, J. G., De Vos, K., Schacht, E., Baets, R., Bienstman, P., "Label-free biosensing with a slot-waveguide-based ring resonator in silicon on insulator," IEEE Photonics J. 1, 197-204 (2009).

[37] Yang, A. H. J., Moore, S. D., Schmidt, B. S., Klug, M., Lipson, M. and Erickson, D., "Optical manipulation of nanoparticles and biomolecules in sub-wavelength slot waveguides," Nature 457, 71-75 (2009).

[38] Robinson, J. T., Chen, L. and Lipson, M., "On-chip gas detection in silicon optical microcavities," Opt. Exp. 16, 4296-4301 (2008).

[39] Toccafondo, V., Garcia-Ruperez, J., Banuls, M. J., Griol, A., Castello, J. G., Peransi-Llopis, S. and Maquieira, A., "Single-strand DNA detection using a planar photonic-crystal-waveguide-based sensor," Opt. Lett. 35, 3673-3675 (2010).

[40] Skivesen, N., Tetu, A., Kristensen, M., Kjems, J., Frandsen, L. H. and Borel, P. I., "Photonic-crystal waveguide biosensor," Opt. Exp. 15, 3169-3176 (2007).

[41] Lee, M. and Fauchet, P. M., "Two-dimensional silicon photonic crystal based biosensing platform for protein detection," Opt. Exp. 15, 4530-4535 (2007).

[42] Lee, M. and Fauchet, P. M., "Nanoscale microcavity sensor for single particle detection," Opt. Lett. 32, 3284-3286 (2007).

[43] Zlatanovic, S., Mirkarimi, L. W., Sigalas, M. M., Bynum, M. A., Chow, E., Robotti, K. M., Burr, G. W., Esener, S. and Grot, A., "Photonic crystal microcavity sensor for ultracompact monitoring of reaction kinetics and protein concentration," Sens. Act. B 141, 13-19 (2009).

[44] Dorfner, D., Zabel, T., Hurlimann, T., Hauke, N., Frandsen, L., Rant, U., Abstreiter, G. and Finley, J., "Photonic crystal nanostructures for optical biosensing applications," Biosens. Bioelect. 24, 3688-3692 (2009).

[45] Kang, C., Phare, C. T., Vlasov, Y. A., Assefa, S. and Weiss, S. M., "Photonic crystal slab sensor with enhanced surface area," Opt. Exp. 18, 27930-27937 (2010).

[46] Mandal, S., Goddard, J. M. and Erickson, D., "A multiplexed optofluidic biomolecular sensor for low mass detection," Lab Chip 9, 2924-2932 (2009).

[47] Konopsky, V. N. and Alieva, E. V., "Photonic Crystal Surface Waves for Optical Biosensors," Anal. Chem. 79, 4729-4735 (2007).

[48] Guo, Y., Ye, J. Y., Divin, C., Huang, B., Thomas, T. P., Baker, J. R. and Norris, T. B., "Real-time biomolecular binding detection using a sensitive photonic crystal biosensor," Anal. Chem. 82, 5211-5218 (2010).

[49] Jane, A., Dronov, R., Hodges, A. and Voelcker, N. H., "Porous silicon biosensors on the advance," Trends in Biotech. 27, 230-239 (2009).

[50] Orosco, M. M., Pacholski, C., Miskelly, G. M. and Sailor, M. J., "Protein-coated porous-silicon photonic crystals for amplified optical detection of protease activity," Advan. Mat. 18, 1393-1396 (2006).

[51] Fan, S. and Joannopoulos, J. D., "Analysis of guided resonances in photonic crystal slabs," Phys. Rev. B 65, 235112 (2002).

[52] Lin, Bo, Li, P. and Cunningham, B. T., "A label-free biosensor-based cell attachment assay for characterization of cell surface molecules," Sens. Act. B 114, 559-564 (2006).

[53] Chan, L. L., Gosangari, S. L., Watkin, K. L. and Cunningham, B. T., "A label-free photonic crystal biosensor imaging method for detection of cancer cell cytotoxicity," Apoptosis 12, 1061-1068 (2007).

[54] Lidstone, E. A., Chaudhery, V., Kohl, A., Chan, V., Wolf-Jensen, T., Schook, L. B., Bashir, R. and Cunningham, B. T., "Label-free imaging of cell attachment with photonic crystal enhanced microscopy," Analyst 136, 3608-3615 (2011).

[55] http://www.srubiosystems.com/, last visited on 17/05/2012.

[56] Grepstad, J. O., Kaspar, P., Solgaard, O., Johansen, I. -R., and Sudbo, A. S., "Photonic-crystal membranes for optical detection of single nano-particles, designed for biosensor application," Opt. Exp. 20, 7954-7965 (2012).

[57] Di Falco, A., O'Faolain, L. and Krauss, T. F., "Photonic crystal slotted slab waveguides," Phot. Nano Fun. Appl. 6, 38-41 (2008).

[58] Di Falco, A., O'Faolain, L. and Krauss, T. F., "Dispersion control and slow light in slotted photonic crystal waveguides," Appl. Phys. Lett. 92, 083501 (2008).

[59] Di Falco, A., O'Faolain, L. and Krauss, T. F., "Chemical sensing in slotted photonic crystal heterostructure cavities," Appl. Phys. Lett. 94, 063503 (2009).

[60] Jagerska, J., Zhang, H., Diao, Z., Le Thomas, N. and Houdre, R., "Refractive index sensing with an air-slot photonic crystal nanocavity," Opt. Lett. 35, 2523-2525 (2010).

[61] Lai, W. -C, Chakravarty, S., Wang, X., Lin, C. and Chen, R. T., "On-chip methane sensing by near-IR absorption signatures in a photonic crystal slot waveguide," Opt. Lett. 36, 984-986 (2011).

[62] Lai, W. -C, Chakravarty, S., Wang, X., Lin, C. and Chen, R. T., "Photonic crystal slot waveguide absorption spectrometer for on-chip near-infrared spectroscopy of xylene in water," Appl. Phys. Lett. 98, 023304 (2011).

[63] Wang, B., Dundar, M. A., Notzel, R., Karouta, F., He, S. and van der Heijden, R. W., "Photonic crystal slot nanobeam slow light waveguides for refractive index sensing," Appl. Phys. Lett. 97, 151105 (2010).

[64] Kwon, S. -H., Sunner, T., Kamp, M. and Forchel, A., "Optimization of photonic crystal cavity for chemical sensing," Opt. Exp. 16, 11709-11717 (2008).

[65] Lin, S., Hu, J., Kimerling, L. and Crozier, K., "Design of nanoslotted photonic crystal waveguide cavities for single nanoparticle trapping and detection," Opt. Lett. 34, 3451-3453 (2009).

[66] Kurt, H., Erim, M. N. and Erim, N., "Various photonic crystal bio-sensor configurations based on optical surface modes," Sens. Act. B 165, 68-75 (2012).

[67] Kita, S., Hachuda, S., Otsuka, S., Endo, T., Imai, Y., Nishijima, Y., Misawa, H. and Baba, T., "Super-sensitivity in label-free protein sensing using a nanoslot nanolaser," Opt. Exp. 19, 17683-17690 (2011).

[68] Lee, M. R., Miller, B. L. and Fauchet, P. M., "Two-dimensional photonic crystal slot microcavity sensor for virus-sized particle detection," Integrated Photonics and Nanophotonics Research and Applications Conference, Boston, Massachusetts (2008).

[69] Luff, B. J., Wilkinson, J. S., Piehler, J., Hollenbach, U., Ingenhoff, J. and Fabricius, N., "Integrated optical Mach-Zehnder biosensor," J. Lightwave Tech. 16, 583-592 (1998).

[70] Prieto, F., Sepulveda, B., Calle, A., Llobera, A., Dominquez, C. and Lechuga, L. M., "Integrated Mach-Zehnder interferometer based on ARROW structures for biosensing applications," Sens. Act. B 92, 151-158 (2003).

[71] Zhang, H., Zhang, J., Chen, S., Song, J., Kee, J. S., Yu, M. and Lo, G. -Q., "CMOS-compatible fabrication of silicon-based sub-100-nm slot waveguide with efficient channel-slot coupler," IEEE Phot. Tech. Lett. 24, 10-12 (2012).

[72] Wu, S. Y., Ho, H. P., Law, W. C., Lin, C. and Kong, S. K., "Highly sensitive differential phase-sensitive surface plasmon resonance biosensor based on the Mach-Zehnder configuration," Opt. Lett. 29, 2378-2380 (2004).

[73] Ymeti, A., Greve, J., Lambeck, P. V., Wink, T., van Hovell, S. W. F. M., Beumer, T. A. M., Wijn, R. R., Heideman, R. G., Subramaniam, V. and Kanger, J. S., "Fast, ultrasensitive virus detection using a Young interferometer sensor," Nano Lett. 7, 394-397 (2007).

[74] Jain, A., Yang, A. H. and Erickson, D., "Gel-based optical waveguides with live cell encapsulation and integrated microfluidics," Opt. Lett. 37, 1472-1474 (2012).

[75] Lawerence, B. D., Cronin-Golomb, M., Georgakoudi, I., Kaplan, D. L., and Omenetto, F. G., "Bioactive silk protein biomaterial systems for optical devices," Biomacromolecules 9, 1214-1220 (2008).

[76] Fan, X. and White, I. M., "Optofluidic Microsystems for chemical and biological analysis," Nature Phot. 5, 591-597 (2011).

[77] Timurdogan, E., Alaca, B. E., Kavakli, I. H., and Urey, H., "MEMS biosensor for detection of Hepatitis A and C viruses in serum," Biosens. Bioelect. 28, 189-194 (2011).

[78] Koev, S. T., Fernandes, R., Bentley, W. E., and Ghoddsi, R., "A cantilever sensor with an integrated optical readout for detection of enzymatically produced homocysteine," IEEE Transactions on Biomedical Circuits and Systems 3, 415-423 (2009).

[79] Barrios, C.A. "Ultrasensitive nanomechanical photonic sensor based on horizontal slot-waveguide resonator." IEEE Phot. Tech. Lett. 18, 2419–2421 (2008).

[80] Ziegler. C., "Cantilever based biosensors," Anal. Bioanal. Chem. 379, 946-959 (2004).

[81] Wanekaya, A. K., Chen, W., Myung, N. V., and Mulchandani, A., "Nanowire-based electrochemical biosensors," Electroanalysis 18, 533-560 (2006).

[82] He, B., Morrow, T. J., and Keatin, C. D., "Nanowire sensors for multiplexed detection of biomolecules," Current. Opinion Chem. Bio. 12, 522-528 (2008).

[83] Zhang, G. –J., Zhang, L., Huang, M. J., Luo, Z. H. H., Tay, G. K. I., Lim, E -J. A., Kang, T. G., and Chen, Y., "Silicon nanowire biosensor for highly sensitive and rapid detection of Dengue virus," Sens. Act. B. 146, 138-144 (2010).

[84] Berdondini, L., Imfeld, K., Maccione, A., Tedesco, M., Neukom, S., Koudelka-Hep, M., and Martinoia, S., "Active pixel sensor array for high spatio-temporal resolution electrophysiological recordings from single cell to large scale neuronal networks," Lab Chip 9, 2644-2651 (2009).

[85] Lee, C. –S., Baker, S. E., Marcus, M. S., Yang, W., Eriksson, M. A., and Hamers, R. J., "Electrically addressable biomolecular functionalization of carbon nanotube and carbon nanofiber electrodes," Nano Lett. 4, 1713-1716 (2004).

Chapter 3

Slotted Photonic Crystals

3.1 Introduction

All of the biosensor devices featured within this work are based on slotted photonic crystals. Much early work [1-3] within this area was carried out by Dr Andrea Di Falco in our group. This thesis therefore builds on Dr Di Falco's early work, demonstrating that this and other new devices based on slotted photonic crystals are capable of target-specific biosensing when combined with microfluidics and functionalization. A number of problems had to be overcome to make this a reality, and many new devices and ideas were generated, all of which will be covered in due course within this thesis. As this device is a combination of two structures, namely a slot waveguide and a photonic crystal, it is best to first consider some background detail behind each separately, to understand fully its principle of operation.

3.2 Slot Waveguides

First proposed in 2004 by Michal Lipson's group at Cornell University, slot waveguides [4] have seen much interest in a number of applications due to their unusual optical properties. They allow strong spatial confinement of light within a narrow air slot inside a material of high refractive index. Standard optical waveguide designs rely on total internal reflection as a means of guiding and confining light. This phenomenon requires that the medium cladding the waveguide be of lower refractive index than the waveguide itself. The case of the slot waveguide, where light is confined inside a lower refractive index medium, therefore seems a bit strange. This can be explained, however, by the imperfect spatial confinement of light by total internal reflection.

Light incident on a boundary between two non-absorbing dielectrics of permittivity ε_1 and ε_2 experiences a combination of transmission and reflection effects. The Maxwell boundary conditions require that the tangential components of the electric field **E** and the magnetic field **H**, and the normal components of the electric flux density **D** and the magnetic flux density **B**, be continuous across the boundary in order to satisfy conservation of energy. As $\mathbf{D}=\varepsilon\mathbf{E}$, the boundary condition for the electric flux density can be expressed in the form [5]:

$$\left[\varepsilon_1\mathbf{E}_{i0} + \varepsilon_1\mathbf{E}_{r0} - \varepsilon_2\mathbf{E}_{t0}\right]\cdot\hat{\mathbf{n}} = 0 \qquad (3.1)$$

Where $\hat{\mathbf{n}}$ is a unit vector normal to the boundary, the 0 subscript refers to the maximum value, and the *i*, *r* and *t* subscripts refer to the incident, reflected and transmitted fields respectively.

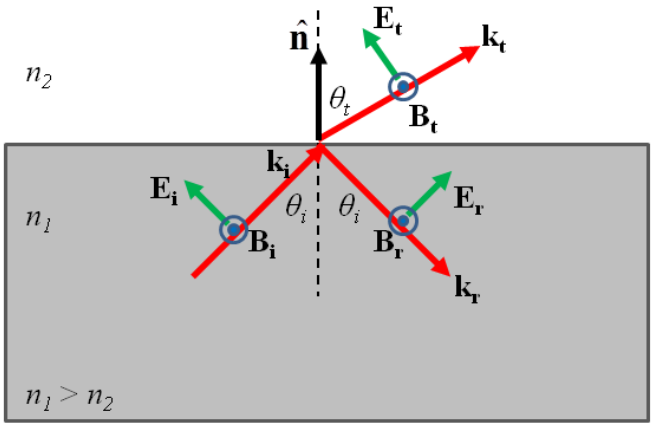

Figure 3.1: Transmission and reflection of light at interface between two dielectrics. Polarisation parallel to the plane of incidence.

In the case of the electric field being parallel to the plane of incidence (see Fig 3.1), eqn (3.1) becomes:

$$n_1^2\left(E_{i0}-E_{r0}\right)\cos\theta_i - n_2^2 E_{t0}\cos\theta_t = 0 \tag{3.2}$$

Where $n=\sqrt{\varepsilon}$ (for a dielectric) is the refractive index of the medium. Considering only the normal components ($E\cos\theta$), eqn (3.2) becomes:

$$\frac{E_{tn}}{E_{in}-E_{rn}} = \frac{n_1^2}{n_2^2} \tag{3.3}$$

The normal component of the electric field just inside n_2 (the low index) is therefore larger than that just inside n_1 (the high index) by a factor of n_1^2/n_2^2.

For total internal reflection, the transmitted angle in Snell's Law becomes complex in nature, with a purely imaginary cosine angle, and the transmitted wave propagates only along the interface [5]. The purely imaginary nature of the normal component (i.e. the cosine angle) of the transmitted field means that it decays exponentially from the maximum value in eqn (3.3) into the cladding from the boundary. This field is said to be **evanescent** in nature. High refractive index contrast boundaries can result in quite a large discontinuity in the normal

component of the electric field inside the low index medium, for example at an air/silicon interface, the discontinuity immediately inside the air would be almost a factor of 12 greater [4].

Consider therefore a standard ridge waveguide fabricated in silicon and surrounded by air. As light propagates along the waveguide, a large discontinuity in field will also propagate through the air close to the waveguide walls. Many of the devices discussed in Chapter 2 utilise this evanescent tail for sensing purposes. Light guided along a ring resonator, for example, will penetrate a short distance from the guiding medium into the surrounding cladding medium. If the refractive index changes in this cladding, for example, due to binding of biomolecules on the ring's surface, this will translate to a change in phase which will in turn alter the resonance of the ring.

If we now consider two optical waveguides close enough that these field discontinuities can interact, which necessitates their separation to be within the decay length of the evanescent field, then these two discontinuities can combine and be enhanced within the narrow air region separating them. Two closely spaced waveguides, or equivalently a narrow slot in a single waveguide, can therefore form a mode of propagation in which most of the light intensity is contained within the low refractive index region, even though total internal reflection is used for guiding. The sharp evanescently decaying discontinuities at each slot wall combine to produce high levels of field inside the air slot. This is the basis behind the operation of slot waveguides [4].

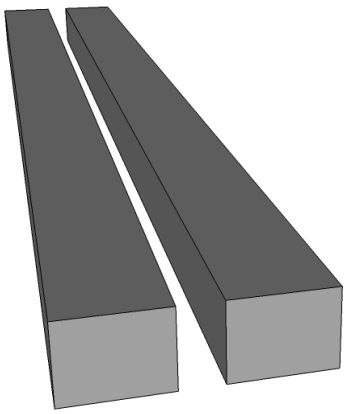

Figure 3.2: Slot waveguide geometry. A narrow air slot is introduced into a ridge waveguide. Alternatively, this can be viewed as two separate waveguides separated by a small region of air. Light is guided mostly in air.

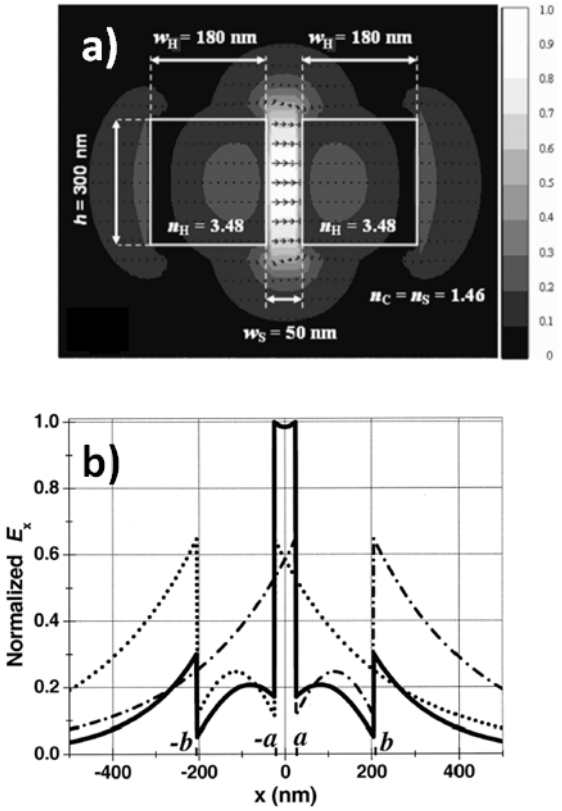

Figure 3.3: (a) Field enhancement inside slot waveguide, showing transverse E-field of quasi-TE mode. (b) Individual and combined normalized transverse E-field of TM modes of each waveguide separated by slot (both reproduced with permission of the Optical Society of America from [4], Copyright 2004).

The enhanced light confinement to low refractive index media offered by these structures has led to their use in a number of applications. Biosensor and optical traps have been discussed in Chapter 2. Slots have also been explored for light sources. Lipson's group propose a silicon slot ring resonator infiltrated with erbium doped silica as a potential light source [6, 7]. Slots have also found use in quantum optics applications [8]. The principles behind them have also been suggested as part of an enhanced light absorbing thin film solar cell [9], optical modulators [10], nonlinear enhancement [11, 12] and for polarization splitters [13]. As will be seen in the following sections, combining the slot waveguide effect with photonic crystals can further enhance light confinement to regions of low refractive index.

3.3 Photonic Crystals

First proposed by Yablonivitch [14] and John [15], but with origins stretching back as far as Bragg and Rayleigh, photonic crystals have been the centre of much research in integrated optics due to the control of light they offer. In such structures light can be confined to high quality factor cavities, directed, split and even slowed down. Photonic crystals consist of periodic arrangements of material of different dielectric constant. The physics describing the behaviour of light within them is in many ways analogous to the behaviour of electrons in semiconductors. In both cases it is the periodicity of the structure that is most important: a periodic structure can only support certain wavelengths. In the case of semiconductors it is a periodic arrangement of atoms, and hence electric potential, that results in the formation of allowed electronic bands. Similarly, for photonic crystals the periodic arrangement of dielectric material results in the formation of allowed **photonic bands**. In its simplest form, the one-dimensional case, the photonic crystal is recognizable as a Bragg mirror.

In a Bragg mirror, the refractive index of the medium is alternated between two values in one direction. Reflections are produced at each interface between the two media. For layers of index n_1 and n_2, and of given thickness h_1 and h_2, these reflections can interfere such that a particular wavelength λ is strongly reflected from the mirror when satisfying the condition:

$$n_1 h_1 + n_2 h_2 = m\frac{\lambda}{2} \tag{3.4}$$

known as the **Bragg condition**, where m is an integer. The main point is that the periodicity of the layers must be an integer number of half-wavelengths for strong reflection. The result of this is a **stopband** of frequencies which cannot propagate through the structure, the effect being maximised when both layers are a quarter-wavelength thick. This effect is highly wavelength specific, unlike Fresnel reflection which is also present. The balance between these two effects, Bragg and Fresnel reflection, influences the width of the stopband: the dominant effect being determined by the refractive index contrast.

Two dimensional photonic crystals [16] have a varying dielectric function in two directions. They are typically created using a triangular or square lattice of air or silica filled holes in a semiconductor medium such as silicon or gallium arsenide. The photonic crystals used within this thesis all use a 2-D triangular lattice of air holes in a silicon membrane. Note that the physics of a planar 2-D photonic crystal slab differs slightly from that of a purely 2-D photonic crystal due to their finite height.

When waves move through a periodic structure they scatter and interfere with themselves. When the Bragg condition is met, interference from this scattering results in diffraction of the wave, causing it to be sent out of the structure. Outside of this condition, those waves which can be physically supported by the periodic structure, and continue to propagate through it, are known as **Bloch waves**. Bloch waves consist of plane waves modulated by a periodic envelope function $\boldsymbol{u_{kn}}$ which is related to the lattice of the periodic structure by [17]:

$$\mathbf{H}_{kn}(\mathbf{r}) = \mathbf{u}_{kn}(\mathbf{r})e^{i\mathbf{k}\cdot\mathbf{r}} \tag{3.5}$$

Where **H** is the magnetic field, **k** a wavevector and **r** a unit directional vector. All allowable modes in a photonic crystal can be written in Bloch mode form. As they are harmonic in nature, a fundamental set of k vector values that make up the **Brillouin zone** (as in solid state physics) can be used to construct all possible modes. Mirror symmetry results in these being classified into Transverse Electric (TE) and Transverse Magnetic (TM) modes, which can be further subdivided into odd and even modes due to their orthogonal geometry [17]. Like the electrons in a semiconductor, photons in a photonic crystal can be thought to occupy certain energy bands corresponding to allowed modes of propagation in the crystal lattice. Two continuums of modes, one corresponding to air (or low index) and the other to dielectric (or high index) guided modes, are separated by a bandgap region. Those frequencies which satisfy the Bragg condition lie within this **photonic bandgap** region, and are forbidden to propagate through the lattice. Like the 1-D Bragg mirror, 2D photonic crystals can be thought of as very efficient wavelength dependent mirrors, with frequencies within the bandgap being strongly reflected. The strong wavelength dependence of these 'mirrors' give the photonic crystal its key functionality. Carving defects into the periodic lattice, for example by removing holes, allows defect states to be created within the photonic bandgap. The lattice surrounding the defect still acts as a mirror for these frequencies, thus frequencies which would normally be rejected can be confined to and guided by defect states within the photonic crystal.

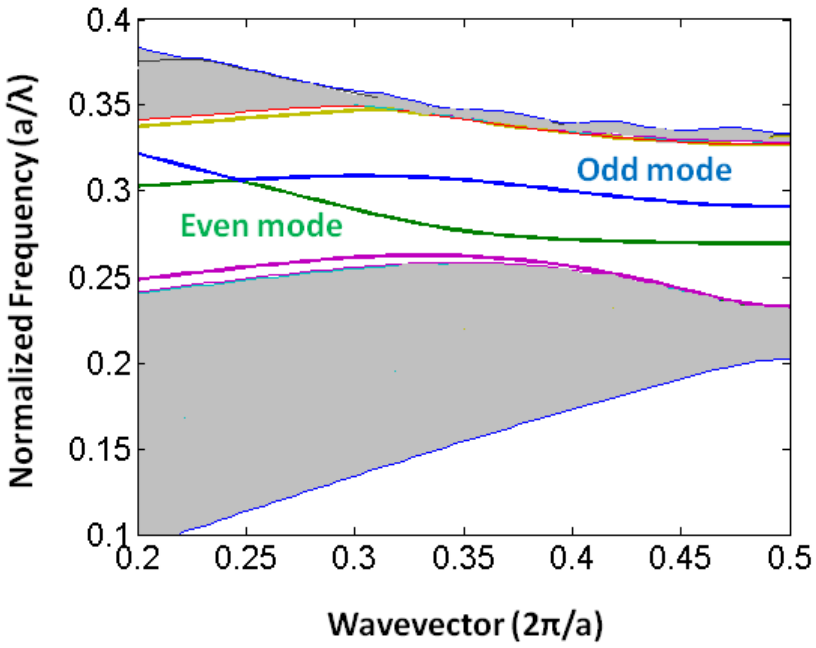

Figure 3.4: Photonic band diagram of 2D photonic crystal with W1 defect. Even and odd defect guided modes shown.

One of the most common defects is to remove a single row of holes within the crystal, creating a **W1** waveguide. This creates the defect modes shown within the photonic bandstructure depicted in Fig 3.4. Forbidden frequencies can be guided in plane through the crystal by this defect; an example of guiding light via photonic bandgap effects. In the case of 2-D slab photonic crystals, light confinement out-of-plane is provided by total internal reflection.

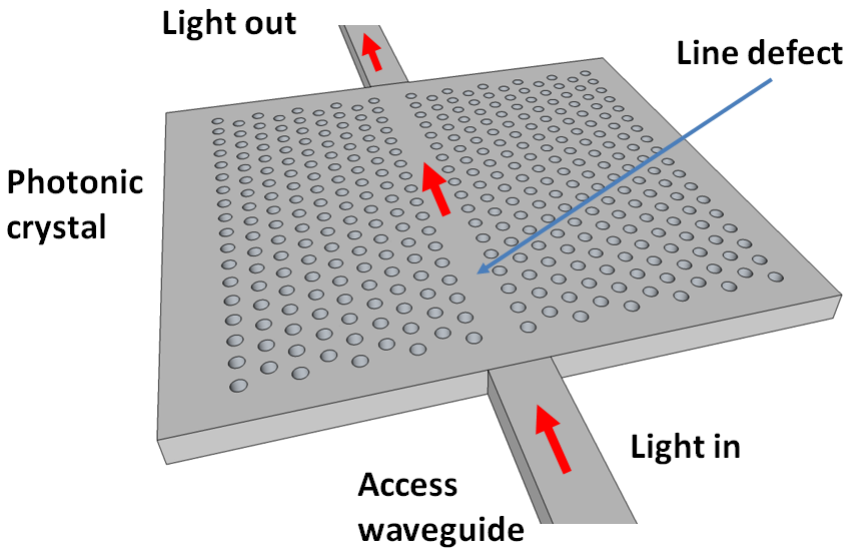

Figure 3.5: Schematic of a 2-D slab photonic crystal with a W1 defect. Light is delivered to and from a photonic crystal via access waveguides. Defect consists of single row of holes being removed, which allows normally forbidden frequencies to exist within the crystal. Holes on either side of line defect behave as very efficient mirrors for forbidden frequencies, and thus can be used to guide light.

When more localized defects are utilized, **cavities** with high quality factor can be created. In this case a single allowed state is created within the bandgap rather than the extended defect of the W1. Several cavity designs exist, two of the most simple being the **H0** (the removal of a single hole) or the **L3** (removal of three holes) type cavities. These can be optimized by adjusting the size and position of holes surrounding the defects. Two of the highest quality factor cavities are that of the **local width modulated** [18] cavity and the **heterostructure** [19] cavity. In the width modulated case, quality factors in excess of 1 million can be achieved by locally shifting a few holes outwards from a W1 (or other) line defect [20]. In the case of the heterostructure, the lattice period is locally increased around a few periods of a W1, also producing quality factors in excess of 1 million [21]. In both cases, a resonance forbidden in the lattice is introduced by locally reducing the amount of air (i.e. reducing the frequency) around a defect.

In addition to cavities, photonic crystals can employ another method of temporal confinement, known as **slow light** [22, 23]. In this case the dispersion curve of a line defect mode can be tailored through structural (rather than material) changes. Shifting the innermost rows of holes parallel to the W1 pulls up or down one part of the dispersion curve, whilst shifting those of the second closest rows pulls another. With careful design a region of constant, high group index

can be realized over a certain bandwidth by engineering the gradient of the dispersion curve to be relatively flat. The bandwidth of this region is inversely proportional to the required delay [23]. Whilst the same result can be obtained by altering the radii of the holes, from a fabrication point of view it is easier to accurately control different positions of holes [24]. Physically, slow light behaviour results from coherent backscattering at each unit cell of the photonic crystal forming slow moving interference patterns within the waveguide [25]. Engineering the dispersion curve of the waveguide allows these resonances to be tuned over a certain bandwidth. Structural slow light can therefore be viewed as a sort of extended cavity. The main advantage of slow light is that the slowing of a light results in pulse length compression, which in turn leads to higher intensity and increased light-matter interactions. In other words, the slow light effect makes a shorter photonic crystal waveguide comparable to a longer structure operating in the normal fast light regime. The downside is that higher propagation losses are also present due to the higher intensities enhancing scattering processes [25]; though through careful design the benefits can outweigh these problems, which can be exploited in applications such as nonlinear optics, optical memories and sensing [23]. Compared to cavities, slow light offers more bandwidth but typically a lower field enhancement.

3.4 Slotted Photonic Crystals

Slotted photonic crystals combine the advantages of spatial confinement of light in air provided by slot waveguides, and the temporal confinement of light provided by photonic crystals, in a single structure. This is advantageous for applications such as sensing (as discussed in the previous chapter) and optical modulators [26-28], because most of the light interacts with the contents of the slot. Simply, a slotted photonic crystal can be viewed as an air slot defect within the guiding region of a standard W1 photonic crystal as shown in Fig 3.6. Early work in this area [1, 2] has shown, however, that the optical properties of slotted photonic crystals are very different to that of the W1.

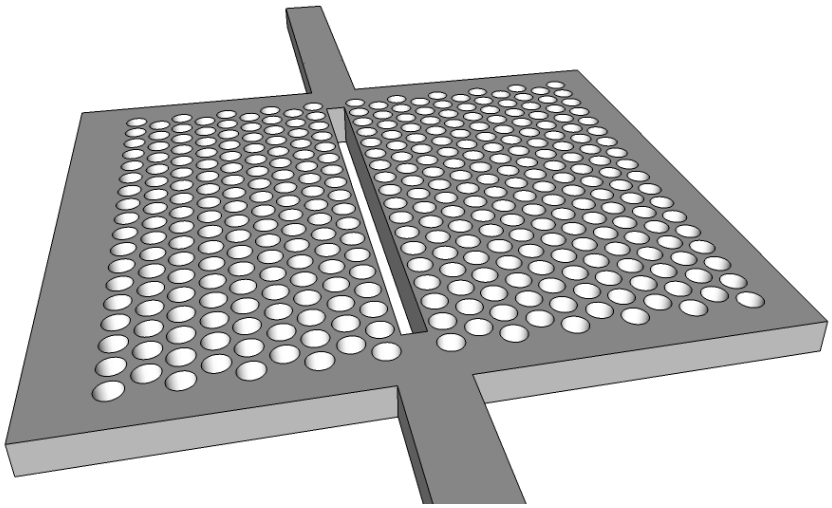

Figure 3.6: Sketch of slotted photonic crystal geometry. Slot waveguide defect introduced to guiding region of W1 photonic crystal.

A slotted photonic crystal pulls a defect mode up from the dielectric band [1], rather than down from the air band as is the case for the W1, as shown in the typical band diagram of Fig 3.7. Comparing Fig 3.7 with Fig 3.4, it is evident that the fundamental modes of the W1 and the modes of slotted photonic crystals have gradients of opposite sign. As will be seen in the next chapter, this introduces problems associated with efficiently coupling light into the structure. The cut-off of the mode is observed at high frequency, rather than the low frequency of the W1 case, and is also strongly dependent on the width of the slot [2]. Several cavity designs have been explored for slotted photonic crystals, including heterostructure [3, 29], local line width modulated [30, 31], L3 like [32], and a varying slot width [33] approach amongst others [34-36]. In the case of the heterostructure [3], the lattice is locally compressed, rather than the normal expansion [19], due to the defect coming from the dielectric band (this will be explored further in Chapter 6). In addition to cavities, line defects have also been investigated, for example to realise slow light as detailed in Section 3.3. Several different designs exist for slow light slotted photonic crystals such as corrugating the slot [37], or adjusting the position [38] or radii [27] of the first two rows of holes adjacent to the slot. Cavities and slow light increase the amount of time the light interacts with the contents of the slot. Combining this with the strong overlap provided by the slot architecture leads to a system that is optimized for many optical sensing applications.

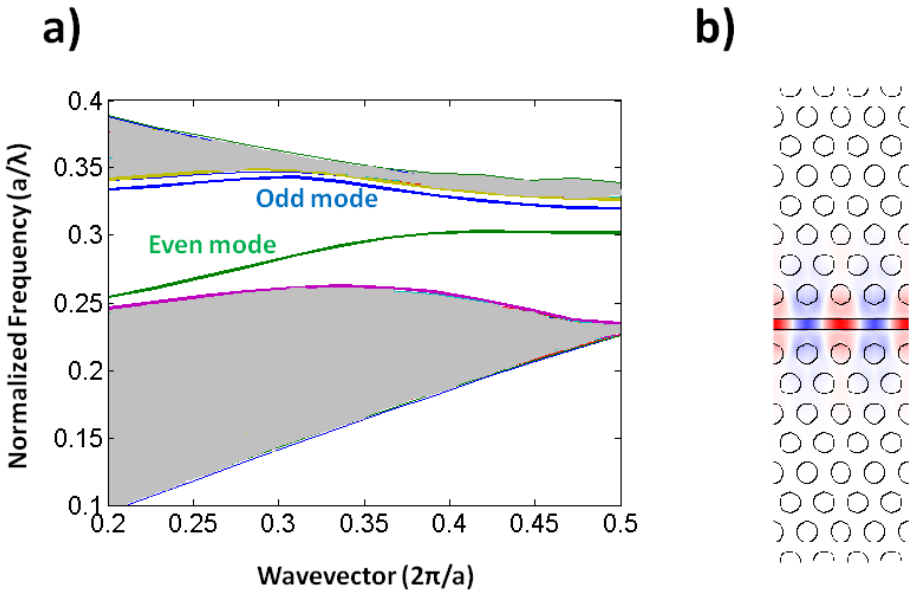

Figure 3.7: (a) Photonic band diagram of 2-D slot photonic crystal. (b) Mode profile.

3.5 Fabrication

Many different platforms exist for fabricating photonic crystals. All of the devices presented in this thesis were fabricated in Silicon-on-Insulator (SOI), which consists of a 220 nm top layer of silicon, below which there is a 2 µm layer of silica separating it from a bulk silicon substrate. I fabricated the structures inside a class 10,000 cleanroom using the protocol outlined below. I performed all steps. A basic overview of this procedure is expressed in Fig 3.8.

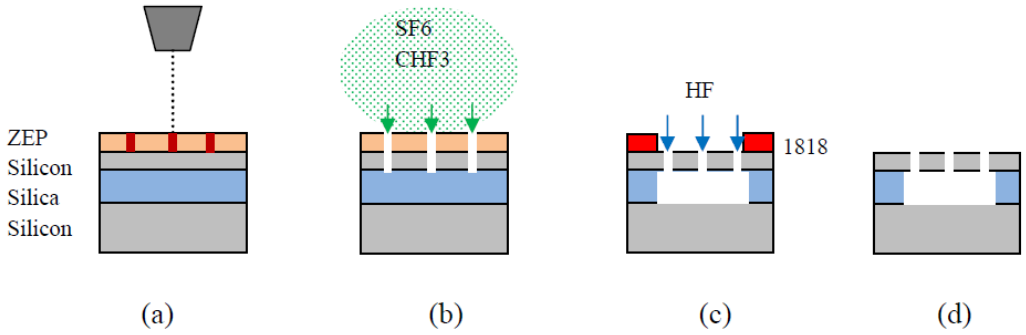

Figure 3.8: Photonic crystal membrane fabrication steps. (a) ZEP e-beam resist coated SOI substrate exposed to electrons in electron beam writer. (b) Sample developed exposing surface in pattern of design. Silicon etched using plasma of reactive ions. (c) Silica under photonic crystals removed using hydrofluoric acid through an S1818 photoresist patterned window. (d) S1818 removed and final membrane sample cleaved.

File preparation

Files corresponding to the desired photonic crystal design were prepared in Elphy CAD. The designs were then processed by a proximity error correction script, which calculates the dose factor of each feature taking into account potential overexposure due to other closely spaced features.

E-beam resist preparation

Small squares of SOI (typically of side 1-2cm) were cleaved from a bulk wafer using a diamond tipped scribe. These were cleaned separately in both acetone and isopropanol (IPA) filled beakers inside an ultrasonic bath at full power. Samples were then removed from the beaker using plastic tweezers and dried under a stream of nitrogen gas. Following cleaning, a sample was spun at 3500 r.p.m for 1 min with ZEP e-beam resist inside a spinner. The chemical properties of this resist alter when exposed to a beam of electrons (or UV light). The thickness of the resist was checked by a Dektak surface profiler. After checking the surface for any contamination spots, the sample was baked at 180 °C inside a hotplate for 10 min, before placing it inside a black carbon bag to prevent exposure to UV light.

Electron beam lithography

Patterns corresponding to the photonic crystal design can be created in the resist using electron beam (e-beam) lithography. The resist coated sample was scratched deliberately in the corner, fixed on a stage using pins and loaded into an e-beam writer (Raith, 30 kV). After pumping the chamber down to vacuum, the scratch on the surface was used as a reference for coarse focusing of the electron beam for the desired aperture. Spots at 50,000x and 80,000x magnification were then burned to aid in the correction of the fine focus and stigmation. After correcting the writefield and loading the desired position list of files, the beam writing procedure was performed. Table 3.1 below shows typical parameters I used for writing the slotted photonic crystals.

Table 3.1: Typical e-beam parameters.

Structure	EHT (kV)	Aperture (μm)	Writefield (μm)	Area Dose (μAs/cm^2)	Step Size (μm)	Dose Factor
Photonic crystal	30	10	100	52	0.02	1
Slot	30	10	100	52	0.02	2-8
Access waveguide	30	30	100	52	0.1	1.8
Tapered waveguide	30	10	100	52	0.02	1

Development

After completion of the exposure, the sample was unloaded from the e-beam and taken to the cleanroom for development. This step removes resist from the sample that was exposed by the electron beam, exposing the silicon surface in the desired pattern. A beaker of xylene was heated to 23 °C (checked with thermometer probe) on a hotplate. After placing the sample into the xylene, the beaker was transferred to an ultrasonic bath at 10% strength for 30 s. The beaker was removed from the ultrasonic bath, and the sample removed to a beaker of IPA after a total of 45 s inside the xylene to stop development. The developed sample was then dried in nitrogen and checked under a microscope. Dose test squares were used to check the progress of the development.

Reactive ion etching

To transfer the photonic crystal pattern of the resist into the silicon I used a dry etching step. Following development, the sample was loaded into a custom built reactive ion etching (RIE) device, and the chamber pumped down to vacuum. The chamber was then filled with a 1 : 1 blend of CHF_3 and SF_6 gases, and adjusted to the correct pressure using a butterfly valve and gas flow controllers. To ensure stability, this mixture was pre-conditioned for 10 min. The sample was then etched by striking a plasma in the chamber. Ions created in this plasma directionally etch through the top silicon layer exposed through the photoresist. A typical etch recipe for SOI is presented in Table 3.2.

Table 3.2: Typical RIE parameters.

Gases (flow rate)	Power (W)	Base Pressure (mBar)	Etch Pressure (mBar)	Etch Time (s)
CHF_3 (100) + SF_6 (100)	21	$3x10^{-6}$	$5.9x10^{-2}$	110

Resist removal

To remove the ZEP e-beam resist after etching, the sample was flood exposed to UV light in a Karl Suss mask aligner for 5 min and then cleaned in a beaker of trichloroethylene in an ultrasonic bath for 1 min. Following this I rinsed it in acetone and IPA in the ultrasonic bath. The cycle of trichloroethylene, acetone and IPA was repeated. To ensure full resist removal, a **piranha** solution was then used. This is composed of 1 part hydrogen peroxide (H_2O_2) to 3 parts sulphuric acid (H_2SO_4). Extreme care must be taken as this solution can explode when brought into contact with any bases. The sample was immersed in this solution for 5 min (using metal tweezers for moving), before rinsing in deionised water (DI).

Photolithography

To remove the silica underneath the top layer silicon, and thus make a suspended membrane structure, a mask must be first made so that only the photonic crystals are membraned and not the whole substrate (as it would be liable to collapse). To do this the sample was again cleaned in acetone and IPA following the DI water rinse of the previous step. After drying in nitrogen gas, I spun S1818 photoresist on the sample at 5000 r.p.m. for 1 min in a spinner, and baked on a hotplate at 100 °C for 2 min. The baked sample was then loaded into a Karl Suss mask aligner with a photomask of linewidth corresponding to slightly less than the length of the photonic crystals. The mask was aligned to the photonic crystals on the sample using the micrometer screws on the mask aligner. After alignment, the sample was exposed to UV light for 40 s. It was then removed and developed in MF 319 developer for 35 s, and rinsed in DI. The final result was that only the photonic crystals were not covered by resist.

HF acid silica removal

To remove the silica underneath the crystals, I used hydrofluoric acid (HF), as this etches through oxides. A solution of 1 part HF acid (49% conc.) to 5 parts DI was made up in a plastic beaker. Extreme caution must be exercised, as HF acid can be fatal if mishandled. Special resistant gloves were worn along with apron and safety glasses on top of the usual cleanroom attire, and danger signs displayed. A large beaker of DI water and HF antidote gel were also kept nearby in case of spills. The sample was immersed in this solution for 15-20 min, before removal using plastic tweezers into a beaker of DI. The resist was then removed using acetone and IPA (**no ultrasonic**), followed by a piranha clean if necessary.

Cleaving

The membrane sample was then cleaved with aid from a diamond tipped scribe pen so that the edge facets intersect the access waveguides used to guide light to and from the photonic crystals. Following cleaving, the sample was rinsed in acetone and IPA, and dried in nitrogen gas.

SEM analysis

The final structures were examined using a Hitachi scanning electron microscope (SEM). The samples were fixed to stubs using double-sided carbon tape and loaded into the SEM through the vacuum interlock chamber. Features were first identified using the low magnification setting. Images were taken at high magnification after correcting focus and stigmation. An example of an image I took is shown in Fig 3.9.

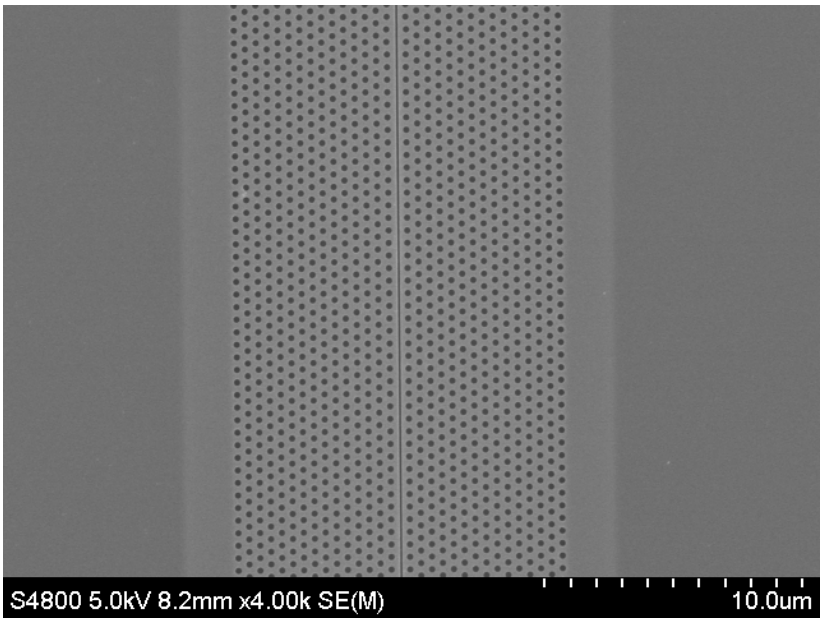

Figure 3.9: SEM image of slotted photonic crystal fabricated in SOI.

3.6 Optical Characterization

I characterized the optical behaviour of each sample using a simple endfire transmission setup as shown in Fig 3.10. Light from a single mode fibre coupled to a broadband ASE (Amplified Spontaneous Emission) source (1520-1620 nm, 50 mW) was collected and collimated by an aspheric lens and sent through free space, through a polarisation beam splitter cube (TE polarisation), to a 60x lens. The spot from this lens was focused onto an access waveguide on the edge facet of the SOI. This was checked from top using an infrared camera with a 20x objective; the sample being illuminated by a white light source. Light passing through the sample to the back facet was then collected and collimated by a 40x times lens, and sent through free space to a focusing aspheric lens onto the facet of a single mode fibre. This light was then split using a splitter fibre, with one arm going to a photodetector, the other to an optical spectrum analyser (OSA). After achieving best possible alignment by moving the lens mounts by micrometer screw and using the camera and the voltage from the photodetector as a reference, measurements of the transmission spectrum were taken with the OSA.

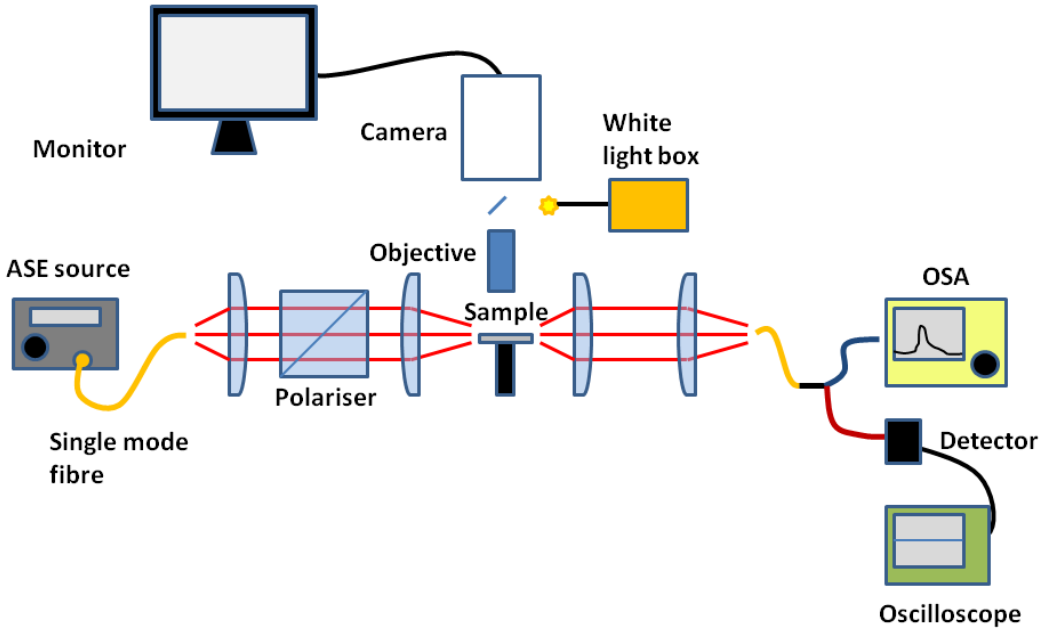

Figure 3.10: Optical endfire setup for transmission measurements. TE polarised light from broadband ASE source focused onto sample edge facet using aspheric lenses. Light collected from back facet split between OSA and photodetector. Sample observed from above using microscope objective and IR camera. Alignment optimized using photodetector signal and camera as reference.

In the case of slow light measurements a modified version of this setup was used based on a Mach-Zehnder interferometer as shown in Fig 3.11. In this case, light from the ASE was split into two arms, one arm being the same as before, the other a simple reference. Light from both arms was combined before being sent to the OSA. The length of the reference arm was reduced until there were approximately 10 fringes per nm. For every waveguide three measurements were taken: transmission from each arm alone and the interference of the two. In the case of a

single arm, the other was blocked accordingly. In the slow light regime, the fringe spacing becomes compressed due to the group delay between each arm increasing.

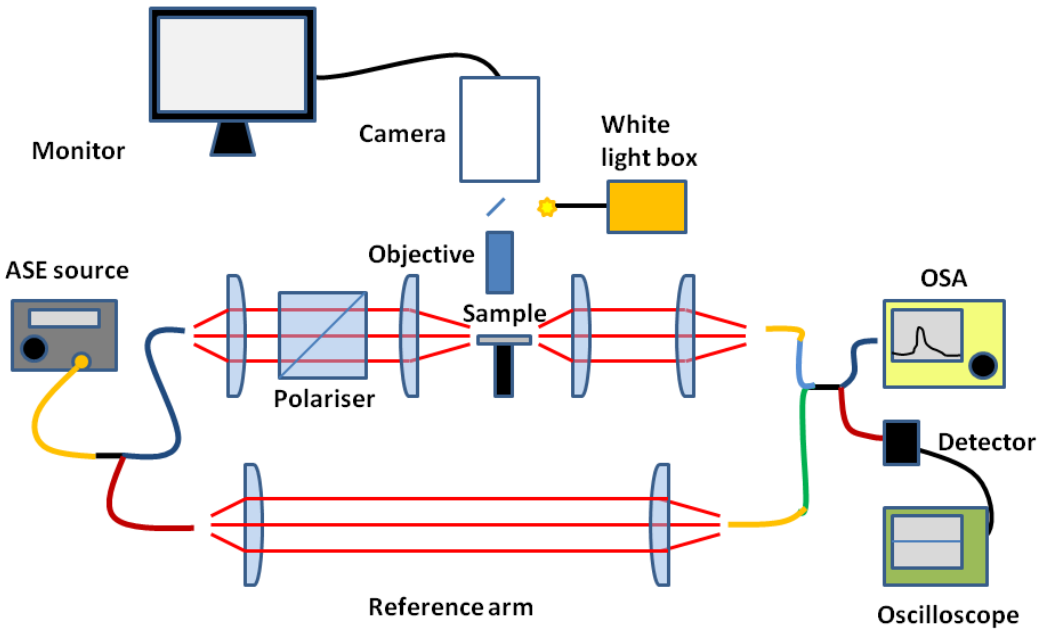

Figure 3.11: Optical setup for slow light measurements based on a Mach-Zehnder interferometer. A reference arm is introduced to the basic transmission setup. Group delay can be extracted from measurements of each arm individually and the interference of the two.

To calculate values for the group index the spectra from each measurement are analysed. The spectral density of an interferogram *I(ω)* is based on the spectral densities of the sample arm *S(ω)* and the reference arm *R(ω)* by the relation [39]:

$$I(\omega) = S(\omega) + R(\omega) + \sqrt{S(\omega)R(\omega)}\left(\exp\left[i\Phi(\omega) - i\omega\tau\right] + c.c.\right) \tag{3.6}$$

Where c.c. refers to complex conjugates, ω is the frequency, τ is the delay and [39]:

$$\Phi = \phi_S - \phi_R \tag{3.7}$$

is the phase difference between the sample, ϕ_S, and reference, ϕ_R, arms. The three terms in eqn (3.6) can be recovered from the Fourier transform of the interferogram: the first two from the

transmission of each separate arm, the third from the interference of both. Corresponding measurements were also taken from a reference channel waveguide. The third term in eqn (3.6) is used to extract Φ. The difference in group delay $\Delta\tau_g$ in each arm for both sample and reference channel waveguide is found by differentiating $\Phi(\omega) - \omega\tau$ with respect to frequency, and using the equation [39]:

$$n_g = \frac{(\Delta\tau_g^{PhC} - \Delta\tau_g^{ref})c}{L} + n_{ref} \tag{3.8}$$

Where L is the length and n_{ref} is the effective index of the reference waveguide, c is the speed of light, and n_g the group index. From this analysis, the group index of the photonic crystal can be found as a function of wavelength.

References – Chapter 3

[1] Di Falco, A., O'Faolain, L. and Krauss, T. F., "Photonic crystal slotted slab waveguides," Phot. Nano. Fun. Appl. 6, 38-41 (2008).

[2] Di Falco, A., O'Faolain, L. and Krauss, T. F., "Dispersion control and slow light in slotted photonic crystal waveguides," Appl. Phys. Lett. 92, 083501 (2008).

[3] Di Falco, A., O'Faolain, L. and Krauss, T. F., "Chemical sensing in slotted photonic crystal heterostructure cavities," Appl. Phys. Lett. 94, 063503 (2009).

[4] Almeida, V. R., Xu, Q., Barrios, C. A. and Lipson, M., "Guiding and confining light in void nanostructure," Opt. Lett. 29, 1209-1211 (2004).

[5] Jackson, J. D., [Classical Electrodynamics, 3rd Edition, Chp. 7], John Wiley & Sons, New York (1999).

[6] Barrios, C. A. and Lipson, M., "Electrically driven silicon resonant light emitting device based on slot-waveguide," Opt. Exp. 13, 10092-10101 (2005).

[7] Preston, K. and Lipson, M., "Slot waveguides with polycrystalline silicon for electrical injection," Opt. Exp. 17, 1527-1534 (2009).

[8] Hiscocks, M. P., Su, C. –H., Gibson, B. C., Greentree, A. D., Hollenberg, L. C. L., and Ladouceur, F., "Slot-waveguide cavities for optical quantum information applications," Opt. Exp. 17, 7295-7303 (2009).

[9] Yu, Z., Raman, A., and Fan, S., "Fundamental limit of nanophotonic light trapping in solar cells," PNAS 107, 17491-17496 (2010).

[10] Koos, C., Vorreau, P., Vallaitis, T., Dumon, P., Bogaerts, W., Baets, R., Esembeson, B., Biaggio, I., Michinobu, T., Diederich, F., Freude, W., and Leuthold, J., "All-optical high-speed signal processing with silicon-organic hybrid slot waveguides," Nature Phot. 3, 216-219 (2009).

[11] Di Falco, A., Conti, C., and Assanto, G., “Quadratic phase matching in slot waveguides,” Opt. Lett. 31, 3146-3148 (2006).

[12] Trita, A., Lacava, C., Minzioni, P., Colonna, J. –P., Gautier, P., Fedeli, J. –M., and Cristiani, I., “Ultra-high four wave mixing efficiency in slot waveguides with silicon nanocrystals,” Appl. Phys. Lett. 99, 191105 (2011).

[13] Lin, S., Hu, J., and Crozier, K. B., “Ultracompact, broadband slot waveguide polarization splitter,” Appl. Phys. Lett. 98, 151101 (2011).

[14] Yablonovitch, E., “Inhibited spontaneous emission in solid-state physics and electronics,” Phys. Rev. Lett. 58, 2059-2062 (1987).

[15] John, S., “Strong localization of photons in certain disordered dielectric superlattices,” Phys. Rev. Lett., 58, 2486-2489 (1987).

[16] Krauss, T. F., De La Rue, R. M., and Brand, S., “Two-dimensional photonic-bandgap structure operating at near-infrared wavelengths,” Nature 383, 699-702 (1996).

[17] Joannopoulos, J. D., Johnson, S. G., Winn, J. N., and Meade, R. D., [Photonic Crystals: Molding the Flow of Light, 2nd Edition], Princeton University Press, New Jersey, (2008).

[18] Kuramochi, E., Notomi, M., Mitsugi, S., Sinya, A. and Tanabe, T., “Ultrahigh-Q photonic crystal nanocavities realized by the local width modulation of a line defect,” Appl. Phys. Lett. 88, 041112 (2006).

[19] Song, B. –S., Noda, S., Asano, T. and Akahane, Y., “Ultra-high-Q photonic double-heterostructure nanocavity,” Nature Mat. 4, 207-210 (2005).

[20] Tanabe, T., Notomi, M., Kuramochi, E., Shinya, A., and Taniyama, H., “Trapping and delaying photons for one nanosecond in an ultrasmall high-Q photonic-crystal nanocavity,” Nature Phot. 1, 49-52 (2007).

[21] Takahashi, Y., Tanaka, Y., Hagino, H., Sugiya, T., Sato, Y., Asano, T., and Noda, S., “Design and demonstration of high-Q photonic heterostructure nanocavities suitable for integration,” Opt. Exp. 17, 18093-18102 (2009).

[22] Baba, T., “Slow light in photonic crystals,” Nature Phot., 2, 465-473 (2008).

[23] Krauss, T. F., “Why do we need slow light?,” Nature Phot. 2, 448-450 (2008).

[24] Li, J., White, T. P., O’Faolain, L., Gomez-Iglesias, A., and Krauss, T. F., “Systematic design of flat band slow light in photonic crystal waveguides. Opt. Exp. 16, 6227-6232 (2008).

[25] Krauss, T. F., “Slow light in photonic crystal waveguides,” J. Phys. D 40, 2666-2670 (2007).

[26] Chen, X., Chen, Y. –S., Zhao, Y., Jiang, W., and Chen, R. T., “Capacitor-embedded 0.54 pJ/bit silicon-slot photonic crystal waveguide modulator,” Opt. Lett. 34, 602-604 (2009).

[27] Brosi, J. –M, Koos, C., Andreani, L. C., Waldow, M., Leuthold, J. and Freude, W., "High-speed low-voltage electro-optic modulator with a polymer-infiltrated silicon photonic crystal waveguide," Opt. Exp. 16, 4177-4191 (2008).

[28] Wulbern, J. H., Hampe, J., Petrov, A., Eich, M., Luo, J., Jen, A. K. –Y., Di Falco, A., Krauss, T. F., and Bruns, J., "Electro-optic modulation in slotted resonant photonic crystal heterostructures," Appl. Phys. Lett. 94, 241107 (2009).

[29] Kwon, S. -H., Sunner, T., Kamp, M. and Forchel, A., "Optimization of photonic crystal cavity for chemical sensing," Opt. Exp. 16, 11709-11717 (2008).

[30] Yamamoto T., Notomi, M., Taniyama, H., Kuramochi, E., Yoshikawa, Y., Torii, Y., and Kuga, T., "Design of a high-Q air-slot cavity based on a width-modulated line-defect in a photonic crystal slab," Opt. Exp. 16, 13809-13817 (2008).

[31] Gao, J., McMillan, J. F., Wu, M. –C., Zheng, J., Assefa, S., and Wong, C. W., "Demonstration of an air-slot mode-gap confined photonic crystal slab nanocavity with ultrasmall mode volumes," Appl. Phys. Lett. 96, 051123 (2010).

[32] Gao, J., Green, W. M., Vlasov, Y., Assefa, S., Yang, X., and Wong, C. W., "Demonstrations of an air-slot photonic crystal nanocavity with ultrasmall mode volumes for enhanced light-matter interactions," Conference on Lasers and Electro-optics, Baltimore, CFE5 (2009).

[33] Jagerska, J., Zhang, H., Diao, Z., Le Thomas, N. and Houdre, R., "Refractive index sensing with an air-slot photonic crystal nanocavity," Opt. Lett. 35, 2523-2525 (2010).

[34] Kita, S., Hachuda, S., Otsuka, S., Endo, T., Imai, Y., Nishijima, Y., Misawa, H. and Baba, T., "Super-sensitivity in label-free protein sensing using a nanoslot nanolaser," Opt. Exp. 19, 17683-17690 (2011).

[35] Lee, M. R., Miller, B. L. and Fauchet, P. M., "Two-dimensional photonic crystal slot microcavity sensor for virus-sized particle detection," Integrated Photonics and Nanophotonics Research and Applications Conference, Boston, Massachusetts (2008).

[36] Foubert, K., Lalouat, L., Cluzel, B., Picard, E., Peyrade, D., de Fornel, F., and Hadji, E., "An air-slotted nanoresonator relying on coupled high Q small V Fabry-Perot nanocavities," Appl. Phys. Lett. 94, 251111 (2009).

[37] Caer, C., Le Roux, X., Do, V. K., Marris-Morini, D., Izard, N., Vivien, L., Gao, D., and Cassan, E., "Dispersion engineering of wide slot photonic crystal waveguides by Bragg-like corrugation of the slot," IEEE Phot. Tech. Lett. 23, 1298-1300 (2011).

[38] Di Falco, A., O'Faolain, L., and Krauss, T. F., "Slotted photonic crystal devices: slow light and applications," Slow and Fast Light, Honolulu, STuC6 (2009).

[39] Gomez-Iglesias, A., O'Brien D., O'Faolain, L., Miller, A., and Krauss, T. F., "Direct measurement of the group index of photonic crystal waveguides via Fourier transform spectral interferometry," Appl. Phys. Lett. 90, 261107 (2007).

Chapter 4

Increased Coupling in Slotted Photonic Crystals

4.1 The Problem

4.1.1 Introduction

Whilst the unique optical properties of slotted photonic crystals are advantageous in many applications, this uniqueness also creates additional challenges for coupling light into these structures. As seen in the previous chapter, their modes have very different dispersive properties to those of a standard W1 photonic crystal waveguide; most notably, the gradient of their dispersion curve is of opposite sign. When these differing structures are coupled together, the group velocity mismatch (from the difference in sign) results in coupling into a backwards propagating mode, resulting in strong reflection at the interface. In addition, there is also a mismatch in the shape of the slotted photonic crystal mode compared to that of the ridge waveguides used to deliver light to them. To take full advantage of the slotted architecture, a suitable coupler must be found.

4.1.2 Solutions in the Literature

For regular slot waveguides, one typical solution to reduce mode shape mismatch is to use a sharply tapered ridge waveguide [1]. The same approach has been used for slotted photonic crystals, by firstly coupling the mode from ridge waveguide to slot waveguide via a taper, and then subsequently from slot waveguide to slotted photonic crystal [2]; the idea is sketched in Fig 4.1. Whilst this approach is relatively simple and goes some way to reducing the spatial mismatch of the modes, it introduces multiple interfaces (taper : slot and slot : slotted photonic crystal at both entry and exit) which all need to be optimized. For example, to optimize the slot : slotted photonic crystal interface, one needs to use a tapering of the hole position over several periods. More importantly, however, this design does not take into account the differences in dispersive properties introduced by the presence of the photonic crystal, in particular, the difference in group velocity sign.

Due to the periodicity of photonic crystals, all allowed optical modes can be constructed from the first Brillouin zone. This is the set of wavevectors lying between $-\pi/a$ and π/a within the band diagram. Above π/a, all modes are constructed from multiples of these fundamental wavevectors, thus secondary Brillouin zones and bandgaps exist due to periodicity. When waveguides are used to couple light into standard W1 photonic crystals, group velocity matching is ensured through coupling in the second Brillouin zone, where the two modes have the same sign of group index [3]. This is more difficult in the case of coupling between slot waveguides and slotted photonic crystals, as the fundamental modes have opposite sign in the second Brillouin zone. To ensure that they have the same sign, the effective index of the slot waveguide must be made low enough such that the two modes cross in the first Brillouin zone as shown in Fig 4.2, which depicts the results of MPB and corresponding FDTD (Finite Domain Time Difference) simulations I carried out. To achieve coupling to the fundamental slotted photonic crystal guided mode in the first Brillouin Zone, the rails of the slot waveguide must be

made narrow. Whilst this is technically possible, it puts limitations on the slot widths that can be used. From a practical point of view it also introduces problems in fabrication. As air slotted photonic crystals have to made in suspended membranes to maintain vertical symmetry, sharply terminated tapers have to be supported somehow, otherwise they are prone to collapse or misalign (see Fig 4.1(b)). The narrow rails add further to the fragility of the structure. One way to get around these problems is to couple to higher order slot modes, but such modes lack the high field concentration of the fundamental slot mode, which is the main reason for using the slotted geometry.

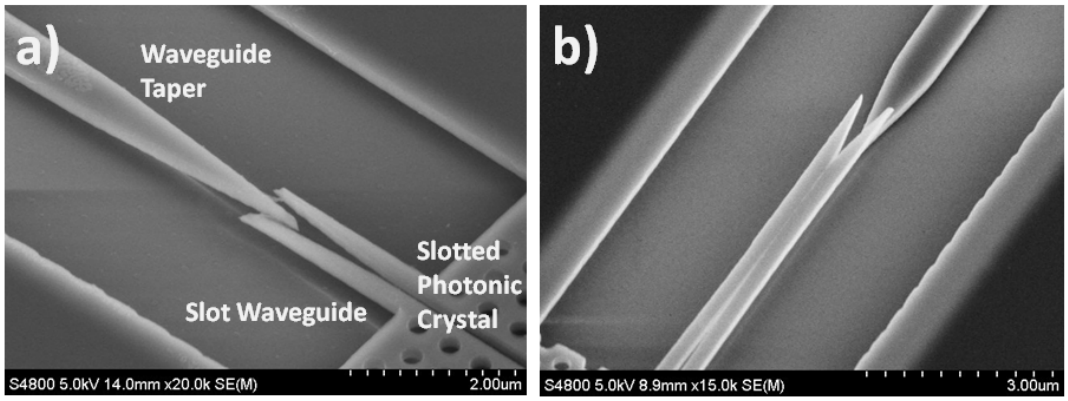

Figure 4.1: a) SEM image of taper based coupler for waveguide : slot waveguide : slotted photonic crystal interface. b) Collapsed taper when under-etched.

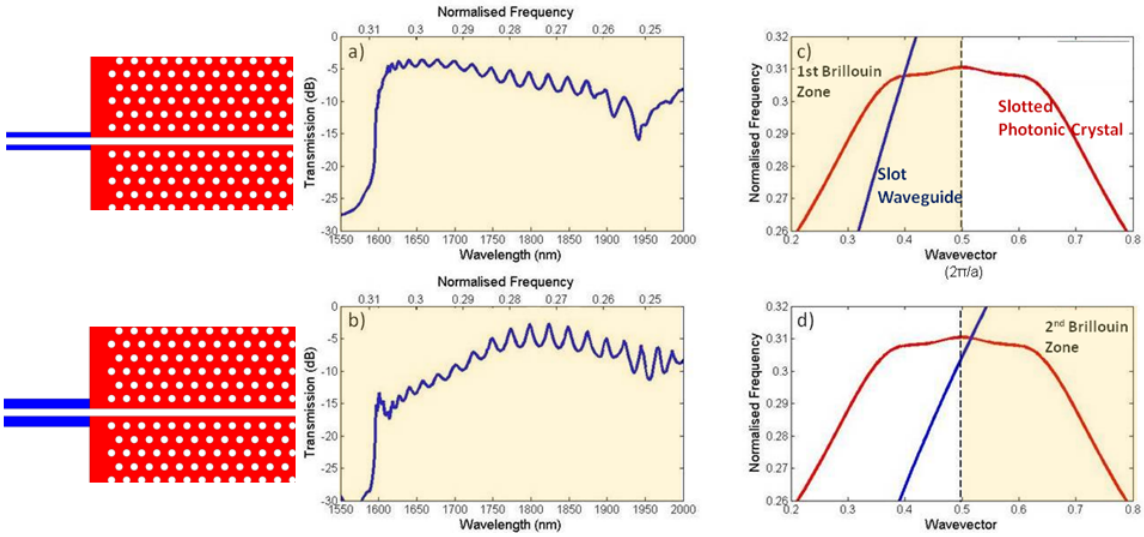

Figure 4.2: Coupling between slot waveguide and slotted photonic crystal. a) & c) Coupling in 1st Brillouin zone using narrow slot rails (196 nm wide) results in good transmission due to group velocity and phase matching. b) & d) Coupling in 2nd Brillouin zone using wide slot rails (294 nm wide) results in poor transmission due to group velocity mismatch.

Another coupling method suggested in the literature is to use multimode interference based structures [4]. In this case a standard input ridge waveguide is locally increased in width at the interface with the slotted photonic crystal. By adjusting the length of this region, the phase difference between the fundamental and second-order modes can be adjusted to give the best mode profile for coupling into the slotted photonic crystal. Whilst an enhancement of 20 dB in coupling was achieved [4], the bandwidth is limited (to about 35 nm). I therefore decided to investigate other potential solutions.

4.2 Resonant Coupler

4.2.1 Basic Principles for Standard Photonic Crystals

It has been shown by several authors [5-9] that lattice defects near the edge of a standard photonic crystal can be used to improve their directional emission. One design from the group of Sajeev John [10] uses enlarged defect rods at the entrance and exit of a square lattice, rod based photonic crystal. As light exits a photonic crystal waveguide, it undergoes diffraction. If such resonant defects are placed at the interface, they can act as secondary sources of light when excited by the higher diffraction orders. For frequencies above the defect resonance (which can be tuned via the rod radius), a π phase shift results, thus light scattered from the defects can cancel out the higher diffraction orders via destructive interference [10]. The other way to view this is that the defect acts as a very broadband cavity. Light couples from this cavity into a forward propagating mode of the photonic crystal. The final result is a self-collimated beam that can be used to achieve very strong coupling with other structures, and operates over large bandwidth as shown in Fig 4.3. To my knowledge, similar designs have not been exploited for slotted photonic crystals previously. Using this idea as inspiration, I explored the use of resonant lattice defects for improving coupling to slotted photonic crystals.

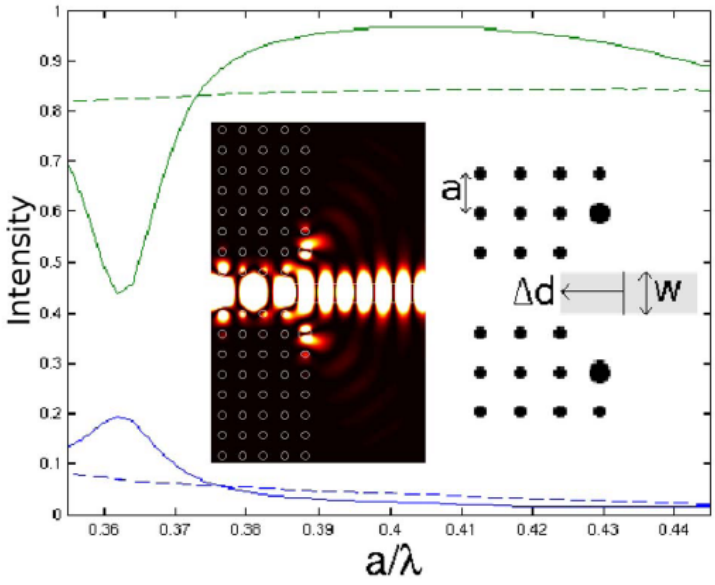

Figure 4.3: Intensity as a function of frequency for transmitted (green) and reflected (blue) light between a standard square lattice photonic crystal with resonant defect coupler and small-mode-area solid core fiber (reproduced with permission of APS from [10], Copyright 2008). Light scattered from resonant defects destructively interferes with higher diffraction orders, producing self-collimating beaming effect.

4.2.2 Slotted Photonic Crystal Coupler - Simulations

To test whether a similar scheme to [10] could be applied to slotted photonic crystals, I conducted simulations using the FDTD method. The addition of the slot introduces another set of parameters that has to be taken into consideration, most notably the width and termination point of the slot. A triangular lattice of air holes is also considered here, rather than the square lattice of dielectric rods used in [10]. Like [10], surface modes were eliminated by cleaving the photonic crystal between rows of holes, rather than within a hole itself. A sketch showing the part of the simulated structure and the relevant parameters is given in Fig 4.4, the most important parameters being the radius of the defect holes *r*, the termination distance of the slot *s* and the width of the input access waveguide *w*. A lattice period of 490 nm, hole radius 150 nm, slot width 180 nm and effective index 2.5 were chosen for all the simulations which were carried out in 2D with a pulse centred on 1550 nm. The full simulation area consisted of a 40 period long slotted photonic crystal, input and exit access waveguides and resonant defects at each interface, with perfectly matched layer (PML) boundary conditions. As it is hard to optimize three parameters at the same time, the simulations were first run for a standard slotted photonic crystal waveguide (i.e. no resonant coupler design). The only parameter varied was the slot termination point *s*. After establishing the optimum value for this, the full coupler interface was added and further simulations were carried out to optimise all three parameters *r*, *s* and *w*. The final results are shown in Fig 4.5.

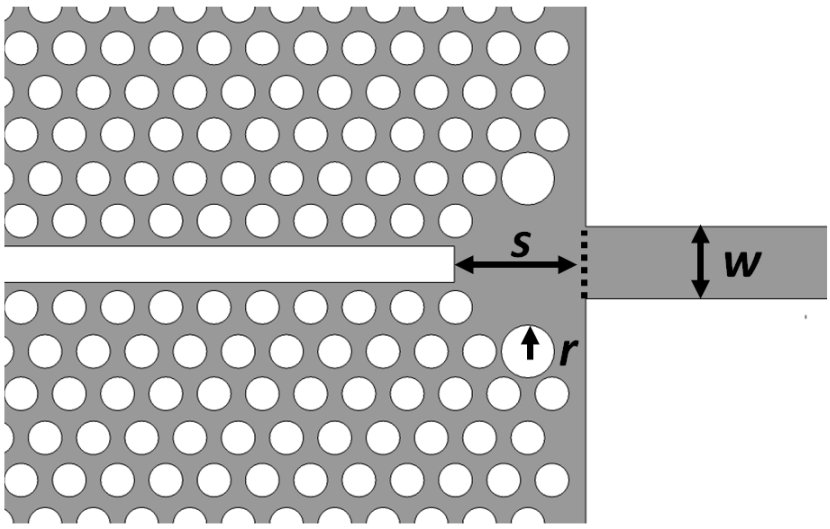

Figure 4.4: Resonant slot photonic crystal coupler geometry. Resonant defect holes placed near interface with access waveguide. Transmission depends on access width *w*, slot termination point *s*, and defect radius *r*.

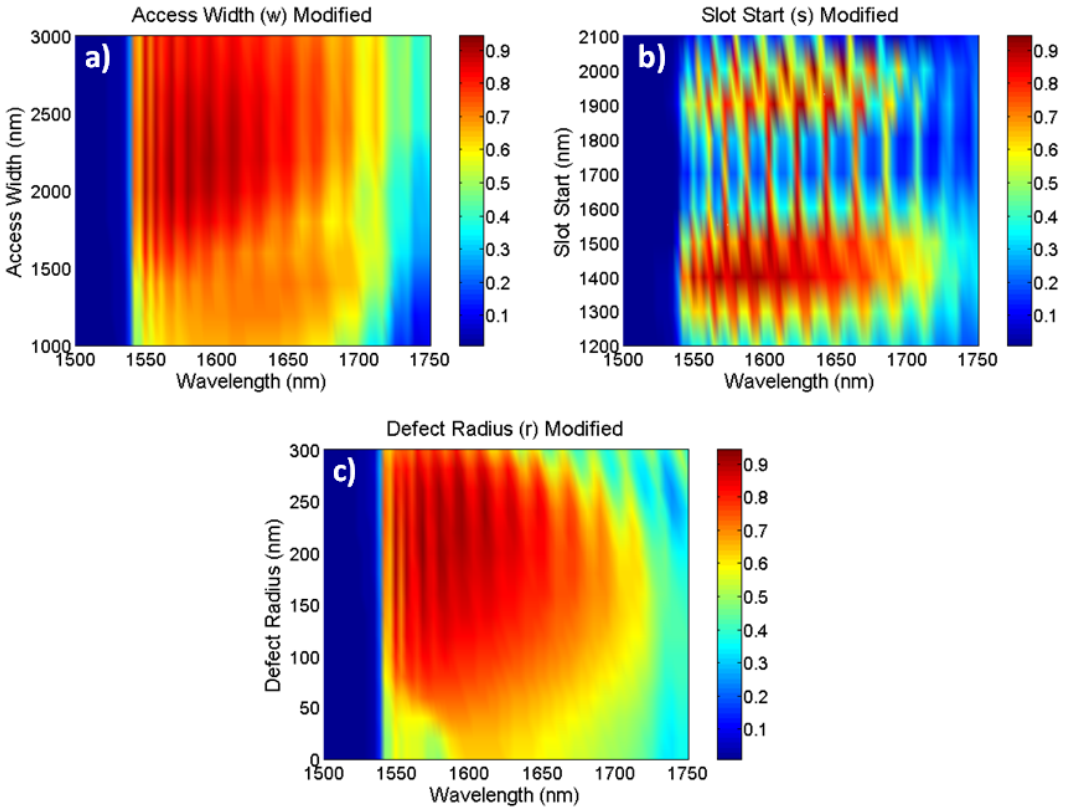

Figure 4.5: 2D FDTD simulations of slotted photonic crystal resonant coupler. Linear transmission at each wavelength as a function of a) *w*, b) *s* and c) *r*. One parameter out of the three was varied at a time from the optimum values of w = 2200 nm, s = 1400 nm and r = 220 nm.

As can be clearly seen from Fig 4.5, the termination point of the slot *s* has the greatest influence on the transmission properties of the coupler. Taking the best set of parameters, the optimum transmission spectrum achieved in these simulations is shown in Fig 4.6 a). From this, in the window of 1550 -1650 nm, the average coupling efficiency is -0.6 dB. As the simulation area consists of two interfaces, this value becomes -0.3 dB per interface. The bandwidth of 100 nm compares favourably with that of [4] (35 nm), whilst providing very small coupling losses. A small ripple remains in the transmission spectra due to the finite length of the slot. It is desirable to have high transmission and low ripple, so I chose the ratio of the zeroth order of the Fourier transform (transmitted spectrum) over the amplitude of the harmonic (ripple due to reflection) as a useful figure of merit (Fig 4.6 b). Fig 4.6 a) displays the transmission against wavelength at the highest value of this figure of merit.

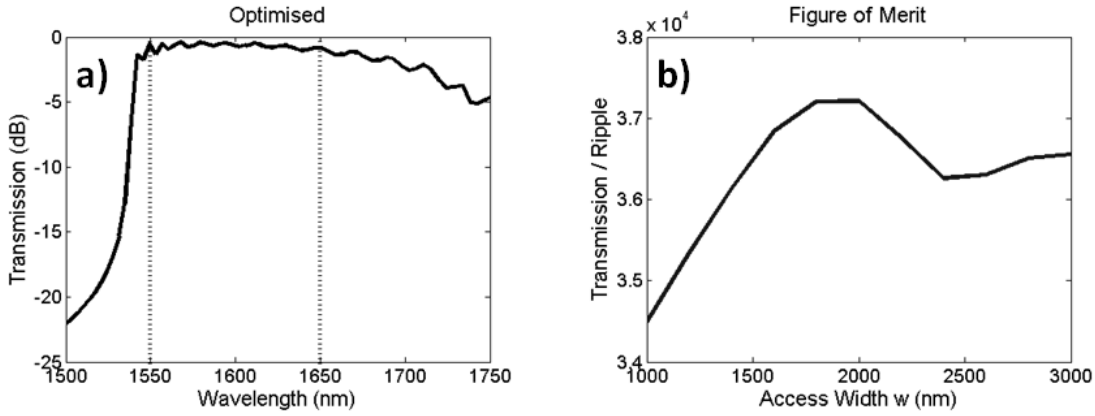

Figure 4.6: a) Transmission spectrum for optimum parameters in dB scale. b) Figure of merit for interface parameters. Keeping s = 1400 nm and r = 220 nm, this graph shows, the ratio of the zeroth order (transmission) to the first order (reflection) of the Fourier transform of the transmission spectra as a function of w. High transmission and low ripple is desired. At w = 2000 nm this ratio is maximised, producing the optimum spectrum shown in a).

4.2.3 Experimental Results

In order to test this design experimentally, I fabricated a number of structures on an SOI chip as detailed in Chapter 3. The target parameters were the same as the simulations. The parameters achieved experimentally were estimated from SEM images to be: 40 period long slotted photonic crystal of period 490 nm, radius 145 nm, slot width 150 nm, defect radius r of 220 nm and access waveguide width w of 2200 nm. All values are within an error of roughly 20 nm. The values of r and w were chosen as they provided the best performance in simulations (Fig. 4.5). The parameter s, which from simulations has by far the strongest impact on the coupling efficiency, was varied in steps of 100 nm from 1300 -1800 nm. Using the setup shown in Chapter 3, I characterized these devices with an ASE source and normalized to blank reference access waveguides fabricated on the same chip. An SEM image of one of the fabricated structures is shown in Fig 4.7, whilst the experimental results are shown in Fig 4.8.

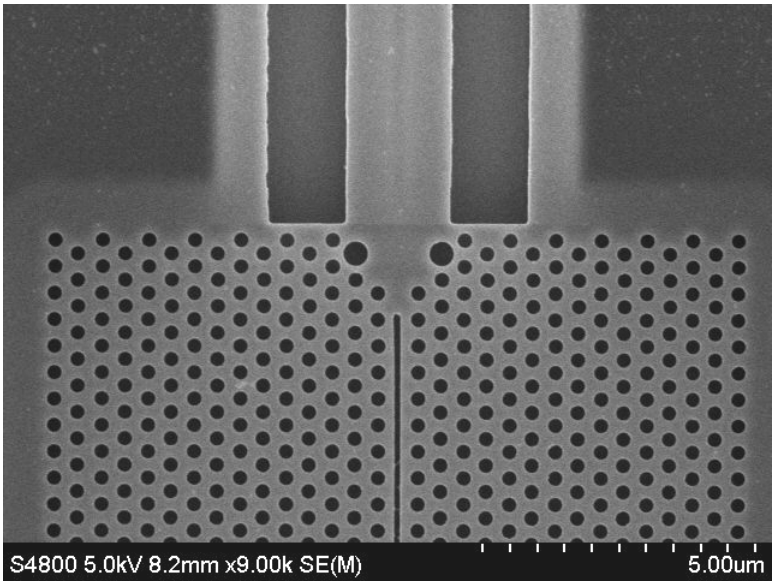

Figure 4.7: SEM image of slotted photonic crystal with resonant defect couplers and access waveguides, fabricated in SOI.

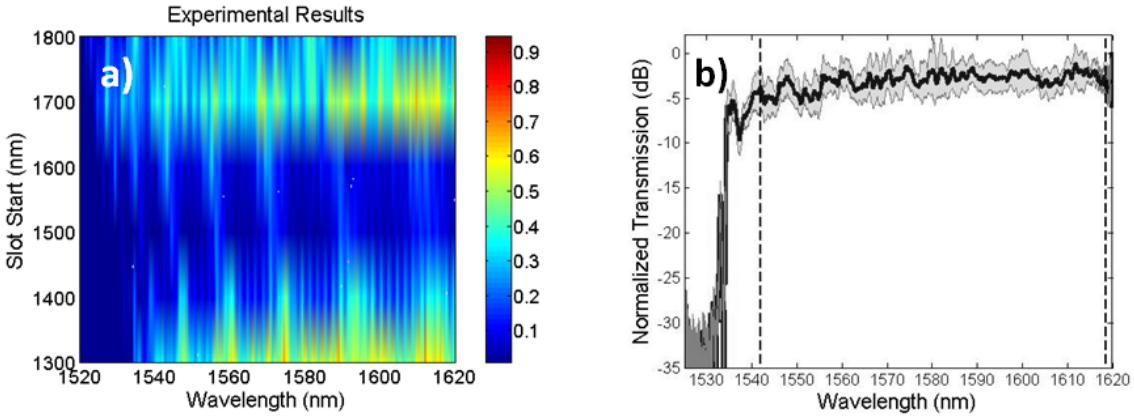

Figure 4.8: Experimental results. a) Linear transmission at each wavelength as a function of *s*. Note the similarity to fig. 4.5b). b) Experimental spectrum on a dB scale. Grey area shows standard deviation. All measurements normalised to four reference channel waveguides.

The comparison with simulations shows a good level of agreement in the behaviour of the transmission spectrum with variation of *s*. In a window of 78 nm, the average coupling loss was found to be -3.0 ± 1.5 dB when normalized to the average of 4 reference waveguides. The error value results from fabrication imperfections between these references. Similar to the simulations, this structure contains two interfaces, thus the average loss per interface is -1.5 dB over the 78 nm window. This value ignores the propagation losses, which will be touched upon later. The value of -3 dB for a two interface structure also compares favourably to [8] (5 dB) and [2] (4 dB), whilst operating over a large bandwidth, and most importantly, coupling to the

desired fundamental slot mode. The structure is also very compact and more robust in terms of fabrication when compared to sharply terminated tapers, which enables us to use the fundamental mode of the slot waveguide with its high field enhancement and strong confinement to air for sensing applications. Further experimental optimisation of the parameters may also be possible. Whilst the waveguides shown in these results are not slow light engineered, it is expected that a similar design will also provide increased coupling in the slow light case. Recently, Zhao *et al* [11] have shown via simulation that the coupler design I present here can indeed enhance coupling into slow light engineered slotted photonic crystals, observing up to 30 dB enhancement in the slow light region.

4.3 Propagation Losses

4.3.1 Introduction

The above results show that the coupling losses into a slotted photonic crystal can be as low as -1.5 dB per interface experimentally (-0.3 dB simulated). Coupling is not the only loss mechanism present; propagation losses also have to be considered. Propagation losses can result from absorption by the medium, and from scattering due to fabrication imperfections or from the geometry of the device itself. In the case of standard photonic crystals, the best reported values are of order 2-4 dB/cm [12]. Little has been published on losses in slotted photonic crystals, however, even though there are some papers on non-photonic crystal slot waveguides [13-16].

4.3.2 Experimental Results

To measure these losses experimentally, slotted photonic crystals of different length and slot width were fabricated together on the same SOI chip as detailed in Chapter 3. In order to make a good measurement of propagation loss, it is best to make the photonic crystals relatively long. As the e-beam machine at St Andrews is limited to a single writefield area of 100 x 100 μm^2 for without stitching errors, the exposure were carried out at LaNN (Laboratory for Nanofabrication of Nanodevices, Padova, Italy) by Dr Massari and Prof. Romanato using an e-beam machine (JEOL JBX-6300FS) capable of much larger writing areas. With this machine, photonic crystals of lengths 50, 100, 200 and 300 μm were exposed. As in the case of the resonant coupler, blank reference ridge waveguides were also included on the same chip for normalization purposes. The rest of the fabrication is the same as in Chapter 3.

In measurements carried out by my colleague Dr Andrea Di Falco with a white light supercontinuum source (Koheras compact) in the setup similar to that shown in Chapter 3 and using the cut-back method (measure different length crystals, with identical length access waveguides), propagation losses could be extracted. Results showing the losses in dB/cm as a function of wavelength for different slot widths are shown in Fig 4.9 with the values of below 10 dB/cm being observed. These results suggest that losses are strongly dependent on wavelength and slot width. Higher losses are observed for narrower slots as the field is more tightly confined to the walls of the slot, and thus feels the surface roughness more. For example, a slotted photonic crystal of slot width 145 nm produced a lowest loss of -8 ± 6 dB/cm, whereas a 115 nm slot produced a lowest loss of -29 ± 10 dB/cm. At wavelengths corresponding to the fast light regime, losses are comparable (~ 10 dB/cm) to standard slot waveguides [13-16] as shown in Table 4.1 below. This suggests that in the fast light regime, most of the light confinement is achieved by the slot, thus scattering from the lattice is reduced. In the slow light

regime losses become much higher as the mode spreads out into the lattice where it experiences enhanced scattering. More precise measurements of propagation losses could be carried out in future by writing longer photonic crystals. These results suggest, however, that with careful design, the losses in slotted photonic crystals can be minimized, allowing such devices to be used as practical sensors.

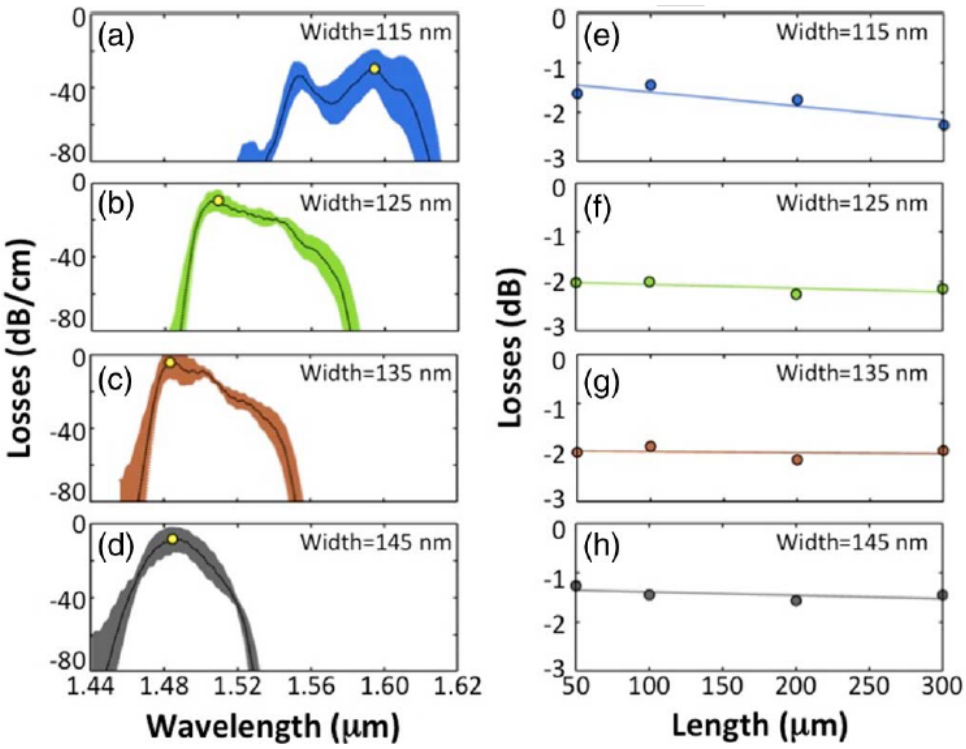

Figure 4.9: Propagation losses in slotted photonic crystal (reproduced with permission of IEEE from [17], Copyright 2012). (a)-(d) Loss measurements in dB/cm as a function of wavelength for 4 slot widths. (e)-(h) Measured losses as a function of waveguide length at highlighted wavelength in (a)-(d).

Table 4.1: Propagation loss comparison

Reference	Device	Material	Slot Width (nm)	Propagation Loss (dB/cm)
This work	Slotted photonic crystal	Silicon	115 125 135 145	29±10 9±5 4±7 8±6
Baer-Jones et al [13]	Slot waveguide ring resonator	Silicon	50 60 70	11.6±3.5 7.7±2.3 8.1±1.1
Spott et al [14]	Asymmetric slot waveguides	Silicon/PMMA	130	1.7±1.1
Zhang et al [15]	Slot waveguide	Silicon	80 100	8.6±0.61 11.1±1.15
Alasaarela et al [16]	Slot waveguide	Silicon/TiO2	Uncoated Coated	71 7±2
Notomi et al [12]	Photonic crystal	Silicon	N/A	2

4.3.3 Discussion

Whilst the propagation losses have been shown to be comparable to slot waveguides, at least in the fast regime, the question remains: how low do the losses have to be to be for a useful application? The main advantage of using slotted photonic crystals is that they allow the peak of the optical mode to interact with the contents of the slot. Reducing the losses would maximise the amount of light interacting with said contents, which is useful for sensing and other applications. The coupling losses can have a large impact (3 dB vs 15 dB), though this has been rectified using the resonant coupler design. Whilst there is a strong variation in the propagation losses with slot width and wavelength, the structures used are typically less than 100 μm in length. For such a structure, a figure of 11 dB/cm gives an absolute loss of 0.11 dB, whereas a figure of 39 dB/cm gives an absolute loss of 0.39 dB/cm. Both of these numbers are quite small when compared to the coupling loss, so do we care? If we use a cavity for sensing (see Chapter 6), whilst the cavity is very small, the effective optical path length can be very long as the resonant wavelength bounces between the cavity mirrors hundreds or thousands of times. Reducing the propagation losses would allow more passes to be made, increasing the interaction time with the sample and producing a sharper (higher quality factor) resonance. Both of these increase the sensitivity of the system. It should also be noted that these propagation loss measurements are for *air-filled* slots, with the primary loss mechanism being scattering from fabrication imperfections. In the sensing measurements of Chapter 6 there are additional losses due to absorption from the water. For slow light structures the losses also become more important due to enhanced scattering resulting from the higher intensities involved. Another point to consider is when several devices are used in series, these losses start to build up and restrict the number of them that can be multiplexed together. It therefore depends on the

application. Whilst for short waveguide structures the propagation losses are not so important, if long optical path lengths are to be used through cavities, slow light or multiplexing, then they can start to become significant. The results also show that the losses are not so much higher than standard photonic crystals to impose restrictions on their use in applications.

References

[1] Wang, Z., Zhu, N., Tang, Y., Wosinski, L., Dai, D., and He, S., "Ultracompact low-loss coupler between strip and slot waveguides," Opt. Lett. 34, 1498-1500 (2009).

[2] Brosi, J. –M, Koos, C., Andreani, L. C., Waldow, M., Leuthold, J. and Freude, W., "High-speed low-voltage electro-optic modulator with a polymer-infiltrated silicon photonic crystal waveguide," Opt. Exp. 16, 4177-4191 (2008).

[3] Gersen, H., Karle, T. J., Engelen, R. J. P., Bogaerts, W., Korterik, J. P., van Hulst, N. F., Krauss, T. F., and Kuipers, L., "Real-space observation of ultraslow light in photonic crystal waveguides," Phys. Rev. Lett. 94, 073903 (2005).

[4] Chen, X., Jiang, W., Chen, J., Gu, L., and Chen, R. T., "20 dB-enhanced coupling to slot photonic crystal waveguide using multimode interference coupler," Appl. Phys. Lett. 91, 091111 (2007).

[5] Moreno, E., Garcia-Vidal, F. J., and Martin-Moreno, L., "Enhanced transmission and beaming of light via photonic crystal surface modes," Phys. Rev. B 69, 121402 (2004).

[6] Morrison, S., and Kivshar, Y. S., "Engineering of directional emission from photonic-crystal waveguides," Appl. Phys, Lett. 86, 081110 (2005).

[7] Frei, W. R., Tortorelli, D. A., and Johnson, H. T., "Topology optimization of a photonic crystal waveguide termination to maximize directional emission," Appl. Phys. Lett. 86, 111114 (2005).

[8] Chen, C. –C., Pertsch, T., Iliew, R., Lederer, F., and Tunnermann, A., "Directional emission from photonic crystal waveguides," Opt. Exp. 14, 2423-2428 (2006).

[9] Kurt, H., "Theoretical study of directional emission enhancement from photonic crystal waveguides with tapered exits, IEEE Photon. Techn. Lett. 20, 1682-1684 (2008).

[10] Bauer, J., and John, S., "Broadband optical coupling between microstructured fibers and photonic band gap circuits: Two-dimensional paradigms," Phys. Rev. A 77, 013819 (2008).

[11] Zhao, Y., Zhang, Y. –N., Wu, D., and Wang, Q., "Wideband slow light with large group index and low dispersion in slotted photonic crystal waveguide," J. Lightwave Tech. 30, 2812-2817 (2012).

[12] Notomi, M., Tanabe, T., Shinya, A., Kuramochi, E., Taniyama, H., Mitsugi, S., and Morita, M., "Nonlinear and adiabatic control of high-Q photonic crystal nanocavities," Opt. Exp. 15, 17458-17481 (2007).

[13] Baehr-Jones, T., Hochberg, M., Walker, C., and Scherer, A., "High-Q optical resonators in silicon-on-insulator-based slot waveguides," Appl. Phys. Lett. 86, 081101 (2005).

[14] Spott, A., Baehr-Jones, T., Ding, R., Liu, Y., Bojko, R., O'Malley, T., Pomerene, A., Hill, C., Reinhardt, W., and Hochberg, M., "Photolithographically fabricated low-loss asymmetric silicon slot waveguides," 19, 10950-10958 (2011).

[15] Zhang, H., Zhang, J., Chen, S., Song, J., Kee, J. S., Yu, M., and Lo, G. -Q., "CMOS-compatible fabrication of silicon-based sub-100-nm slot waveguide with efficient channel slot coupler," IEEE Photon. Tech. Lett. 24, 10-12 (2012).

[16] Alasaarela, T., Korn, D., Alloatti, L., Saynatjoki, A., Tervonen, A., Palmer, R., Leuthold, J., and Honkanen, S., "Reduced propagation loss in silicon strip and slot waveguides coated by atomic layer deposition," Opt. Exp. 19, 11529-11538 (2011).

[17] Di Falco, A., Massari, M., Scullion, M. G., Schulz, S. A., Romanato, F., and Krauss, T. F., "Propagation losses of slotted photonic crystal waveguides," IEEE Photon. J. 4, 1536-1541 (2012).

Chapter 5

Microfluidics

5.1 Microfludics Basics

5.1.1 Introduction

Whilst the previous chapters have shown that light can be squeezed down into nanoscale slots, and that this is advantageous for optical sensing, the delivery of the sample solution to these sensors has yet to be addressed. One of the advantages of the slotted photonic crystal sensing architecture is the small footprint, on the order of 10-100 μm, thus potentially hundreds of independent sensors could be fabricated on a single chip. It therefore makes sense to control liquids at a similar scale such that samples can be directed to different sensors, whilst also minimizing their volume; something that can be important with precious samples and reagents. This is where **microfluidics** [1, 2] comes into play; it being the control and manipulation of fluids in flow channels less than 1 mm wide. Microfluidics is a rapidly growing field in its own right, but is also being combined with other disciplines such as biophotonics [3]. One of the key features of fluid behaviour within microfluidic channels is that fluid flow is almost entirely laminar. This results from the Reynolds number Re, a dimensionless quantity, which gives the ratio between inertial and viscous forces, being defined as:

$$\mathrm{Re} = \frac{\rho U_0 L_0}{\eta} \tag{5.1}$$

Where ρ is the density, η is the shear viscosity and U_0 is the flow velocity of the fluid, whilst L_0 is a characteristic length scale of the flow. The Reynolds number can be used to give an indication of the flow regime (for example, laminar or turbulent), with the transition between the two occurring around Re ≈ 2000. The small size of microfluidic channels, result in viscous forces dominating inertial ones, thus Re is always much lower than 2000, ensuring laminar flow [1]. For a typical microfluidic channel of width 100 μm, and filled with water (ρ = 1000 kg/m^3, $\eta \approx 10^{-3}$ Pa.s) flowing at a rate of 100 μm/s, then Re ≈ 0.01. The lack of turbulence in a microfluidic channel means that two fluids within the same channel mainly mix by diffusion, a relatively slow process, thus they can propagate together in parallel over a length equivalent to several 10's or even 100's of channel widths [1] without significantly mixing. The length of channel required to achieve full mixing is determined by the Péclet number, which gives the ratio between convection (bulk transport) and diffusion, and is defined as [1]:

$$\mathrm{Pe} = \frac{U_0 L_0}{D} \tag{5.2}$$

Where *D* is the diffusion constant. The volumes of liquids within microfluidic channels is also very low, often sub-nanolitres, which is useful in applications with precious samples. The small size of the channels also affects other fluid properties such as capillary forces, which can be used to draw fluids into the channel for self-pumping chips (a full review is given by [1]).

5.1.2 Platforms and uses

Microfluidic chips have been fabricated in a number of materials using many different techniques. One of the most common materials is an elastomeric polymer called poly(dimethylsiloxane), or for short, **PDMS**. As will be seen shortly, this is the primary material I used for the devices described in this thesis. Using a technique known as **soft lithography**, microfluidic devices can be rapidly fabricated in PDMS with feature sizes down to 30 nm [4]. PDMS is optically transparent and flexible. This flexibility can be exploited in making components such as pneumatic microvalves and pumps [5] in the microchannels. Other polymers such as Poly(methylmethylacrylate) (PMMA) can be used to make microchannels via hot embossing [6], laser ablation [7] or injection moulding [8]. Also common is the use of glass based microfluidics, which can be realised through techniques such as wet etching [9]. Some other interesting material platforms include treated paper [10] and thread [11]. It is probably fair to say that no one material has become the accepted standard, though PDMS is perhaps the most common. PDMS, like other platforms, is itself not without problems [12]: it is gas permeable (can also be an advantage), is naturally hydrophobic and can swell in and absorb organic solvents [13] (as will be discussed more in Chapter 6). It is, however, relatively cheap, simple and fast to use, can be chemically bonded to glass via oxygen plasma treatment, is biocompatible, and, as mentioned above, it is flexible, which can be exploited for microfluidic components.

Microfluidics has seen much interest in the area of lab-on-a-chip research (discussed in Chapters 1 and 2). Like photonics, a number of microfluidic components can be integrated together on a single chip such as the aforementioned valves and pumps. These can also be combined with microelectronic devices, and as is the case here, with nano/microphotonic components. Key technological abilities offered by the microfluidics approach include hydrodynamic focusing [14] where ‘sheath’ liquids are used to focus a stream of and/or sort particles [15], oil droplet manipulation [16] for controlling and studying interfaces between liquids and capsules for transporting material, and electroosmosis [17] where a liquid containing ions, within a surface charged microchannel, can be moved by applying an electric field along the channel. In this thesis, I integrate microfluidic channels with the slotted photonic crystals as a way to address the sensors with samples of very low volume, whilst also preventing fast evaporation. I also explored microvalve structures, which potentially would allow automation of the device and greater control over sampling; something which could be useful in remote sensing applications. As a starting point, the fabrication methods I used for microfluidic channels are presented.

5.2 Microfluidic Channel Fabrication

5.2.1 PDMS

PDMS devices are the primary platform for microfluidics in my work, though glass is also briefly touched upon. PDMS (184 Sylgard) comes in two liquid parts: base elastomer and curing agent. When mixed together and left to cure, this forms a solid elastomer. If this process is carried out on top of a master mould containing the negative of the desired channel design, an imprint of the mould can be left in the cured PDMS when it is peeled away. This is known as

soft lithography [4]. A diagram of the full process is shown in Fig 5.1. To form a master mould with the desired channel design (typically 100-200 μm wide channels), I cleaned a piece of silicon in acetone and IPA whilst inside an ultrasonic bath, and dried in nitrogen gas. SU-8 negative photoresist (2050 : 2000.5 in a ratio of 10 : 1) was spun on top of the substrate. To achieve a thickness of 40 microns I used a spin speed of 1000 r.p.m. The sample was then baked on a hotplate at 65 ℃ for 5 min, followed by 95 ℃ for 15 min. To create the desired pattern, this sample was loaded into a mask aligner and exposed to UV light through a photomask of the channel pattern for 2 min. Following this, the sample was post exposure baked at 65 ℃ for 1 min and 95 ℃ for 10 min. The pattern was then revealed by developing in EC solvent for 3 min, and rinsing in IPA. To ensure good adhesion of the SU-8 to the silicon substrate, the sample was hard baked overnight in a 180 ℃ oven.

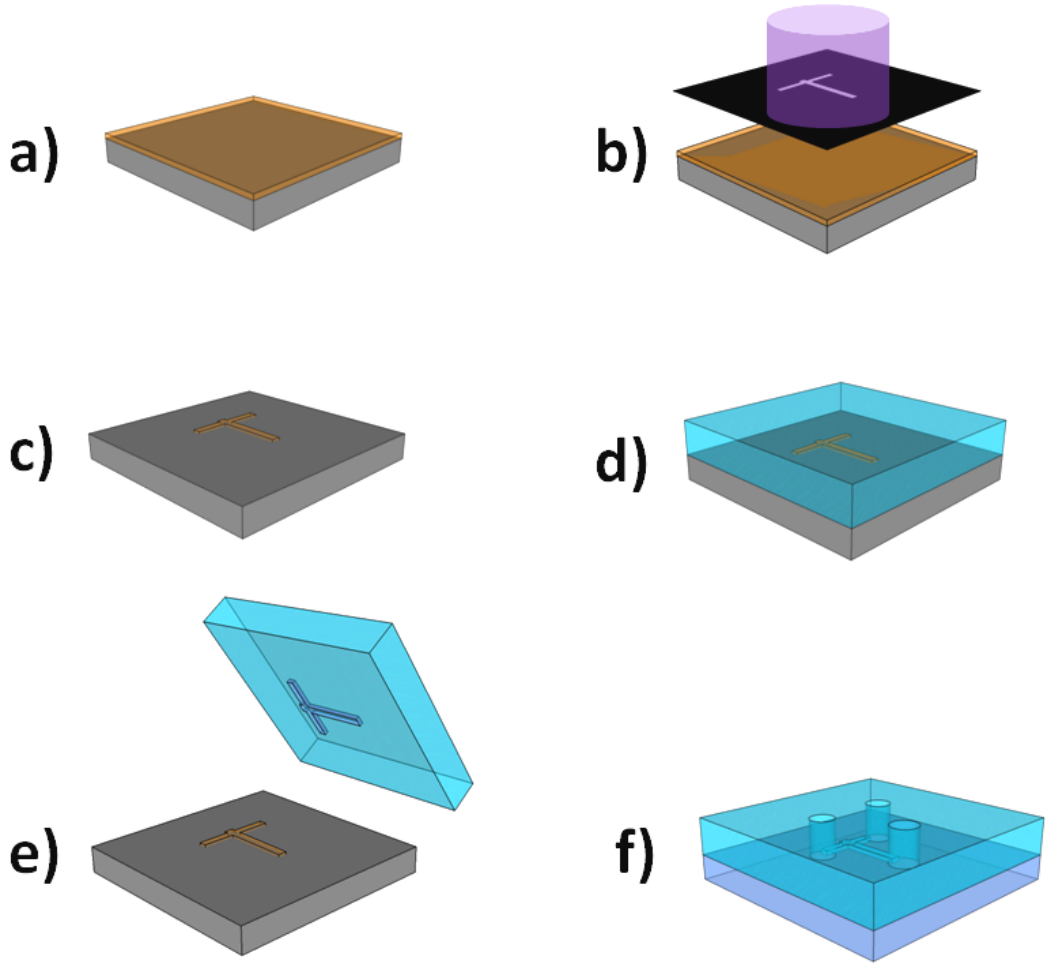

Figure 5.1: Soft lithography method of fabricating PDMS microfluidics. a) SU-8 photoresist of thickness equal to desired channel height is spun and baked on clean silicon substrate. b) Sample exposed to UV light through photomask of channel design. c) Followed by, post-exposure bake, development and hard baking to complete mould. d) Liquid PDMS base and curing agent poured on top of mould and allowed to solidify. e) Solid PDMS containing imprint carefully peeled from mould. This mould can be used repeatedly for making PDMS imprints. f) Access holes punched in to PDMS in order to connect pipes. PDMS and bottom cover (e.g. glass) then treated with oxygen plasma and bonded together.

PDMS base and curing agent were mixed in a ratio of 10 : 1.3 by volume, and degassed in a vacuum chamber to remove bubbles. I then carefully poured this over the master mould inside a plastic petri dish, and left it inside a 65 °C oven for over 4 hours to solidify. The solid PDMS was carefully pealed from the mould and cut to size with a blade. Access holes for tubing were punched through the microchannels where required. To seal the bottom of the channel, I used a coronal discharge gun to treat the PDMS stamp with oxygen plasma [18] for 30 s, creating free OH groups on its surface [19]. When placed in contact with another surface with similar free groups, such as oxygen treated glass, PDMS, PMMA or silicon, the two surfaces can form covalent siloxane (Si-O-Si) bonds [19]. Each surface was treated with the oxygen plasma for 30 s, before rinsing in methanol. This allows the two surfaces to be placed in contact and aligned (the methanol acting as a lubricant). To ensure good bonding this process must be carried out within a few minutes of oxygen treatment, thus I used methanol as it evaporates fast (using IPA produced mixed results). After contact, the samples were placed in a 65 °C oven for over 4 hours. I found that better bonds resulted when using PDMS that was cured on the same day (ideally it was poured ~4 hours before bonding). The final sample had tubing of diameter slightly greater than the access holes, compressed into these holes to take liquids in and out of the microchannel. These moulds could be re-used numerous times to make PDMS microchannels.

5.2.2 Glass

For glass microchannels I used a similar process to [20, 21]. To begin, I cleaned a glass microscope slide in acetone and IPA inside an ultrasonic bath. S1818 photoresist was then spun at 1000 r.p.m., and baked for 2 min at 100 °C. I repeated this on the same sample to give two layers. The resist was then exposed to the channel design in a mask aligner for 3 min, before developing in MF 319 for 2 min 30 s. This I hard baked at 150 °C for over an hour to enhance its chemical resistance and to improve adhesion. An etchant solution based on [20, 21] was made up with the following constituents: 80 mL DI, 5 mL HF (49 %), 5 mL HCl and 30 mL NH_4F using appropriate safety measures. This solution is more directional in its etching than concentrated HF, allowing the mask to survive longer and preventing significant underetching. The presence of HCl creates smoother channels by removing precipitated particles [20, 21]. The photoresist coated slide was left in this solution for 1 hour. The sample was then rinsed in DI, and the resist removed in acetone and IPA, and followed by a Piranha clean if necessary. The etch depth I found to be around 60 µm using a Dektak surface profiler, implying an average etch rate of 1 µm/min. Access holes were then drilled into the channel using a diamond tipped drill bit. To form a bottom cover, a second glass slide was cleaned in Piranha solution for 5 min along with the etched slide. Similar to [20], the un-etched slide was coated with Norland 60 UV optical adhesive by spinning it at 5000 r.p.m. I then brought the etched slide into contact, and exposed the two slides together in the mask aligner for 6 min. Images of the final results are shown in Fig 5.2.

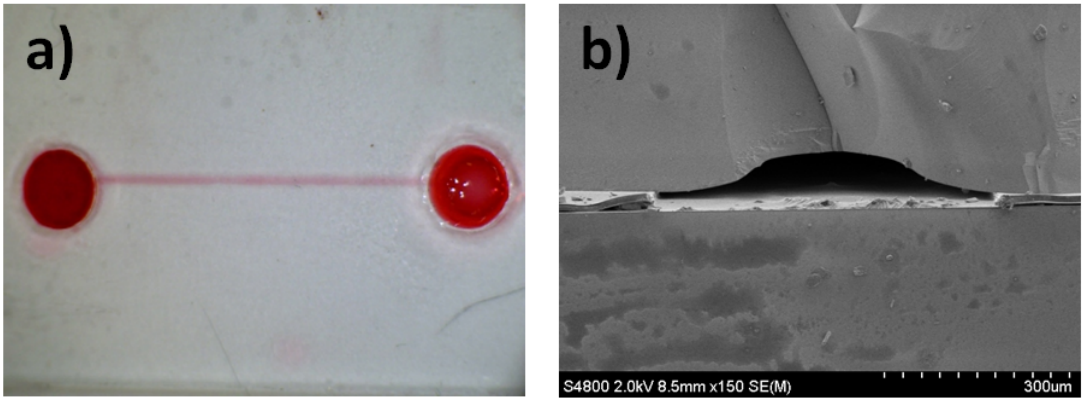

Figure 5.2: Glass microfluidic channels fabricated by wet etching. a) Channel containing red dye. Liquid injected through access holes. b) SEM image of channel cross section obtained by cleaving the sample.

5.3 Integration with Slotted Photonic Crystals

In addition to PDMS and glass, I also considered other materials such as PMMA and acetate sheets for microfluidic channels. In the end I chose PDMS as the best option for integrating with the slotted photonic crystals. Using glue, as in the case of the glass, to seal the device is tricky as the photonic crystals need to be left clean in order to function as a sensor. One option in this case is to use a stamp-and-stick method [22]. For PDMS, however, no glue is required. As explained above, oxygen plasma treatment can be used to chemically bond the PDMS to the silicon, with alignment being achieved using methanol as a lubricant. If glue is used, there is only one chance of correct alignment to the photonic crystals; any mistake requires the sample to be cleaned. Also, as seen above, glass microchannel fabrication involves the use of dangerous chemicals, and additional steps such as drilling access holes. This has to be done for each sample. In the case of the PDMS, the SU-8 master mould can be re-used, making the process much faster and repeatable. It is also easier to fabricate valves in PDMS.

Whilst in the above section, surfaces were bonded to PDMS by oxygen plasma treating both materials, in the case of the silicon containing the slotted photonic crystals I used a slightly different protocol. Instead, I first immersed the photonic crystal sample in Piranha solution. Piranha solution ensures that the surface is free from organic material, whilst adding OH groups on the silicon surface. Both of these properties are useful for the biosensing experiments as they ensure that the surface is very clean, and as will be seen in the next chapter, the OH groups can be used to functionalize the surface. The presence of the OH groups also makes the surface more hydrophilic, which improves the wetting properties of the photonic crystals, something that is important for the device to function properly as a sensor. Whilst many of these properties are also achieved by using the coronal discharge gun, I found that when used with silicon (a semiconducting material) there were large arcs between the surface and the gun filament that could potentially damage the photonic crystal membranes. The use of piranha solution is also perhaps better at cleaning than the hand held gun.

I found the following protocol to produce the most reliable results. PDMS was poured on top of an SU-8 mould consisting of a straight line channel of dimensions 40 µm high, 200 µm wide, 1.2 cm long (fabricated as in Section 5.2.1). This I left in a 65 °C oven for only 4 hours to cure. As before, the PDMS was removed, cut to size, and access holes punched through. The access waveguides of the photonic crystals had to be sufficiently long, and the width of the PDMS sufficiently narrow, that they were able to be bonded together without covering the edge facets of the waveguides, whilst also preventing leaks in the microfluidics. To ensure this was the case I wrote access waveguides of 4 mm in length on either side of the photonic crystals, and punched 2 mm access holes into the PDMS. After cutting the PDMS chip to size, I rinsed it in IPA within an ultrasonic bath and dried with nitrogen gas in order to ensure the surface was clean. The piece of SOI containing the photonic crystals was then immersed in piranha solution for 15 min, before rinsing in DI, acetone and IPA (no ultrasonic). This I placed on top of a microscope slide, inside a small plastic petri dish, under a microscope. The PDMS surface containing the microchannel was then exposed to oxygen plasma on top of a plastic petri dish for 30 s using the coronal discharge gun, before rinsing both the SOI and PDMS in methanol. The two surfaces were placed in contact under the microscope, and aligned using a pair of tweezers. The alignment of the microchannel to the photonic crystals (which I checked using the microscope) has to be completed before the lubricating methanol evaporates, and shortly after oxygen treatment, in order to achieve good bonding at the desired location. Once aligned, the sample was left for a few minutes to allow the methanol to evaporate, before I carefully transported the petri dish containing the sample to a 65 °C oven, and left it to bond overnight. After removing from oven, I glued the chip on top of a glass sample holder using silver conductive paint, and inserted tubing into the access holes. Images of the final results are shown in Fig 5.3. No leaks were detected.

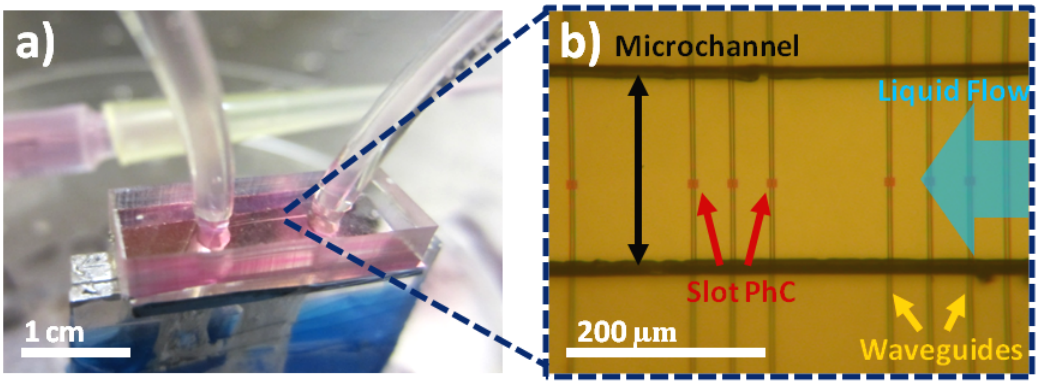

Figure 5.3: Slotted photonic crystals with integrated microfluidics. a) PDMS microchannel bonded on top of SOI chip. Sample glued to glass holder. Tubing inserted into access holes, to which syringes can be connected. b) Optical microscope image of channel with slotted photonic crystals inside. Access waveguides take light to and from photonic crystals.

5.4 Microvalves

5.4.1 Introduction

The successful integration of microfluidics with slotted photonic crystals allowed biosensor chips to be constructed. The resulting biosensing work is shown in the following chapters. Here, continuing the microfluidics theme, my investigations into microvalves to control sampling on-chip are presented. This would be of benefit in remote sensing applications. Many existing microvalves are based on the design by Quake's group [5], which rely on pneumatic actuation. Quake's valve is constructed from multiple layers of PDMS: one thin membrane layer in which the liquid channel is defined, on top of which is bonded another perpendicular channel. When pressurised gas is passed through this top channel, it deforms the channel membrane below, preventing flow. Whilst these valves are relatively simple to fabricate, small, and can be packed in very high densities, they require an external source of gas, which significantly adds to the bulk of the device. They are also normally open valves, which are not always desired. Other solutions that do away with this gas source, and are thus truly miniature, would be of interest in lab-on-a-chip and remote sensing applications. Many different microvalve mechanisms have been reported, good reviews of which can be found in [23, 24]. Most commonly, valve actuation takes place via thermal methods. One type of valve relies on heating a blockage of hydrogel [25, 26] inside a microchannel causes it to drastically shrink in its size, opening the channel. Others are based on shape memory alloys (SMAs) [27-31]. When heated (one simple way is to pass electrical current through the wire itself) a deformed wire tries to recover its original shape. This restoring force is used to perform work. Parlyene based flaps within a channel, which are opened by melting via an embedded heater have also been demonstrated [32].

A common thermal method is to rely on a phase change in a material such a paraffin wax when heated. In one design [33] a chamber underneath a microchannel is sealed with paraffin. When heated by an integrated ITO heater, the volume of the wax expands deforming the channel above it. Another [34] relies on the wax changing to liquid state through heating. Once in liquid form, the paraffin is compressed by a pneumatic control, deforming a microchannel below. Instead of using a separate chamber, other designs place the wax inside the channel itself. One paper [35] using microheaters to melt a large region of embedded paraffin, and vacuum to reset it. Perhaps the simplest design [36] involves melting a small plug of paraffin inside the microchannel via a peltier heater. Reservoirs after the heater are used to catch most of the paraffin. Although this type of valve only affords single shot operation, its simplicity makes it a very attractive option, especially for some of the single use devices that we are interested in.

5.4.2 In-line paraffin microvalve

Instead of using large peltier heaters, I modified the design of [36] to include microheaters fabricated on-chip and smaller regions of wax. For my initial tests, PDMS chips containing two straight, perpendicular and intersecting channels were fabricated as outlined in Section 5.2, and bonded onto microscope slides. Paraffin wax was melted, and sucked through one of channels using a syringe, the hope being that on cooling, the wax would form a solid plug at the intersection with the other channel. I performed this work together with Praveen Ashok, and we noted that it was hard to prevent the liquid wax from flowing through the entire chip. We used multiple syringes to balance the pressure at the intersection, but without success. A secondary idea I had was to make the microchannels in a thin membrane of PDMS. In this case, I spun liquid PDMS on top of the mould at 500 r.p.m. This was cured on a 120 °C hotplate for 5 min before peeling and bonding to a glass slide containing aluminium microheaters. The

microheaters were defined in AZ 4562 photoresist on glass using photolithography. After development, I loaded the samples into a thermal evaporator, in which a 200 nm thick layer of aluminium was deposited on the surface of the device. Redundant metal was lifted off using acetone. Heater dimensions were: length 5 mm, wire width 25 µm, coil period 130 µm. Larger blocks of PDMS were then attached in order to connect tubes properly at the access holes. The bonded sample was placed inside a custom made press built by Praveen Ashok and myself, sandwiched between a peltier heater, and a pair of fixed tweezers. The tweezers were aligned such that they pressed down on either side of the intersection between the two channels. The thin and flexible nature of the PDMS meant that one of the two channels was closed by this external pressure from the tweezers. Solid wax was inserted into the other channel, and the peltier turned on. Liquid wax then flowed through the open channel. Once full, the peltier was cooled and the pressure from the tweezers removed, leaving one channel full of wax, and the other free except for the intersection, as shown in Fig 5.4 a) and b). I then carried out electrical tests using a power supply and needle probes connected to the microheater's contact pads. A microscope and camera were used from above to view the actuation. Images of a device being actuated are shown in Fig 5.4 c)-e).

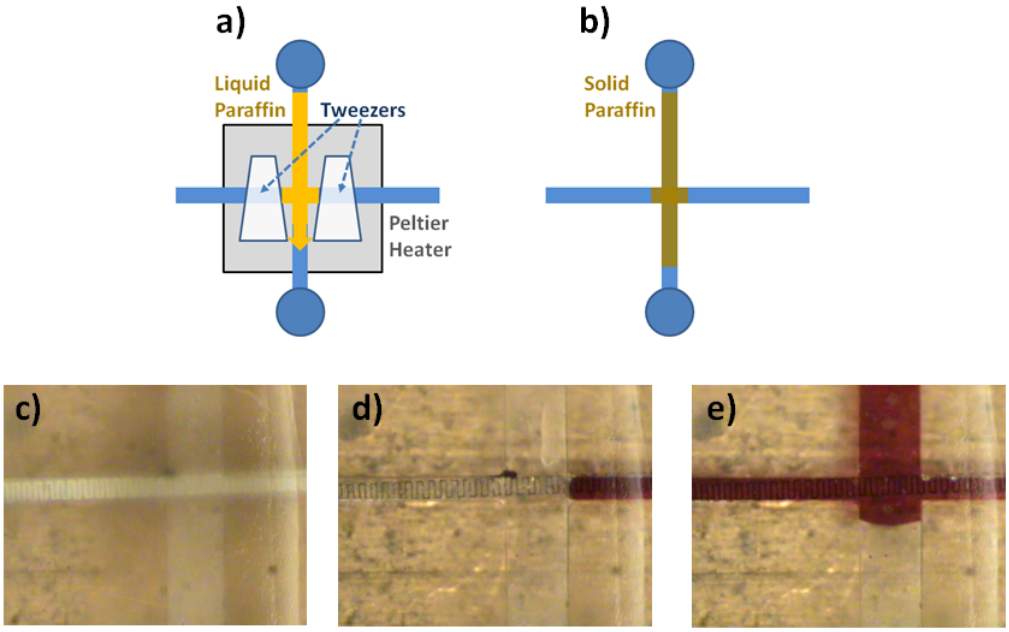

Figure 5.4: In-line wax microvalve. a) Wax loading technique. One channel closed on either side of intersection by pressure from tweezers on PDMS membrane. The wax was melted by a peltier heater and was then able to flow through the open channel. b) Final result after removing heat and pressure; the channel is now sealed c)-e) Images of valve actuation at the intersection using the integrated microheater coil.

Tests showed that the actuation time could be varied depending on the current used. At 40 mA current, a voltage of 7.6 V was required, which resulted in an actuation time of less than 5 s, and thus an energy consumption of less than 1.5 J. Depending on the combinations of these parameters, energies between 1 - 4.7 J were needed to open the valve. I tested the burst pressure of the valve using pressurised argon gas connected to regulator, and coloured water samples. The valve was found to withstand a differential pressure of 12 psi.

5.4.3 Membrane based wax microvalve

The valve described above is relatively simple and effective, but it requires placing the wax directly into the fluid channel, which could contaminate the analyte. I therefore investigated another valve design, where the wax was kept separate from the channel contents. In this design, a single channel was fabricated in a thin membrane of PDMS and bonded on top of a microheater as in Section 5.4.2. The next step was to bond a second piece of PDMS on top of this, with a 2 mm access hole punched into, such that this hole sat above the membrane channel. Solid microcrystalline wax, more tacky than regular paraffin, was then compressed into this access hole, forcing down and pinning the channel within the thin PDMS membrane layer below. The valve was actuated as before by heating the wax via the microheater. In this case, the melting of the wax releases its downward hold on the membrane, causing the valve to open. Using a current of 100 mA, and a voltage of 13.4 V allowed the valve to be actuated in approximately 1 s using similar microheaters as above. Testing the burst pressure as before, resulted in a value of 8 psi. I integrated several of these valves into a single chip, and used them to control liquid flow from several channels feeding a central reservoir where, for example, a fluorescent detection system could be placed (see Chap 7). Images of the completed device are shown in Fig 5.5.

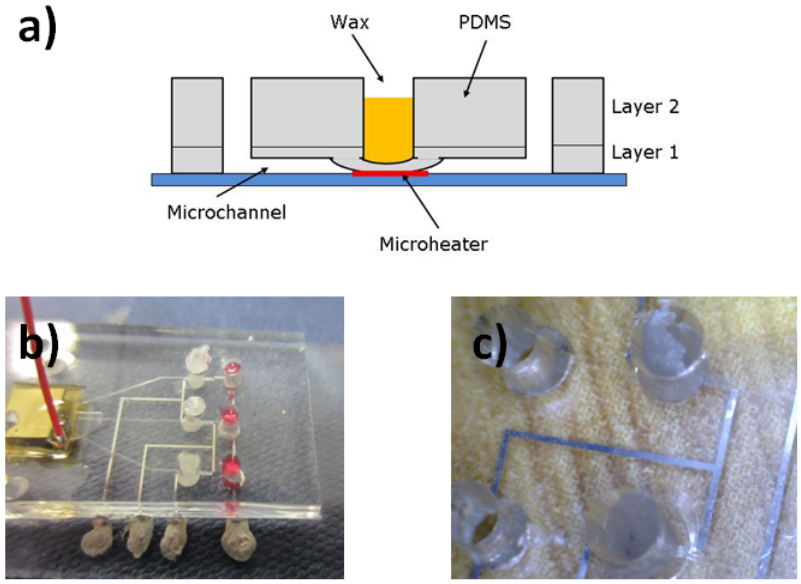

Figure 5.5: Membrane based wax microvalve. a) Principle of operation. Compressed tacky microcrystalline wax in the top layer keeps the membrane channel pinned closed. Heater melts wax, releasing this pressure, opening the channel. b) Several valves in different channels feeding a central reservoir. Valves can be actuated in different sequences using contact pads. c) Close-up of valve regions.

These simple valves can be easily integrated into PDMS. The main disadvantages are their low burst pressure and single shot nature. Despite this, I was able to demonstrate that low power microvalves that do not require any pneumatic base actuation can be integrated into a microchannel. The performance of the wax valves is favourable when compared to others in the literature, given their small size (see Table 5.1). Whilst valves fabricated in more rigid

materials can withstand higher pressures, they cannot use the membrane actuation demonstrated here which keeps the wax away from the channel contents.

Table 5.1: Comparison of wax microvalves

Reference	Valve	Microchannel	Actuation	Valve Dimensions (mm^3)	Energy (J)	Pressure Resistance (Bar)
In-line valve presented here	Microwax	PDMS	Integrated microheater	0.75x0.25x0.05	1 – 4.7	0.83
Membrane valve presented here	Microwax	PDMS	Integrated microheater	2x2x0.5	> 1	0.55
Yoo et al [33]	Paraffin	PDMS	Integrated ITO heater	2x3.5x3.5	-	-
Yang et al [34]	Paraffin	PDMS	Hotplate	2x0.35x0.3	58.9	0.35
Pal et al [35]	Various waxes	Glass	Integrated microheaters	1.4x0.5x0.05	< 5	17.2
Liu et al [36]	Paraffin	Polycarbonate	Peltier	6x1x0.5	1 - 4	2.7

5.4.4 Shape Memory Alloy Valves

In the quest to realise a multiuse valve, I investigated valves based on shape memory alloys. Many such valves have been reported in the literature [27-31], but many of these operate in the normally open state (rather than the more energy efficient closed state), whilst others are not easy to integrate. I therefore briefly looked at developing new designs. A selection of these design studies is shown in Fig 5.6. Whilst all of these designs suffered problems preventing them working as designed, it is conceivable that with more time available, a working device could be demonstrated in the future.

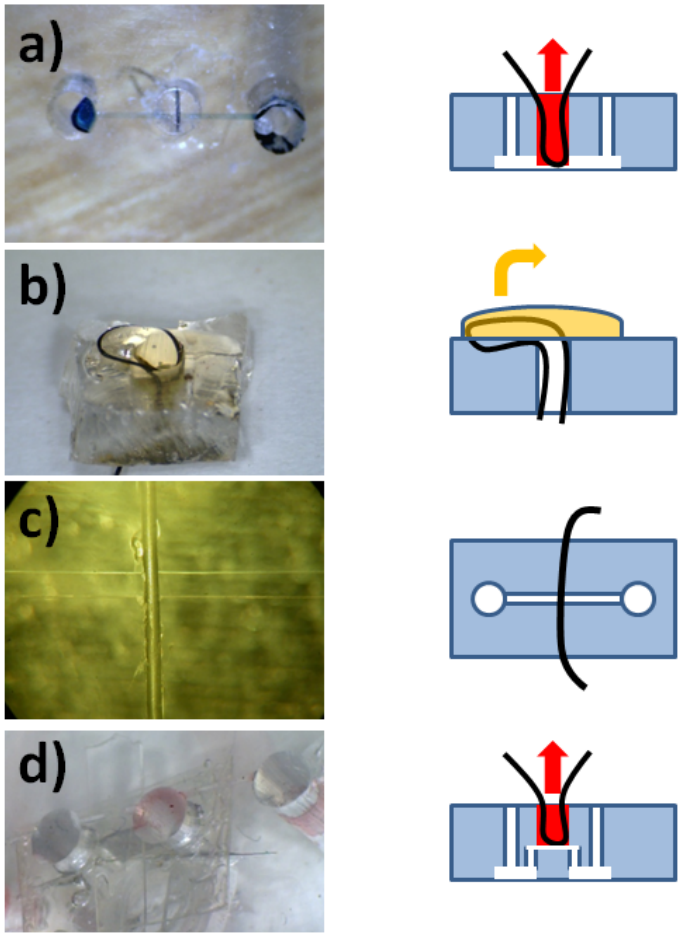

Figure 5.6: Different shape memory alloy (SMA) valve concept designs that were investigated. All designs are work in progress. a) SMA wire pulls up post when actuated. b) SMA pushes open layer of SU-8 on top of access hole. c) Wire blocks flow in perpendicular channel. Actuation lifts up channel roof. d) SMA wire lifts membrane lid covering two ports (image taken from bottom).

References

[1] Squires, T. M., and Quake, S. R., "Microfluidics: Fluid physics at the nanoliter scale," Rev. Modern Phys. 77, 977-1026 (2005).

[2] Whitesides, G. M., "The origins and the future of microfluidics," Nature 442, 368-373 (2006).

[3] Schmidt, H., and Hawkins, A. R., "The photonic integration of non-solid media using optofluidics," Nature Phot. 5, 598-604 (2011).

[4] Xia, Y., and Whitesides, G. M., "Soft lithography," Annu. Rev. Mater. Sci. 28, 153-184 (1998).

[5] Unger, M. A., Chou, H. –P., Thorsen, T., Scherer, A., and Quake, S. R., "Monolithic microfabricated valves and pumps by multilayer soft lithography," Science 288, 113-116 (2000).

[6] Brown, L., Koerner, T., Hugh Horton, J., and Oleschuk, R. D., "Fabrication and characterization of poly(methylmethylacrylate) microfluidic devices bonded using surface modifications and solvents," Lab Chip 6, 66-73 (2006).

[7] Yuan, D., and Das, S., "Experimental and theoretical analysis of direct-write laser micromachining of polymethyl methacrylate by CO_2 laser ablation," J. Appl. Phys. 101, 024901 (2007).

[8] Huang, F. C., Chen, Y. F., and Lee, G. B., "CE chips fabricated by injection molding and polyethene/thermoplastic elastomer film packaging methods," Electrophoresis 28, 1130-1137 (2007).

[9] Woolley, A. T., and Mathies, R. A., "Ultra-high-speed DNA fragment separations using microfabricated capillary array electrophoresis chips," Proc. Natl. Acad. Sci. USA 91, 11348-11352 (1994).

[10] Martinez, A. W., Phillips, S. T., Wiley, B. J., Gupta, M., and Whitesides, G. M., "FLASH: A rapid method for prototyping paper-based microfluidic devices," Lab Chip 8, 2146-2150 (2008).

[11] Li, X., Tian, J., and Shen, W., "Thread as a versatile material for low-cost microfluidic diagnostics," ACS Appl. Mater. Interfaces 2, 1-6, (2010).

[12] Mukhopadhyay, R., "When PDMS isn't the best," Anal. Chem. 79, 3248-3253 (2007).

[13] Lee, J. N., Park, C., and Whitesides, G. M., "Slovent compatibility of poly(dimethylsiloxane)-based microfluidic devices," Anal. Chem. 75, 6544-6554 (2003).

[14] Sundarajan, N., Pio, M. S., Lee, L. P., and Berlin, A. A., "Three-dimensional hydrodynamic focusing in polydimethylsiloxane (PDMS) microchannels," J. Microelectromech. Syst. 13, 559-567 (2004).

[15] Gosset, D. R., Weaver, W. M., Mach, A. J., Hur, S. C., Tse, H. T. K., Lee, W., Amini, H., and Di Carlo, D., "Label-free cell separation and sorting in microfluidic systems," Anal. Bioanal. Chem. 397, 3249-3267 (2010).

[16] Zagnoni, M., and Cooper, J. M., "A microdroplet-based shift register," Lab Chip 10, 3069-3073 (2010).

[17] Santiago, J. G., "Electroosmotic flows in microchannels with finite inertial and pressure forces," Anal. Chem. 73, 2353-2365 (2001).

[18] Haubert, K., Drier, T., and Beebe, D., "PDMS bonding by means of a portable, low-cost corona system," Lab Chip 6, 1548-1549 (2006).

[19] Eddings, M. A., Johnson, M. A., and Gale, B. K., "Determining the optimal PDMS-PDMS bonding technique for microfluidic devices," J. Micromech. Microeng. 18, 067001 (2008).

[20] Lin, C. –H., Lee, G. –B., Lin, Y. –H., and Chang, G. -L., “A fast prototyping process for fabrication of microfluidic systems on soda-lime glass,” J. Micromech. Microeng. 11, 726-732 (2001).

[21] Chen, Q., Li, G., Jin, Q. –H., Zhao, J. –L., Ren, Q. –S., and Xu, Y. –S., “A rapid and low-cost procedure for fabrication of glass microfluidic devices,” J. Microelectromech. Sys. 16, 1193-1200 (2007).

[22] Satyanarayana, S., Karnik, R. N., and Majumdar, A., “Stamp-and-stick room-temperature bonding technique for microdevices,” J. Microelectromech. Sys. 14, 392-399 (2005).

[23] Oh, K., and Ahn, C. H., “A review of microvalves,” J. Micromech. Microeng. 16, R13-R39 (2006).

[24] Zhang, C., Xing, D., and Li, Y., “Micropumps, microvalves, and micromixers within PCR microfluidic chips: Advances and trends,” Biotech. Advan. 25, 483-514 (2007).

[25] Yu, C., Mutlu, S., Selvaganapathy, P., Mastrangelo, C. H., Svec, F., and Frechet, J. M. J., “Flow control valves for analytical microfluidic chips without mechanical parts based on thermally responsive monolithic polymers,” Anal. Chem. 75, 1958-1961 (2003).

[26] Geiger, E. J., Pisano, A. P., and Svec, F., “A polymer-based microfluidic platform featuring on-chip actuated hydrogel valves for disposable applications,” J. Microelectromech. Sys. 19, 944-950 (2010).

[27] Vyawahare, S., Sitaula, S., Martin, S., Adalian, D., and Scherer, A., “Electronic control of elastomeric microfluidic circuits with shape memory actuators,” Lab Chip 8, 1530-1535 (2008).

[28] Reynaerts, D., Peirs, J., and Van Brussel, H., “An implantable drug-delivery system based on shape memory alloy micro-actuation,” Sens. and Act. A, 61 455-462 (1997).

[29] Piccini, M. E., and Towe, B. C., “A shape memory alloy microvalve with flow sensing,” Sens. and Act. A 128, 344-349 (2006).

[30] Pemble, C. M., and Towe, B. C., “A miniature shape memory alloy pinch valve,” Sens. and Act. A 77, 145-148 (1999).

[31] Gui, L., and Ren, C. L., “Exploration and evaluation of embedded shape memory alloy (SMA) microvalves for high aspect ratio microchannels,” Sens. and Act. A 168, 155-161 (2011).

[32] Li, P. –Y. Givrad, T. K., Sheybani, R., Holschneider, D. P., Maarek, J. –M. I., and Meng, E., “A low power, on demand electrothermal valve for wireless drug delivery applications,” Lab Chip 10, 101-110 (2010).

[33] Yoo, J. –C., Her, H. –J., Kang, C. J., and Kim, Y. –S., “Polydimethylsiloxane microfluidic system with in-channel structure for integrated electrochemical detector,” Sens. and Act. B 130, 65-69 (2008).

[34] Yang, B., and Lin, Q., “A latchable microvalve using phase change of paraffin wax,” Sens. and Act. A 134, 194-200 (2007).

[35] Pal, R., Yang, M., Johnson, B. N., Burke, D. T., and Burns, M. A., “Phase change microvalve for integrated devices,” Anal. Chem. 76, 3740-3748 (2004).

[36] Liu, R. H., Bonanno, J., Yang, J., Lenigk, R., and Grodzinski, P., “Single-use, thermally actuated paraffin valves for microfluidic applications,” Sens. and Act. B 98, 328-336 (2004).

Chapter 6

Detection of Biotin using Cavities (Proof-of-Principle)

6.1 Introduction

The results from the previous two chapters, namely increased coupling of light into slotted photonic crystals and integration of microfluidic channels, enabled practical sensor chips to be constructed. As mentioned in Chapter 2, biosensors are distinguished from refractive index sensors by the addition of specific receptors on their surface. These receptors, for example single stranded DNA or antibodies, allow only matching biomolecules to properly bind to them. This introduces another feature in the sensor response. In addition to a bulk refractive index change from the analyte, there will also be a surface refractive index change due to this binding. Changes in surface refractive index result in corresponding shifts in wavelength of the device's spectrum, which can be tracked using sharp spectral features. The bigger the shift, the more material that has bonded. As this process depends on diffusion of the target molecules to receptors on the sensor surface, the response of the sensor, and especially the time-response, will be limited by diffusion. The time-response curve gives an indication of the target concentration, and is specific to the target molecules alone and not to other sample constituents.

Sharp spectral features can be realised through the use of cavities within photonic crystals. The slotted photonic crystal cavity used in this section is a variant of the heterostructure design of the group of Noda [1]. It was designed and previously used by Dr Andrea Di Falco in the group to demonstrate its refractive index sensing capabilities; in his case measuring different concentrations of glucose [2]. In this chapter, the additional layers of microfluidics and surface receptors are included to investigate its usefulness as a biosensor. Proof-of-principle measurements with the avidin-biotin system are presented.

6.2 Slotted Photonic Crystal Cavity

6.2.1 Coupling Mechanisms

As explained in Chapter 3, photonic crystals are effectively very efficient wavelength dependent mirrors; only certain wavelengths can be supported by a lattice of a given period and fill factor. Cavities with high quality factor can be created by locally altering the lattice properties, and hence operational wavelength, of a defect region. This introduces a forbidden bandgap frequency into the otherwise perfect lattice. As it is forbidden, the surrounding lattice acts as a mirror, confining this frequency to the defect alone. Light inside this cavity can bounce between the mirrors hundreds or thousands of times, the limiting factor being the mirror and cavity medium propagation losses.

Although high quality factor cavities can be constructed in photonic crystals, an additional difficulty is the method used to couple light of resonant wavelength into them in the first place. One common waveguide technique is to use a side coupling method. In side coupling, a waveguide region capable of supporting the cavity defect resonant wavelength is placed in parallel, but displaced by several rows, to the cavity region as shown in Fig 6.1 a). This design

contains effectively two line defect photonic crystal waveguides. One of these waveguides supports the cavity resonance, which I will refer to as the 'bus waveguide', whilst the other does not, which I refer to as the 'mirror waveguide'. This difference in behaviour can be realised by altering the position of the first row of holes on either side of the waveguides. The cavity defect is placed in the centre of the mirror waveguide. As light is guided along the bus waveguide, it penetrates into the surrounding lattice, through an exponentially decaying evanescent field. This field can excite the cavity mode if its wavelength matches that of the cavity resonance, and the cavity is sufficiently close to the bus. A dip in the transmission spectrum of the bus waveguide is produced at the resonant wavelength. As it is easier to resolve a peak in transmission against a dark background, versus a dip in transmission from a bright background, the side coupling method shown in Fig 6.1 b) is sometimes used. In this case an input and output bus are used, which are separated by several periods. Light from the input bus can couple into the cavity at the resonant wavelength, before out-coupling into the output bus, the end result being a peak in the transmission spectrum at the cavity resonance. The advantage of using this method is the lack of interfaces and the clarity of the cavity spectrum. The big disadvantage is that when working with resonances of very narrow linewidth, there is very little light to work with for sample alignment purposes.

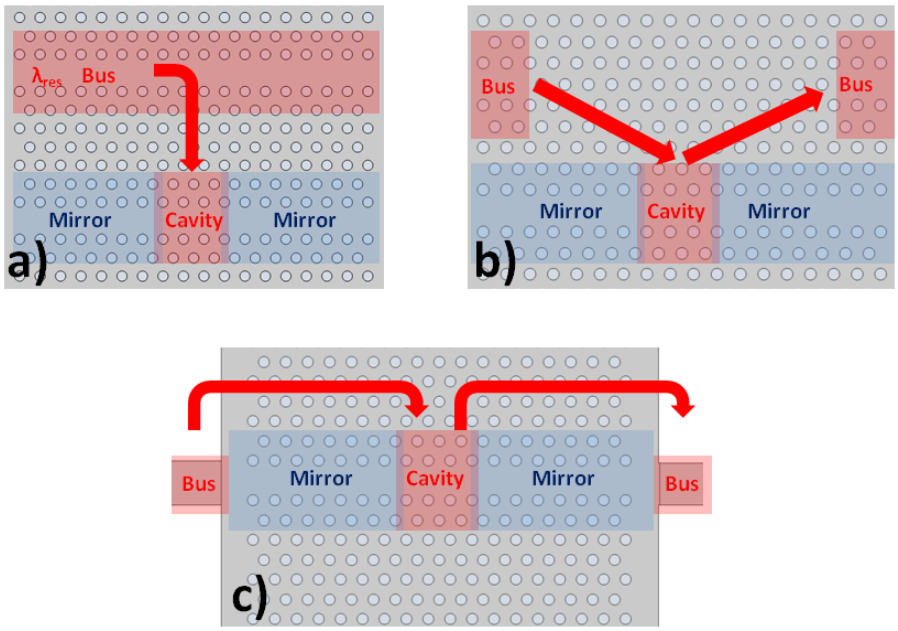

Figure 6.1: Common photonic crystal cavity coupling mechanisms. a) Side coupling from bus waveguide produces dip in transmission spectrum. b) Side coupling using input and output buses produces peak in transmission. c) In-line coupling produces cavity peak plus guided wavelengths of mirror waveguide region.

One approach that gives a cavity peak *and* is also easier to align is that of in-line coupling as shown in Fig 6.1 c). This is used for the devices in this chapter. In this case, light of resonant wavelength couples from the mirror interface, into the cavity, and back out to the waveguide beyond the second mirror. This produces a peak in the transmission spectrum as in the case of Fig 6.1 b). The important difference is that other wavelengths of light which are guided, rather than reflected, by the wavelength dependent mirrors can pass through. This produces a broad region of high signal within the output transmission spectrum which can be used for alignment

purposes. The full spectrum therefore shows a broad region of high transmission, with a stopband at the mirror wavelengths, within which lies the transmission peak of the cavity resonance. The disadvantage of this approach is that there are more interfaces to consider.

6.2.2 Photonic Crystal Heterostructure Cavity

These coupling schemes can be used for the photonic crystal cavities of both Noda [1] and Notomi [3]. In the heterostructure cavity of Noda, the lattice is locally expanded in one direction along a W1 (single row of missing holes) waveguide for a few lattice periods as shown in Fig 6.2 c). The lattice remains unaltered on either side of this defect. The unaltered part has the photonic band structure shown in Fig 6.2 b), the waveguide mode shown being the guided mode of the W1. By expanding the lattice of the defect region, the amount of dielectric in this part of the crystal increases. This effectively lowers the operational frequency of the defect, moving it further down in the band diagram. As frequencies just below the waveguide mode cut-off are within the bandgap and thus not supported by the lattice or the unaltered W1, the defect has a forbidden frequency. This effectively creates a 'mode gap' [1] within the bandstructure as shown in Fig 6.2 d). Only light of a certain frequency can be supported in the defect region, and is confined by the surrounding lattice which acts as a mirror. Notomi's cavity [3] uses similar principles for forming a cavity, except a few holes are moved outwards in a directional perpendicular from the W1 to reduce the frequency below the waveguide mode. In both cases very high quality factors can be reached.

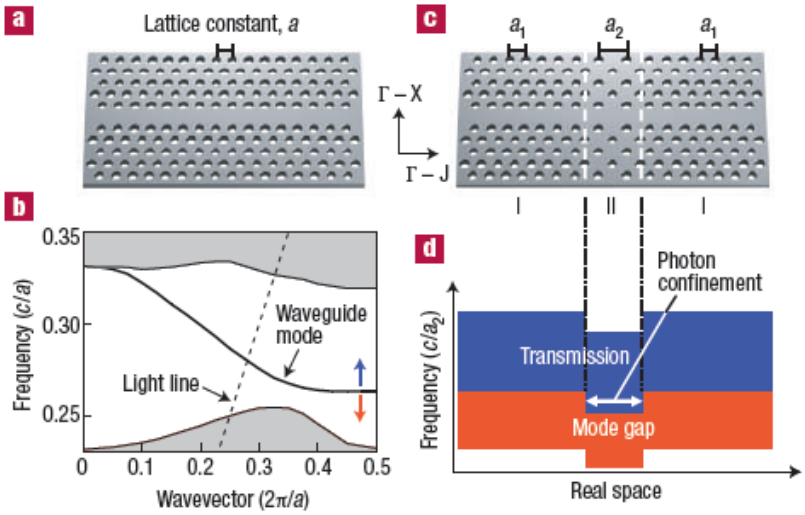

Figure 6.2: Photonic crystal cavity heterostructure design of Noda (reproduced with permission of Nature Publishing Group from [1], Copyright 2005). a) W1 defect and b) its bandstructure. Waveguide mode is pulled down from air band by the removal of holes that creates W1. c) Heterostructure cavity created by locally expanding lattice period in one direction along W1. d) Band diagram in waveguide direction of heterostructure.

6.2.3 Slotted Photonic Crystal Heterostructure Cavity

As was seen in Chapter 3, a slotted photonic crystal waveguide pulls a mode up from the dielectric band, rather than the more familiar pulling down from the air band used by W1 defects. This is due to the fact that a W1 involves the removal of air (holes), whereas a slotted photonic crystal involves the addition (the slot). The different nature of these defects results in the gradient of their fundamental modes being opposite in sign. To form a cavity in the slotted photonic crystal architecture therefore requires the opposite approach to that of the W1. As shown by my colleague Andrea Di Falco, heterostructure cavities within slotted photonic crystal require a *compression*, rather than expansion, of the lattice [2]. As the waveguide mode of the slotted photonic crystal cuts-off at high frequency, a new forbidden frequency can be introduced by increasing the frequency slightly into the bandgap, one way being lattice compression. With this design Dr Di Falco has demonstrated theoretical quality factors of 80,000 in air, 6,000 in water, and experimental values of 50,000 in air and 4,000 in water [2].

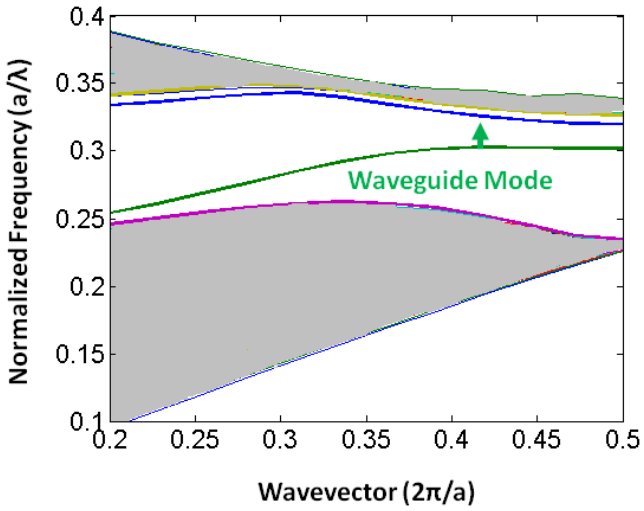

Figure 6.3: Bandstructure of slotted photonic crystal waveguide showing waveguide mode. A small local compression of the lattice period reduces the amount of dielectric, which in turn raises the operational frequency further into the forbidden bandgap region.

Slotted photonic crystal cavities are advantageous for sensing applications as most of the field interacts with contents of the air slot, as shown in the FDTD simulation of Fig 6.4. In conventional photonic crystal cavities and other devices such as ring resonators, most of the light is locked up by total internal reflection inside the dielectric of the waveguide structure, and only the evanescent tail of the optical mode sees the analyte of interest. In the slotted photonic crystal case a change in the refractive index of the slot contents is felt by the peak of the cavity mode, altering the resonant wavelength of the system more strongly. Dr Di Falco has demonstrated the refractive index sensing abilities of these cavities, detecting changes in dissolved sugar concentrations (cast in drops on top of the device) with an experimental sensitivity value of up to 1500 nm/RIU (500 nm/RIU theory) [2]. It should be noted that the experimental sensitivity was observed to be much higher than the theoretical sensitivity as a result of changing wetting properties with dissolved sugar concentration [2]. The work

presented here combines the results of the previous two chapters with surface functionalization chemistry, the goal being to produce a biosensor with these cavities.

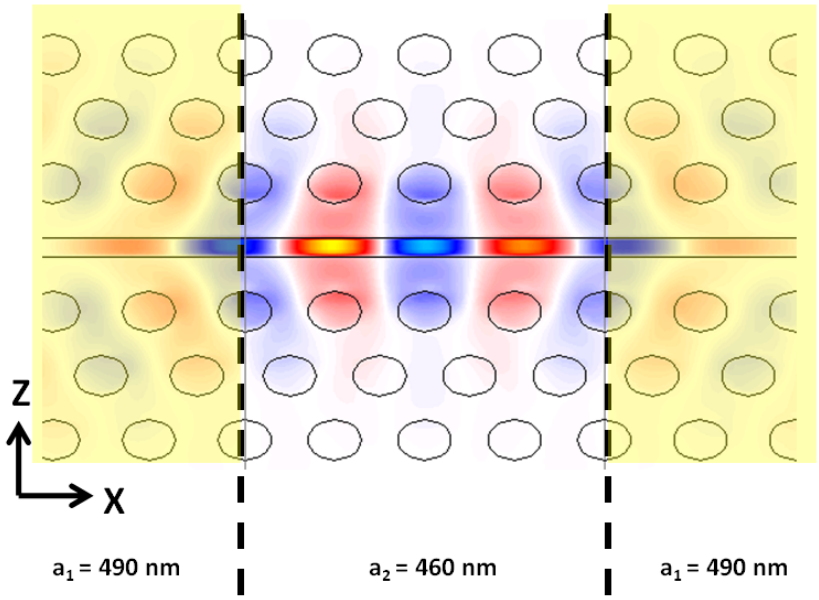

Figure 6.4: 2D FDTD simulation of an air slotted photonic crystal cavity mode showing Ez component. Mirrors are highlighted in yellow. The majority of the field intensity is confined to the slot, a property which lends itself to sensing because of the resulting strong light-matter interaction.

6.3 Biosensing with Slotted Photonic Crystal Cavities

6.3.1 Biotin-Avidin

In order to test the cavity's potential as a biosensor, suitable capture agents and targets had to be chosen. We initially decided to investigate the avidin-biotin system, which was briefly mentioned in Chapter 2. Biotin is a vitamin commonly found in cells, and is thought to be involved in cell growth, metabolic processes and gene expression [4]. It is not produced by humans, but is present in our bodies through ingestion of plants and microorganisms [4]. Avidin is a protein commonly found in egg whites [5]. Biotin and avidin (and its other form streptavidin) have a very high affinity for each other; it is the strongest non-covalent biological interaction known to exist in nature [6]. Humans can in fact suffer from a biotin deficiency, affecting cell growth of hair and nails, when consuming excessive amounts of avidin rich egg whites [4].

This system is often used as a model system for studying protein interactions [7]. It can also be used to help immobilize a variety of antibodies on surfaces. Biotin can be conjugated to many other proteins; such proteins being said to be **biotinylated**. These proteins can then be captured by a (strept)avidin coated surface. Its use here is therefore of great interest as it could be adapted to suit most types of antibody, and thus different types of sensor.

6.3.2 Fabrication

Cavities were fabricated in SOI (as in Chapter 3) using the design shown in Fig 6.4. As the addition of water causes large shifts in the operational wavelength of the cavity, and the light source used has a limited bandwidth of 100 nm, lithographic tuning was used to compensate for this. Lithographic tuning utilises the fact that the spectrum of the photonic crystal can be shifted in wavelength by increasing the radius of the holes and the width of the slot. A range of doses were written to find the optimum parameters for the light source's spectrum. For operation at 1550 nm for water filled devices, a hole radius of 150 nm, and slot width of 180 – 200 nm were used. PDMS microfluidic channels of 40 µm height and 200 µm width were integrated with the chip as in Chapter 5. Devices were characterised using the setup shown in Chapter 3. It was found experimentally that most repeatable results occurred when using the interface design shown in Chapter 4. An SEM image of the structure is shown in Fig 6.5.

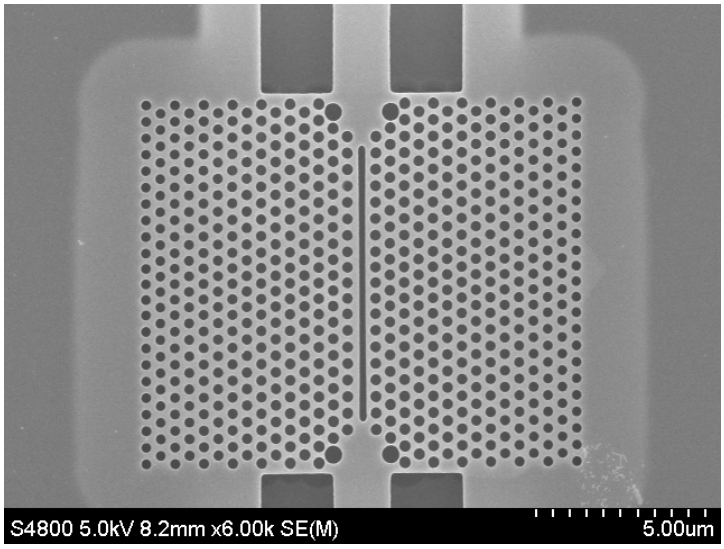

Figure 6.5: SEM image of slotted photonic crystal cavity fabricated in SOI.

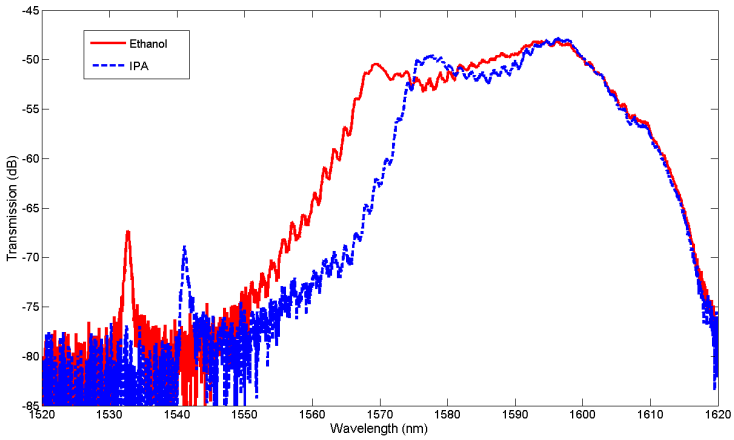

Figure 6.6: Transmission spectra of a slotted photonic crystal cavity with different alcohols injected into integrated microchannel.

As a first test different alcohols were introduced into the microchannel, as shown in Fig 6.6. The cavity peak (around 1532 nm for ethanol) is clearly distinguished from the bulk transmission of the mirror waveguide (above 1550 nm for ethanol). At 1550 nm, ethanol has a refractive index of approximately 1.354 and IPA has 1.378. Given that the shift in resonant wavelength in Fig 6.6 is approximately 10 nm, this corresponds to a refractive index sensitivity of approximately 415 nm/RIU, which is close to the theoretical value of 500 nm/RIU [2].

6.3.3 Functionalization Problems

Biotin can be immobilized on silicon dioxide surfaces using a chemical known as Aminopropyltriethoxysilane (APTES). This chemical binds to free OH groups on the surface of the glass, whilst presenting free NH2 groups for further functionalization. NHS-linked Biotin can attach to these NH2 groups [8]. In order to functionalize the photonic crystals with biotin receptors, a protocol similar to that of De Vos et al [9] was adopted, as they demonstrated biotin functionalization of silicon microphotonic structures.

Before bonding the microfluidics, the SOI chips containing the photonic crystals were immersed in Piranha solution for greater than 20 min to ensure that the surface was clean, hydrophilic, and to expose OH groups on the surface (from the resulting oxidation) to aid functionalization. The microfluidic circuitry was attached as in Chapter 5. After bonding the chip to a sample holder with silver conductive paint, the chip was placed in the optical characterization setup. Following De Vos [9], APTES was diluted in toluene to a concentration of 1% and was injected into the chip to sit for several hours. This step creates the NH2 groups for attaching the biotin. It was found, however, by a Masters project student within my group, Ulagalandha Perumal Dharanipathy, and later by myself, that the toluene within this solution caused the PDMS microfluidics to swell up, and in some cases even melt, destroying both the microfluidic circuitry and the silicon surfaces. The later step of biotin involved DMF, which has similarly detrimental effects on PDMS. I later discovered that this problem has previously been reported in the literature [10]. As noted by Whitesides' group [10], PDMS swells up in the presence of nonpolar organic solvents, one good example of which is toluene, with the amount of swelling varying between solvents.

In order to combat this problem, I tried a number of approaches. Liquid silica solutions such as Fox 14 were coated on the PDMS chip through spinning, and baking on a hotplate. The problem with this method was that Fox 14 requires baking to temperatures in excess of 400 °C, which are not suitable for PDMS (PDMS is thermally stable only up to approximately 180 °C), thus the full glass transition could not be allowed to take place. Another approach was to sputter thin layers of gold into the channel itself, masking the surrounding PDMS surfaces with tape during the procedure so as to protect the parts to be placed in contact with the silicon. This appeared to reduce the swelling in toluene, but resulted in reduced light transmission, suggesting the gold was scattering some of the light at the edges of the channel in contact with the silicon or that the gold was detaching when solutions were flowed through the channel. As I did not succeed in adapting the PDMS to the functionalization chemicals, I decided to change the chemistry. By studying some of the relevant literature [8, 9, 11-13] I realised that silicon surfaces can also be functionalized with APTES dissolved in many different solvents including ethanol and water. Some of these solvents only have very little effect on the PDMS. The immersion times also varied widely from a matter of minutes to 24 hours. After several test runs with different concentrations and timing, the protocol described below was adopted.

6.3.4 Functionalization Protocol

Following the piranha and microfluidic bonding steps mentioned above, ethanol was diluted to a concentration of 95 % in DI water (1 part DI to 19 parts ethanol). Using this solution, APTES was diluted to a concentration of 2 %. This was then injected into the microchannel and left overnight (typically 19 hours in total). No noticeable swelling or deterioration of the PDMS was detected. Using ethanol before and after this step as a reference, APTES was found to cause a shift of greater than 1 nm in the cavity peak wavelength. After this, the channel was flushed several times with ethanol and then DI water, and the whole chip was placed inside a 65 °C oven for over 5 hours in order to allow the APTES to cure. Biotinamidohexanoic acid N-hydoxysuccinimide (NHS linked biotin) ester powder (Sigma–Aldrich, UK) was dissolved in dimethylformamide (DMF) to a concentration of 1 mg/ml. This was then further diluted in phosphate buffered saline (PBS) to a concentration of 100 µg/mL. This was flowed into the cured chip, and left to sit in the channel for over 12 hours in order to saturate the surface with biotin receptors. Using blank PBS before and after biotin immobilization as a reference, biotin was found to induce a wavelength shift of greater than 2 nm. The chip was then flushed several times with PBS. As the APTES and biotin steps both caused shifts in wavelength that did not recover after flushing with ethanol and PBS respectively, this suggests that the functionalization protocol was successful.

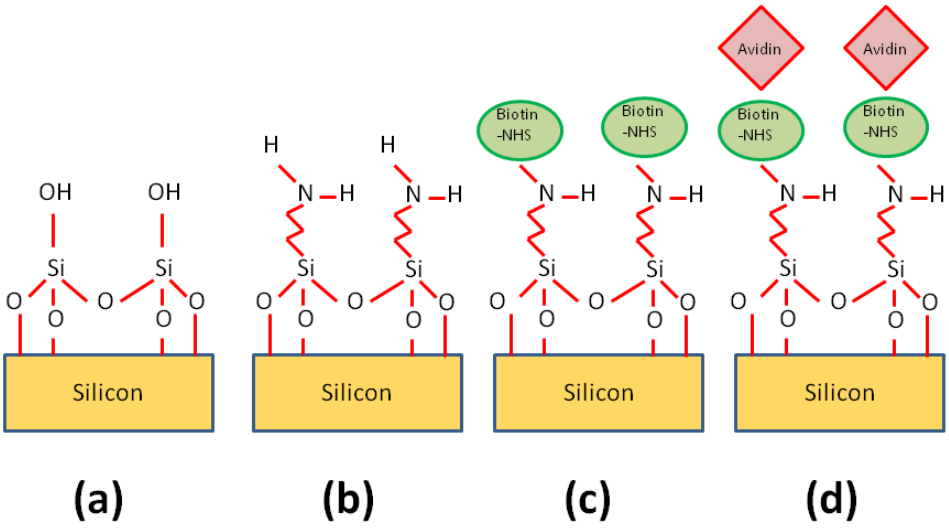

Figure 6.7: Biotin functionalization of silicon surface using APTES. a) Silicon immersed in Piranha solution to expose OH groups on surface. b) APTES links to OH groups on surface and presents NH2 groups. c) NHS linked biotin attaches to NH2 groups. d) Avidin captured by immobilized biotin.

6.3.5 Avidin Biosensing Experiments

To test the performance of the device, avidin from egg-white lyophilized powder (Sigma–Aldrich, UK) was diluted down to 10 µg/ml in PBS. After functionalization and optical alignment, a blank PBS solution was first used, before injecting the avidin, via a syringe and inlet tubing into the chip as shown in Fig 6.8 (see Chapter 3 for full optical setup). During this time the transmission spectra of the slotted photonic crystal was recorded from the optical

spectrum analyser (OSA). The results are shown in Fig 6.9, which depicts the variation in the peak wavelength of the cavity versus time.

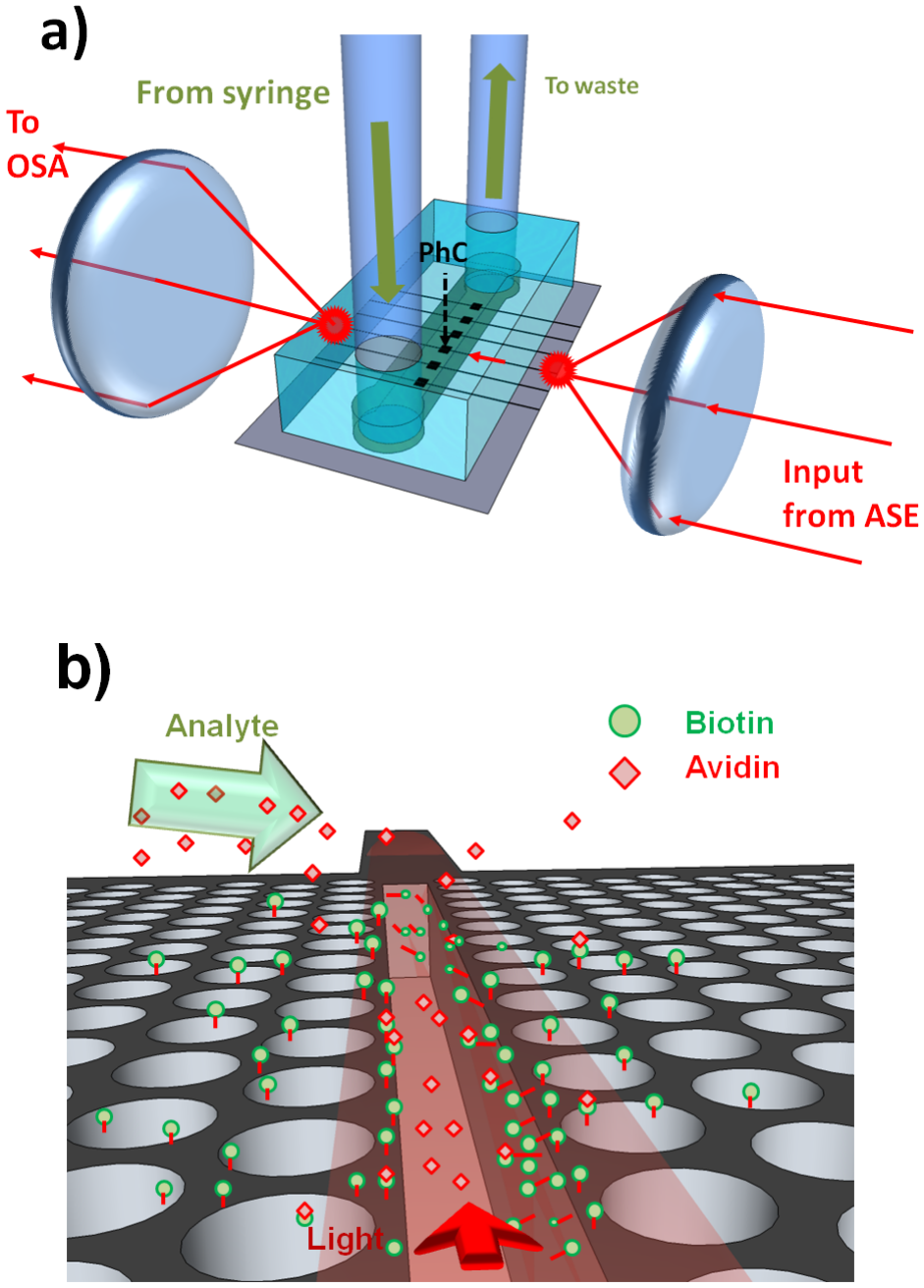

Figure 6.8: Biosensing experimental setup (not to scale). a) Light focused into optical waveguide at front edge. This light is then taken through the photonic crystal (inside the microfluidic channel) and then to the back edge where it is collected. Liquids are passed through the microchannel via connected tubing and syringe. b) Avidin binds to the biotin coated sensor inducing a shift in the cavity peak wavelength.

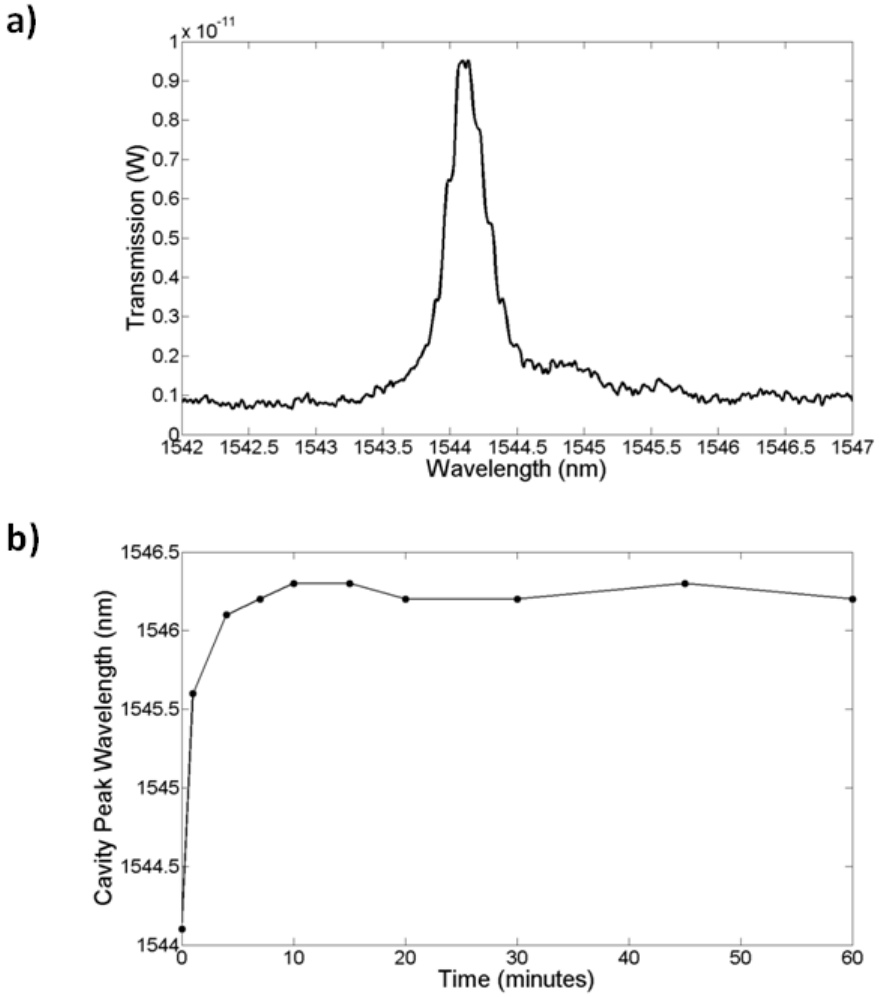

Figure 6.9: Initial avidin biosensing experiments. a) Cavity transmission spectrum. b) Cavity peak wavelength as a function of time for 10 µg/mL concentration.

The results of Fig 6.9 showed that avidin binding produced a large response, and that this response is shaped by diffusion. 30 minutes was also found to be sufficient to reach saturation. In order to test the lowest limit of detection another fresh chip was fabricated and functionalized as before. This time, avidin was serially diluted in PBS from 100 µg/mL down to 1 ng/mL. Each solution was introduced in order of increasing concentration into the chip and left to sit for typically 30 min each. Spectra were taken every minute using the high sensitivity setting on the OSA to reduce noise, and a smallest resolution of 0.05 nm; whilst the cavity peak wavelength was extracted from a Lorentzian fit. Whilst some errors will result from the fit, given that the shifts in wavelength during binding were greater than the linewidth of the cavity, these fitting errors were assumed to be negligible. The results of the binding are shown in Fig 6.10. Note that all of these measurements were performed on a single slotted photonic crystal.

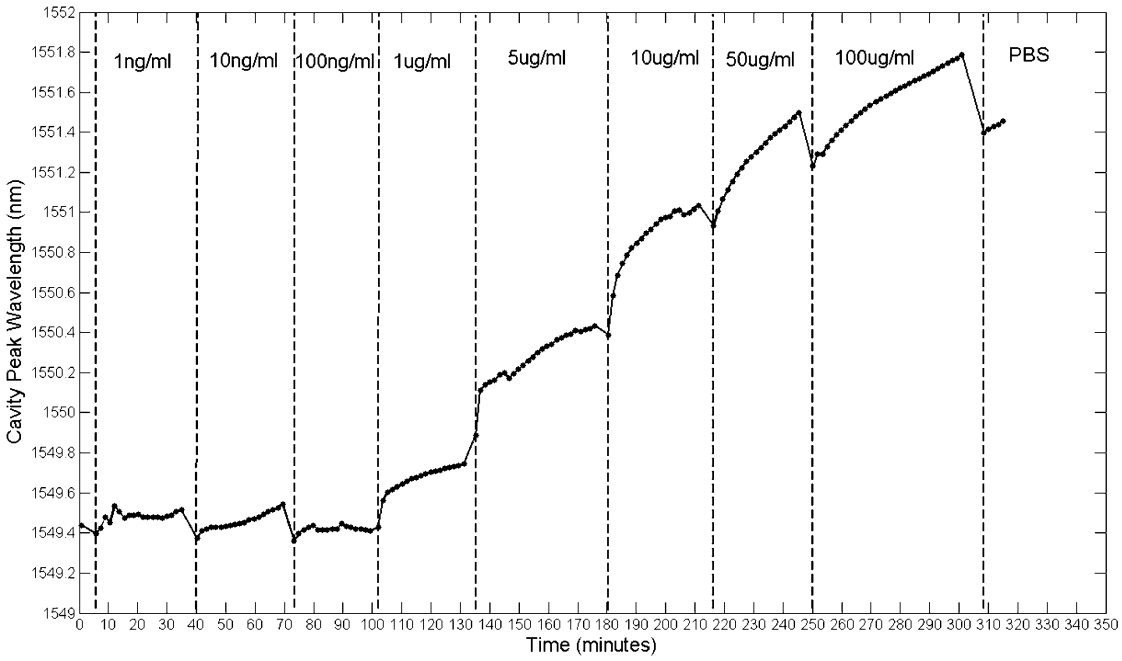

Figure 6.10: Cavity peak wavelength for a single slotted photonic crystal cavity as a function of time for different concentrations of avidin in PBS.

Fig 6.10 highlights again that the time-response of the sensor is dominated by diffusion. Whilst the experiment was only run for 30 min per concentration, leaving it for longer would allow these diffusion curves to plateau at their respective saturation values. Each concentration has a different curve. As expected, lower concentrations have shallower gradients. The little dips in sensor response at each injection point can be attributed to the flushing of material that has not properly bonded to the biotin [14]. A better measure of the actual bound material are therefore these dip points, as here the unbound material has been discarded. Taking these points, Fig 6.11 shows how the sensor response for a thirty minute reaction varies for different avidin concentrations. The lowest concentration that can be clearly observed is 1 µg/mL, though perhaps even 100 ng/mL can also just be resolved. The cavity peaks for each of these points is shown in Fig 6.12. The average quality factor was estimated to be 3,000.

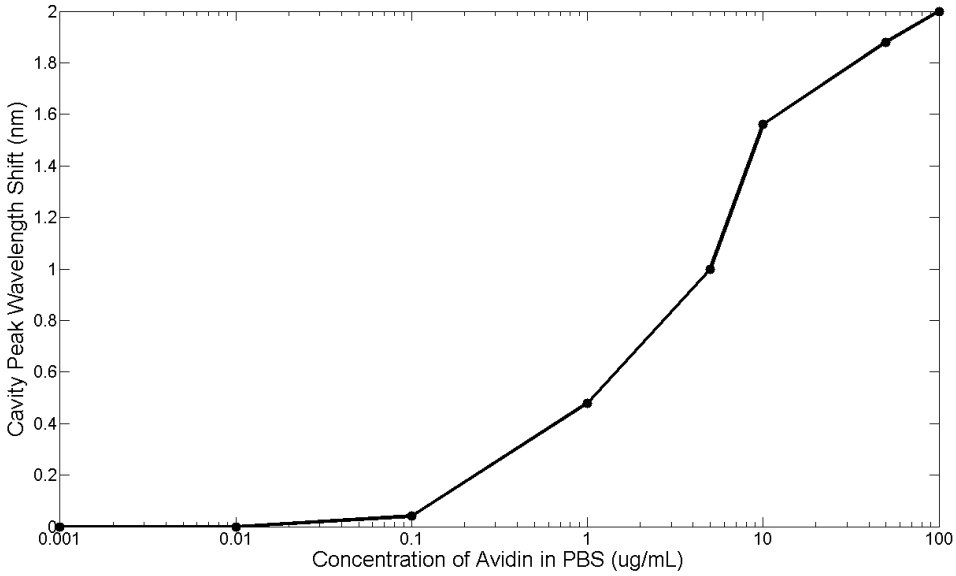

Figure 6.11: Cavity peak wavelength shift after binding for each avidin concentration.

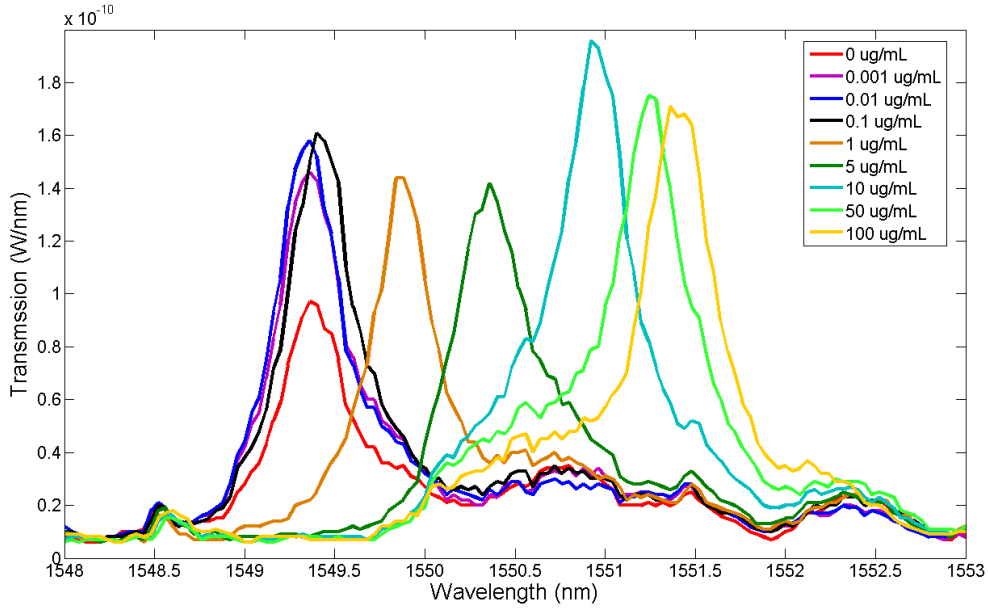

Figure 6.12: Transmission spectra at each of the points in Fig 6.11.

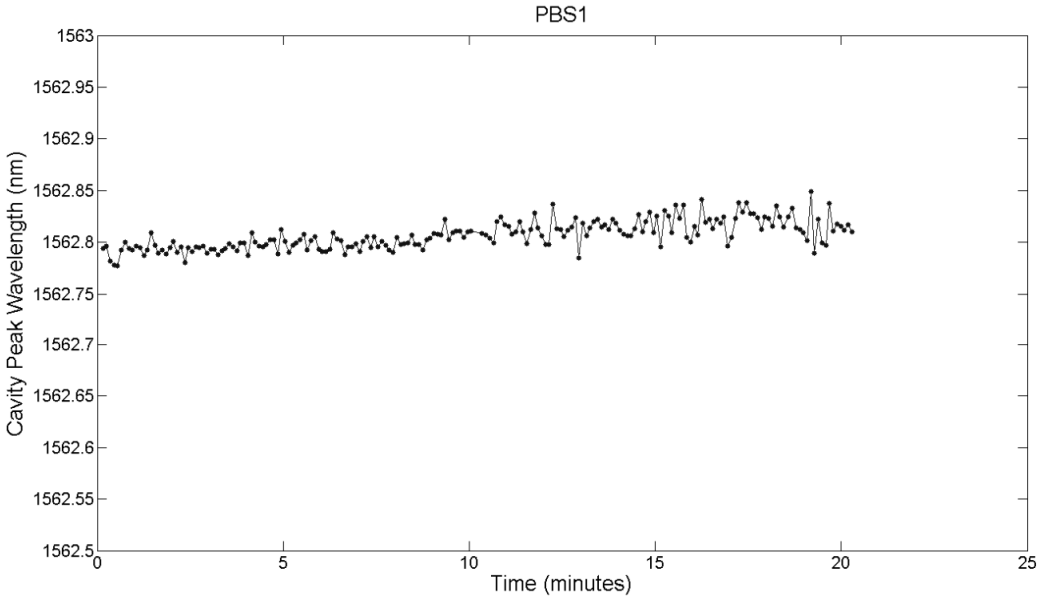

Figure 6.13: Cavity peak wavelength as a function of time for PBS filled microchannel.

6.3.6 Analysis

From Figs 6.10 & 6.11, a dissolved avidin concentration of 1 µg/mL was clearly detected. As avidin has a molecular weight of 68 kDa [15], this corresponds to a molar concentration of 15 nM. Given that the sample stage was not temperature controlled, thermal noise must be taken into consideration. For de-ionised water at a temperature of 20 °C, light of wavelength 1550 nm experiences a thermo-optic coefficient of approximately 10^{-4} RIU/°C [16]. Assuming a maximum temperature fluctuation of 0.5 °C within the lab over the time period for each concentration, and the refractive index sensitivity of the slotted photonic crystal cavity being 500 nm/RIU, this would correspond to a shift in resonant wavelength of 0.025 nm. Even assuming an order of magnitude higher thermo-optic coefficient of 10^{-3} RIU/°C would produce a shift of 0.25 nm. In both cases, the wavelength shift is smaller than the shifts observed for avidin concentrations above and including 1 µg/mL. To experimentally test the thermal stability of the PBS solutions, the cavity peak wavelength for a PBS filled channel was recorded over a 20 min period. The results shown in Fig 6.13 show fluctuations in wavelength of less than ~0.05 nm, which is consistent with a thermo-optic coefficient of $5\text{x}10^{-4}$ RIU/°C. With these numbers, and given the linewidth of the cavity, it is fair to say that binding can be attributed to wavelength shifts of greater than 0.1 nm. Better environmental control should allow this number to be reduced in future. Comparing with other devices shown in Table 2.1 (Chapter 2), an experimental detection limit of 15 nM is impressive given the small size of the slotted photonic crystal cavity. To aid comparison further, an estimate of the surface density and bound mass is also made. For the smallest observed wavelength shift $\delta\lambda$ (in this case taking 0.4 nm for 1 µg/mL) the surface density of bound material σ_p can be estimated from equation [17]:

$$\frac{\partial\lambda}{\lambda} = \sigma_p \alpha_{ex} \frac{2\pi\sqrt{n_m^2 - n_s^2}}{\varepsilon_0 \lambda^2} \frac{n_m}{n_s^2} S \qquad (6.1)$$

where α_{ex} is the excess polarizability of the molecule, n_m is the refractive index of the sensor substrate, n_s is the refractive index of the buffer solution and S is the bulk refractive index sensitivity (see Chapter 2). Taking the values for this experiment: $\alpha_{ex} = 4\pi\varepsilon_0(3.2 \times 10^{-21})$ cm^3 [18], $n_m = 3.4$ (silicon), $n_s = 1.35$ (PBS), $S = 500$ nm/RIU [2], $\delta\lambda = 0.4$ nm and $\lambda = 1550$ nm, the bound surface density is found to be 5×10^8 molecules/mm^2. For avidin, this corresponds to a surface mass density of 60 pg/mm^2. From FDTD simulations of the cavity (see Fig 6.4), the sensing surface area is estimated to be as low as 2.2 μm^2 (based on the surface area of the slot walls within, and the 6 holes surrounding, the cavity), thus the bound mass detected is of the order of 100 ag. As per the discussion in Chapter 2, such numbers should be used with caution, as they are based on assumptions. The concentration limit of detection is the most reliable quantity as this was actively controlled; it should be noted, however, that this value will differ for different antibody-antigen pairs. Although a biotin solution is left in contact with the substrate for several hours in order to ensure saturation, and the specificity of this protocol has already been established [9], non-specific binding could be eliminated by adding suitable blocking agents to the protocol.

Given that the sensing area is only 2.2 μm^2, an observed detection limit of 15 nM is impressive when compared with much larger devices (> 250 μm^2) in the literature (see Chapter 2). This result highlights the increased light-matter interaction of slotted photonic crystal cavities. Wavelength shifts comparable to that of much larger structures can be observed in smaller devices. Compactness allows potential for hundreds of these devices to be integrated onto a centimetre scale chip. When combined with the antibody patterning techniques discussed in Chapter 2, this would allow hundreds of independent biological tests to be conducted simultaneously using a minimum amount of precious analyte. The disadvantage when compared with larger structures is that the target sensing area is much smaller. When dealing with very low concentrations, the target molecule may never see the 2.2 μm^2 sensing area on a reasonable timescale. This is a general limitation of all surface affinity based biosensors. Microfluidics has potential to help here. One simple way of improving performance would be to flow samples *through* the photonic crystal membrane, rather than over it, as demonstrated by Eftekhari *et al* [19]. The disadvantages of this particular approach are the potential for clogging the holes, and also for false signals due to pressure effects distorting the membrane. Water absorption at 1550 nm also impacts on the performance of the device, by reducing the quality factor of the cavity. Shifting to shorter wavelengths would reduce this problem allowing higher sensitivities. 1550 nm was chosen here due to the wide availability of sources and detectors and the group's familiarity with working at this wavelength. The lowest water absorption occurs at visible wavelengths, but this is inaccessible with slotted photonic crystals fabricated in silicon, due to strong absorption of silicon below 1000 nm. Other materials (such as polymers) that are transparent at such wavelengths do not have as high a refractive index as silicon, and are thus not of sufficient index contrast necessary for the slot waveguide effect. Reducing the wavelength also requires downscaling the photonic crystal parameters (radius, slot width, period), which is harder to fabricate and increases potential for clogging. Despite these problems it is conceivable that performance could be improved by using wavelengths around 1300 nm.

Whilst the sensor device has been demonstrated to work with avidin, one of the key aims of my work is to develop practical devices for real applications. Many photonic devices presented in

the past have yet to take this step. The next chapter looks at some applications that have been explored during this project, whilst also looking at other unique sensor designs developed within this work, as well as potential solutions to key limiting problems such as on-chip sources and detectors.

References – Chapter 6

[1] Song, B. –S., Noda, S., Asano, T. and Akahane, Y., "Ultra-high-Q photonic double-heterostructure nanocavity," Nature Mat. 4, 207-210 (2005).

[2] Di Falco, A., O'Faolain, L. and Krauss, T. F., "Chemical sensing in slotted photonic crystal heterostructure cavities," Appl. Phys. Lett. 94, 063503 (2009).

[3] Kuramochi, E., Notomi, M., Mitsugi, S., Sinya, A. and Tanabe, T., "Ultrahigh-Q photonic crystal nanocavities realized by the local width modulation of a line defect," Appl. Phys. Lett. 88, 041112 (2006).

[4] Zempleni, J., Wijeratne, S. S. K., and Hassan, Y., I., "Biotin," Biofactors 35, 36-46 (2009).

[5] Melamed, M. D., and Green, N. M., "Avidin: Purification and composition," Biochem. J. 89, 591-599 (1963).

[6] Holmberg, A., Blomstergren A., Nord, O., Lukacs, M., Lundeberg, J., and Uhlen, M., "The biotin-streptavidin interaction can be reversibly broken using water at elevated temperatures," Electrophoresis 26, 501-510 (2005).

[7] Wilchek, M., Bayer, E. A. and Livnah, O., "Essentials of biorecognition: The (strept)avidin-biotin system as a model for protein-protein and protein-ligand interaction," Immun. Lett. 103, 27-32 (2006).

[8] Lapin, N. A. and Chabal, Y. J., "Infrared characterization of biotinylated silicon oxide surfaces, surface stability, and specific attachment of streptavidin," J. Phys. Chem. B. 113, 8776-8783 (2009).

[9] De Vos, K., Bartolozzi, I., Schacht, E., Bienstman, P., Baets, R., "Silicon-on-insulator resonator for sensitive and label-free biosensing," Opt. Exp. 15, 7610-7615 (2007).

[10] Lee, J. N., Park, C., and Whitesides, G. M., "Slovent compatibility of poly(dimethylsiloxane)-based microfluidic devices," Anal. Chem. 75, 6544-6554 (2003).

[11] Mandal, S., Goddard, J. M. and Erickson, D., "A multiplexed optofluidic biomolecular sensor for low mass detection," Lab Chip 9, 2924-2932 (2009).

[12] De Lisa, M. P., Zhang, Z., Shiloach, M., Pilevar, S., Davis, C. C., Sirkis, J. S., and Bentley, W. E., "Evanescent wave long-period fiber bragg grating as an immobilized antibody biosensor," Anal. Chem. 72, 2895-2900 (2000).

[13] Ksendzov, A. and Lin, Y., “Integrated optics ring-resonator sensors for protein detection,” Opt. Lett. 30, 3344-3346 (2005).

[14] Carlborg, C. F., Gylfason, K. B., Kazmierczak, A., Dortu, F., Banuls Polo, M. J., Maquieira Catala, A., Kresbach, G. M., Sohlstrom, H., Moh, T., Vivien, L., Popplewell, J., Ronan, G., Barrios, C. A., Stemme, G. and van der Wijngaart, W., “A packaged optical slot-waveguide ring resonator sensor array for multiplex label-free assays in lab-on-chips,” Lab Chip 10, 257-396 (2010).

[15] Green, N. M., “The molecular weight of avidin,” Biochem. J. 92, 16-17 (1964).

[16] Kim, Y. H., Park, S. J., Jeon, S. –W., Ju, S., Park, C. –S., Han, W. -T., and Lee, B. H., “Thermo-optic coefficient measurement of liquids based on simultaneous temperature and refractive index sensing capability of a two-mode fiber interferometric probe,” Opt. Exp. 20, 23744-23754 (2012).

[17] White, I. M., and Fan, X., “On the performance quantification of resonant refractive index sensors,” Opt. Exp. 16, 1020-1028 (2008).

[18] Arnold, S., Khoshsima, M., Teraoka, I., Holler, S., and Vollmer, F., “Shift of whispering-gallery modes in microspheres by protein adsorption,” Opt. Lett. 28, 272-274 (2003).

[19] Eftekhari, F., Escobedo, C., Ferreira, J., Duan, X., Girotto, E. M., Brolo, A. G., Gordon, R., and Sinton, D., “Nanoholes as nanochannels: Flow-through plasmonic sensing,” Anal. Chem. 81, 4308-4311 (2009).

Chapter 7

Real World Applications

7.1 Introduction

The previous chapters have shown the development of slotted photonic crystals as a platform for biosensing. The performance of these devices is in line with, or better than, the state-of-the-art (see Table 2.1). As touched upon within Chapters 1 and 2, many other microphotonic devices have been shown to be good biosensors. Very few, however, have addressed two of the key problems preventing them from leaving the research lab, namely:

1. **Real applications for genuine problems**
2. **Full integration of the device**

Whilst it will take a timescale of at least 5-10 years to develop slotted photonic crystal biosensors to a commercial level, this chapter shows initial groundwork already carried out during this project aimed at addressing the two problems above. During the project several collaborations were fostered with people in different disciplines including marine science, medical biology, engineering and physics. By speaking directly to potential end-users, this approach helped identify key problems in other fields that this technology could potentially solve. Many physics tools have suffered in the past from being solutions looking for a problem, whilst many biologists are perhaps not aware of what technologies are out there. To work in the field, which can often be a harsh and limiting environment compared to the lab, issues such as cost, size, power consumption and fragility all come into play. Many technologies are presented as 'proof-of-principle' demonstrations and are not carried through to practical devices. Whilst this is true to some extent for this body of work, significant efforts were made to tackle these issues. This chapter therefore not only looks at exciting applications such as detecting cellular material and toxins with help from these collaborators, but also how to make a fully integrated, practical device. All of these applications and designs are in early stages of development, but with the groundwork established here, it is conceivable that a practical device could be realised in the near future. The main point this chapter will demonstrate is the versatility of the slotted photonic crystal for biosensors, not only in what I can be used to detect, but in the potential for a total analysis system, light source, sensor and spectrometer, all made from slotted photonic crystals.

7.2 Exosomes

7.2.1 Introduction

Some of the initial results from Chapter 6 were presented to biologists at the Medical School, including Dr Simon Powis whose expertise includes exosomes. It was soon realised that there could be real potential for slotted photonic crystals to solve some of the mysteries of exosomes, thus an exciting collaboration was fostered with Dr Powis.

Exosomes are tiny packets of cellular material, roughly 40-100 nm on average in size, that are excreted by many types of biological cells [1]. They are of interest to biologists as much about them is unknown, but they are thought to have potential in many disease diagnostic and therapeutic applications [1, 2]. These packets can almost be thought of as cells in miniature, minus the internal machinery. Exosomes form when regions of a cell's membrane bud inwards, forming a sack-like structure within the cell's cytoplasm [2]. This sack is known as an early endosome. The walls of this sack can then bud inwards themselves forming the little bubbles (vesicles) that constitute exosomes. When this sack of exosomes (multi vesicular body) then fuses with the cell membrane, the exosomes are released from the cell into the surrounding medium [2]. Much of this information has been gained using labels attached to the membrane of a cell, and electron microscopy [1].

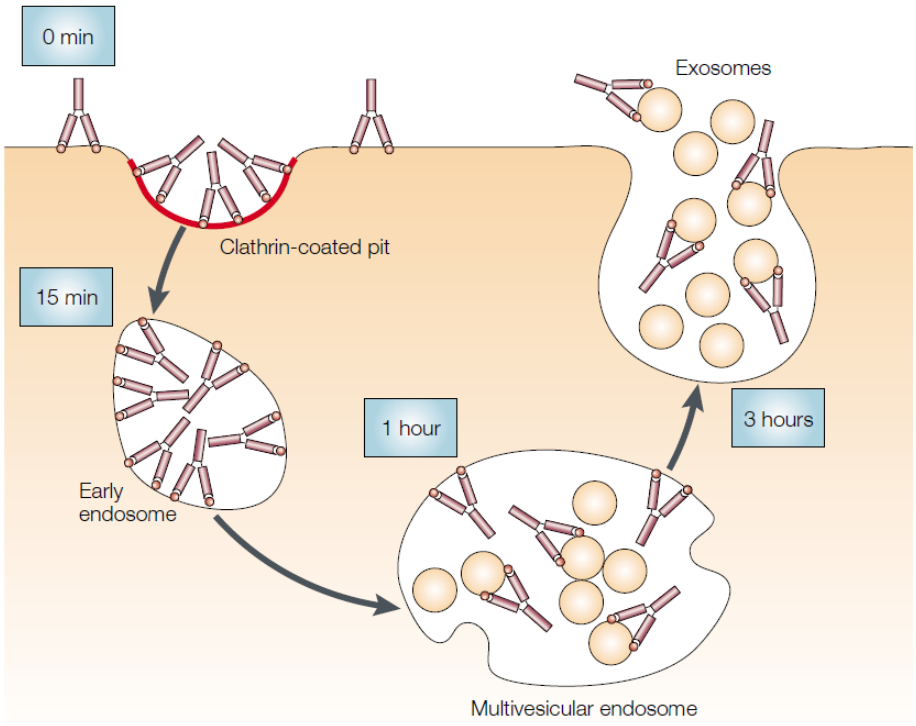

Figure 7.1: Exosome formation model (reproduced with permission of Nature Publishing Group from [2], Copyright 2002). Inward budding of cell membrane creates early an endosome, the subsequent inward budding of which creates exosome packets. Exosomes are released from cell when the endosome fuses with cell membrane. Exosomes can carry proteins that were embedded in the cell membrane during their formation.

Initially, exosomes were thought of as little 'trash bags' for removing waste from the cell, but in recent years their perceived importance has been growing [3]. Exosomes can travel to, and fuse with, other cells. As exosomes are formed from the cell's membrane, they contain proteins and other materials that were embedded within it [4]. Exosomes can therefore carry proteins and other materials such as mRNA and microRNAs between different cells; and are thought to mediate some form of communication link [1]. If these proteins, or some other marker, could be identified on the exosome, then they could be used to infer the state of health of the original

cell [4]. Ideally, biologists would like to identify a marker on their surface that is indicative of disease, such as cancer [5]. The impact of this, if found to be practical, would be huge. Not only would they be of interest in diagnosing diseases such as cancer, but also in therapeutics. Exosomes are thought to be involved in cell stimulation and immune response [5-8]. Understanding this better could allow biologists to use exosomes as a way of delivering tumour rejection antigens or stimulating an immune response [7]. Exosomes also pose questions about fundamental biology. Some believe they may even have virus-like properties, spreading nucleic acids and pathogens amongst cells [1].

Currently, exosomes can be isolated from cells using a series of centrifugation steps. Different spin speeds encourage sedimentation of particles of different size. Combining with filtration steps allows a pellet of exosomes to be formed, which can then be re-suspended in a medium [2]. The proteins on their surface can be identified from immuno-blotting techniques. Given their small size, exosomes cannot be observed using optical microscopes. Usually electron microscopes are needed [1, 4], which necessitates that they be treated somehow in order to be viewed under high vacuum. Whilst high resolution images can be obtained, the substances embedded within them cannot be identified from the image alone. Dr Simon Powis, our collaborator, has been using a machine known as Nanosight [9] to detect exosomes [10]. This machine uses a combination of light scattering and particle tracking to estimate the size distribution of nanoparticles within a medium [9]. We decided to try to see if slotted photonic crystals could be used not only to detect the presence of exosomes in real-time, but also what proteins are present on their surface. This could have potential in fast, label-free diagnostics, and perhaps even in experiments probing some of the fundamental mysteries of exosomes.

7.2.2 Initial Results

As a starting point, we looked at detecting exosomes with slotted photonic crystals without any functionalization. Sensor chips were fabricated as in Chapters 5 and 6. Dr Powis then provided exosomes taken from cell lines known as Jurkat and CEM, suspended in medium. These samples were stored in a fridge prior to the experiments, but could be left at room temperature for periods less than 24 hours. To minimize thermal effects impacting on the experiments, the vials containing the exosmes were removed from the fridge and placed in the optical lab more than 2 hours before the experiment, such that they reached thermal equilibrium. After alignment, serum free medium was first injected into the chip and spectra taken for several minutes to ensure stability. Following this, solutions of exosomes and serum free medium were alternated within the chip for several minutes at a time. As in Chapter 6, the cavity peak wavelength as a function of time was constructed using Lorentzian fits of the cavity spectra obtained from the OSA to extract the central wavelength.

Figure 7.2 a) shows the results. In each injection there is a clear difference in response between the exosomes and the blank medium. After the third injection of exosomes, the difference in response between the exosomes and the medium no longer changes. This behaviour seems to suggest that some material is gradually being coated or trapped in the slot, until some saturation level is reached. This saturation could be because the slot is clogged with exosomes. To test further, a sensor chip that had been previously been injected with exosomes was re-used. If the slot was indeed immobilizing the exosomes, some should be remaining from the last experiment. The results are shown in Fig 7.2 b). This behaviour is quite similar to the saturated response of Fig 7.2 a), suggesting that exosomes were still remaining inside the slot from the previous experiment. Whilst these results are inconclusive, they do suggest that slotted

photonic crystals can discriminate between a blank medium and a medium with exosomes. The next step was to look at functionalising the system, so as to make the test specific.

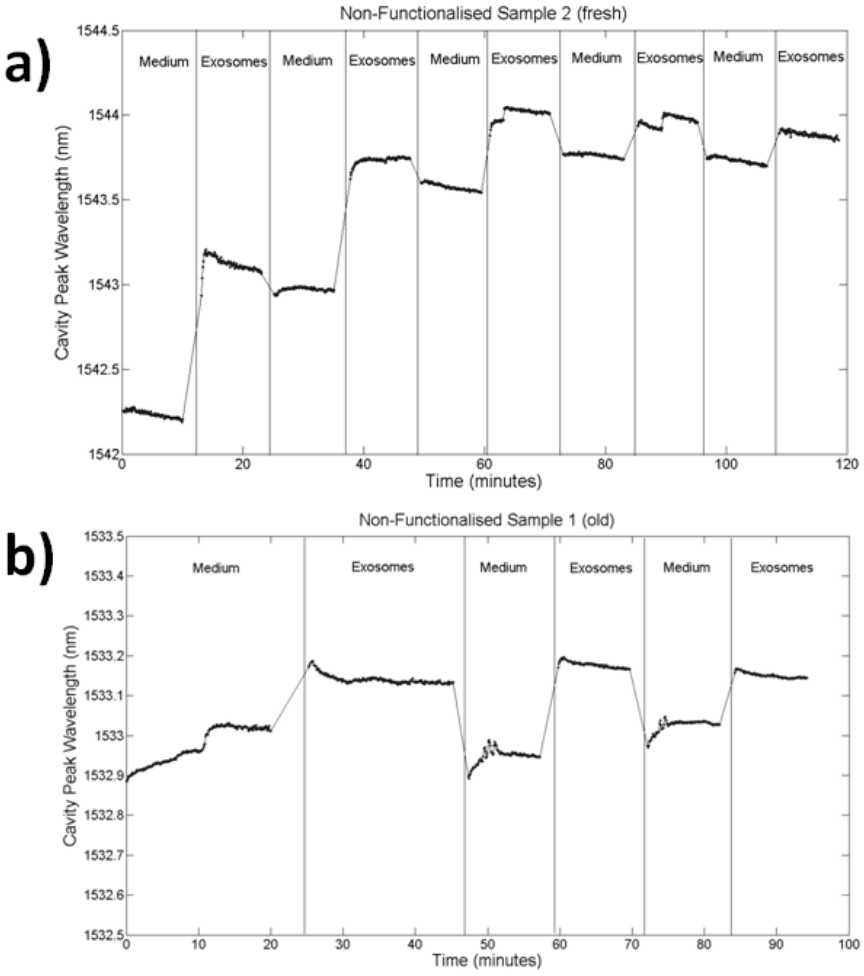

Figure 7.2: Sensor response for exosomes in a) fresh slot photonic crystal chip. b) Re-used chip.

7.2.3 Functionalisation Protocol

Exosomes can carry a variety of different proteins that are of interest in proteomics [4]. Dr Powis's research [10] has shown that exosomes from different cell lines can carry different proportions of proteins. One protein expressed strongly on the surface of the CEM and Jurkat lines was found to be CD45 [10]. If we could coat the sensor with antibodies that capture CD45 protein, this would allow a fast way of specifically detecting these types of exosomes. Fresh sensor chips were made, and Dr Powis provided fresh exosomes in addition to CD45 antibodies. After discussion with Dr Powis, a protocol was established to immobilize the CD45 antibodies on the surface of the slotted photonic crystal device. As they can also link to NH2 groups, the CD45 antibodies were used in conjunction with APTES, the chemical used to immobilize biotin in Chapter 6.

As before, the sensor chip was immersed in Piranha solution for 20 min before bonding the microfluidic circuitry on top. APTES was diluted to a concentration of 2% in 95% ethanol in DI. This was injected into the aligned chip and left to sit overnight. After flushing with ethanol and DI the chip was cured as before. Dr Powis supplied a vial of CD45 antibodies: 200 µL at a concentration of 50 µg/mL. As a first test, blank PBS (phosphate buffered saline) was injected into the sample. Next, the CD45 antibodies were injected and left to sit for a couple of hours. The initial sensor response is shown in Fig 7.3. As the response did not recover after a subsequent wash with pure PBS, this suggested that the antibodies had been immobilized as expected.

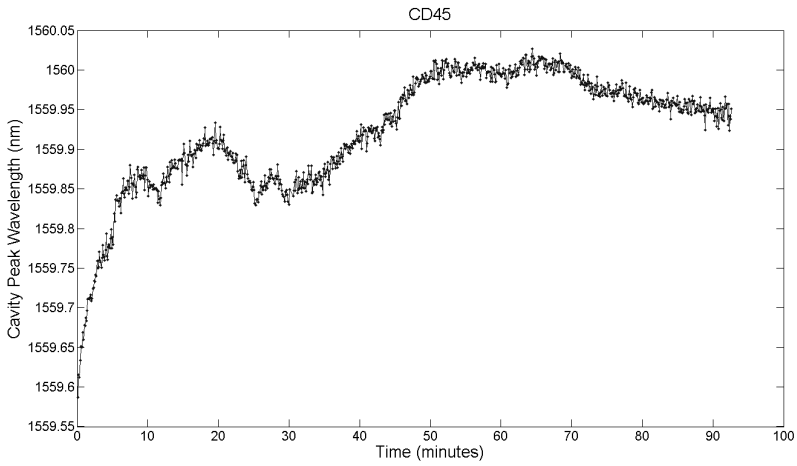

Figure 7.3: Cavity peak wavelength as a function of time after injection with CD45 antibody.

7.2.4 Exosome Detection using CD45 Antibodies

As the functionalization protocol appeared to work, the next step was to try and detect exosomes that carry CD45. After functionalising the chip as above, solutions of the blank medium alone and medium with exosomes were injected. The sensor response for one chip with Jurkat type exosomes, and another with CEM type exosomes, is shown in Fig 7.4.

Immobilization of material can be detected in both cases. In Fig 7.4 a), there is a sharp difference between blank medium and exosomes that does not recover after further flushings, suggesting the exosomes have been immobilized. In the case of CEM, it takes two injections to saturate. In both cases it seems like the exosomes have been captured, but there is a general underlying downward trend in response for blank medium and exosomes. This was observed in many different samples, yet its origin cannot be satisfactorily explained. At first, I thought that the downward trend was due to the presence of phenol red indicator in the samples which is used to monitor the health of the exosomes, but tests with medium not containing phenol red produced similar results. My best guess is that something in the medium attacks the silicon of the sensor, or that a chemical reaction between the antibodies and the medium causes a refractive index change. A downward shift is consistent with a reduction in refractive index, which favours the theory that the effective index of the slot is slowly reducing, possibly also

because the medium is etching the slot walls away. It may be possible in the future to use exosomes in PBS rather than in the medium to try and eliminate this, but this is more tricky to prepare and maintain. To test if these results are truly specific, a negative control test was carried out, as detailed in the next section.

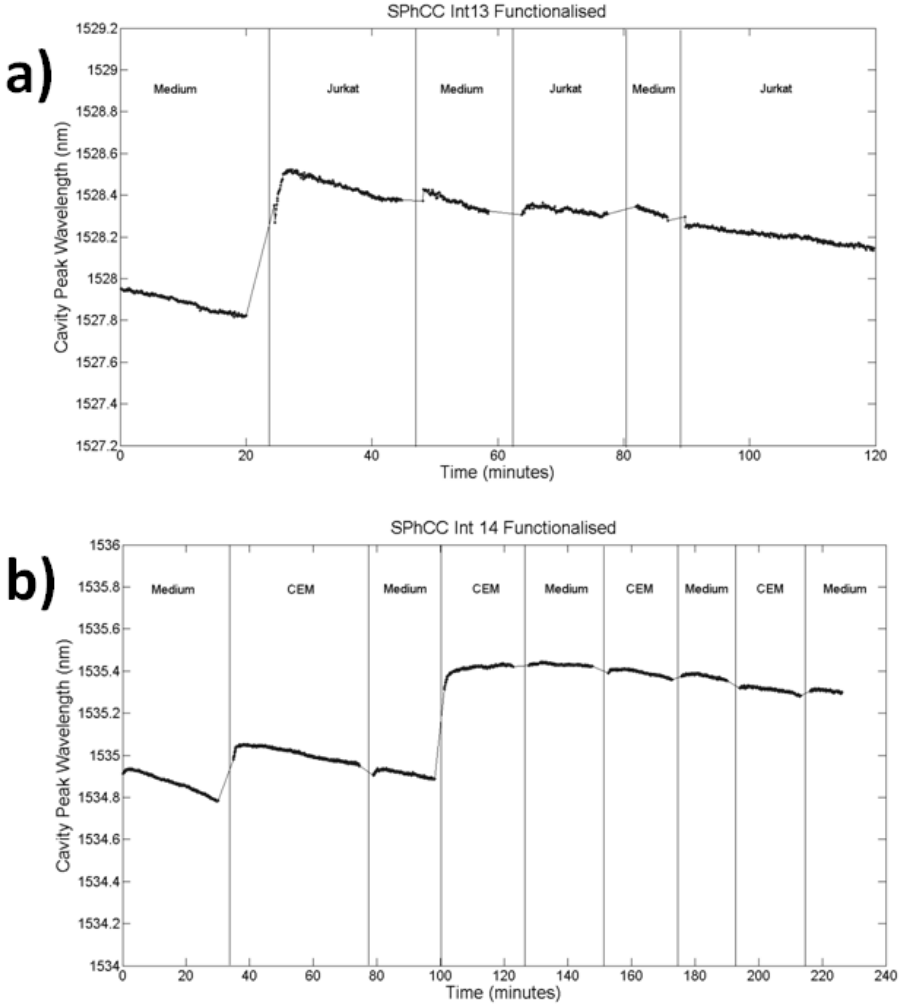

Figure 7.4: Exosome detection using functionalized chips. a) Jurkat line exosomes. b) CEM line exosomes.

7.2.5 Exosome Control Experiment

To test whether we could specifically detect the proteins on the surface of the exosomes with slotted photonic crystals, a negative control test was needed. Whilst Jurkat and CEM exosomes express CD45 on their surface, Dr Powis established that exosomes from the MDA cell line do not. An experiment to test the specificity was planned as follows. The sensor would be functionalised with CD45 antibodies as before, but prior to injecting CD45 containing Jurkat or CEM lines, the CD45 negative MDA line would be injected first. A fresh sensor chip was constructed and functionalized as before. To prevent non-specific absorption, a solution of glycine was used in the microchannel at a concentration of 0.2 % in PBS for 30 min before

injecting the analytes. BSA was not used as a blocker due to concerns that it would clog up the slot. The results of this experiment were unexpected, as a response was noted for both MDA and Jurkat lines, as shown in Fig 7.5 below. As MDA exosomes do not contain CD45 protein on their surface, we do not expect them to be captured by CD45 antibodies. I have several possible explanations for these results:

1. **The functionalization protocol failed**
2. **The exosomes are been trapped physically by the slot, rather than by the antibodies**
3. **Something in the medium, the glycine or the MDA exosomes is altering the results**

The results are even more surprising given the relatively clear behaviour of Fig 7.4. Of the three explanations I can think of, I believe number 2 to be the most likely. Whilst exosomes are generally between 40-100 nm in size, they can even go up to 200 or 300 nm [10]. The slot in the sensor is approximately 180 – 200 nm wide. It is therefore conceivable that individual exosomes could be physically trapped by the slot, or that clumps of smaller exosomes result in the same effect. This still doesn't explain the results of Fig 7.4. One way this could be resolved is to also include point 3. Perhaps the MDA exosomes had a higher fraction of larger exosomes, and blocked the slot up physically, or maybe the MDA exosomes are more adherent than other types of exosome, and are thus most susceptible to non-specific absorption or clumping together. MDA *cells* are higher in their adherence to surfaces than Jurkat and CEM, and as exosomes are composed from the same membrane material as their parent cell, it is possible that the exosomes have inherited some of these properties. Future work will have to address these problems. It is unlikely that the glycine is causing clumping as similar results were obtained when this was omitted. At worst, the glycine is not functioning as a blocking agent, thus allowing non-specific absorption to take place.

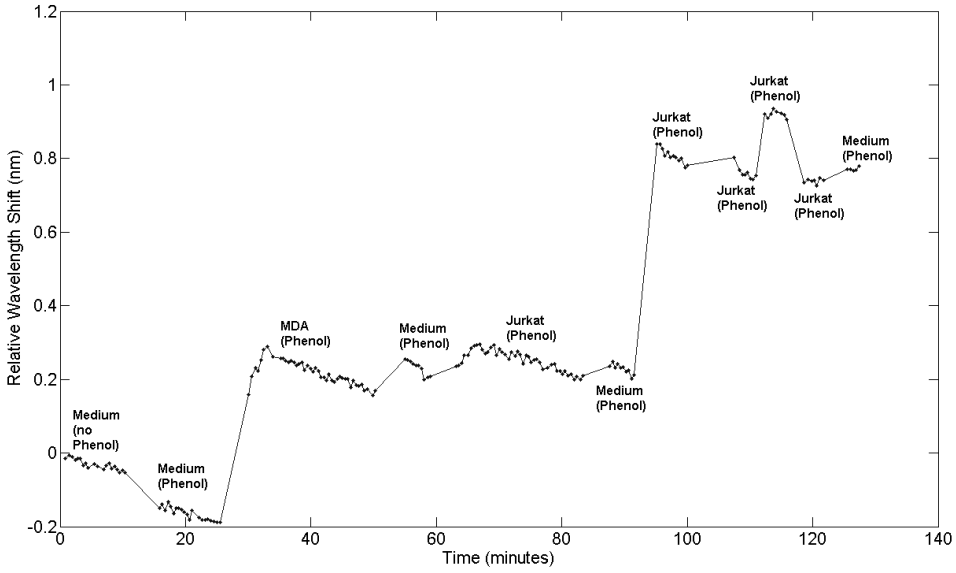

Figure 7.5: Sensor response for C45 negative (MDA) and positive (Jurkat) exosomes using CD45 antibodies.

Potential solutions to the 3 problems above could be to use wider slots (requires a re-design), a different blocking agent, or trying a CD45 negative cell line other than MDA. Despite these issues, it is clear from all of these results that exosomes can be detected with slotted photonic crystals. The question is whether the detection is specific or not, which should be the subject of future work. If it is indeed the different size or adherent properties of exosomes that is producing this difference in results, then this weakness could be turned into a strength; different slot sizes could be used to identify different sizes of exosomes, or different exosomes or health states could be identified from their different adhesion properties to the sensor. In this case no antibodies would be needed, making the device much simpler to make and use.

7.3 Cell Growth on Silicon Photonic Crystals

7.3.1 Introduction

An exciting idea we developed with Dr Powis would be to measure exosome or other media secretion directly from a living cell using slotted photonic crystals. As cells are typically the same size as our photonic crystals (~ 10 μm length) then a proteomic study on a single cell could be performed. The idea would be to grow a single cell on top of the photonic crystal, and then stimulate it with chemicals, light or something else to cause it to secrete substances. The resulting change in refractive index would be detected by the slots. Using antibodies would also allow this to be made specific. This would be of interest for studying direct exosome secretion in real time, but may find use in other applications. For example, a cell's health can be determined by how well it adheres to a substrate. This is of interest in drug screening [11].

7.3.2 Initial Results

Whilst the specificity of the exosome detection still has to be addressed, we decided to test the feasibility of growing cells on top of photonic crystals. To do this, a photonic crystal sample was tested by Dr Rob Marchington and Dr Lani Torres of the group of Prof Kishan Dholakia (University of St Andrews), on top of which they tried to culture Chinese hamster ovary (CHO) cells. These initial results were very poor, as the cells appeared to be shrivelled up, in low numbers, and poorly attached to the surface of the silicon. As cells like hydrophilic surfaces, I decided to try Piranha cleaning a second sample for 10 min immediately before giving it to Dr Torres for culture in an incubator for 48 hours. This ensured that the crystals were free from organic contaminants, and that the sample was hydrophilic as it creates OH groups on the surface of the silicon. The results are shown in Fig 7.6. This time the cells appeared well adhered and healthy due to their flat, elliptical shape. These results therefore demonstrate that cells can be grown on top of a silicon slotted photonic crystal, provided it is made hydrophilic. Once the exosome protocol is finally established, future work could investigate exosome secretion directly from the cell. Some cells, for example, such as MDA or HELA may be ideal, given their good adhesion properties and their interest in exosome studies [12]. Exosome producing cells have been shown to respond to stimulation from calcium ionophores [1]. Another way may be to combine the slotted cavity detection with photoporation [13], the idea being to punch a hole in the cell with a laser, or even to lyse a cell and then to measure the contents coming out with the slotted photonic crystal. These considerations also gave us another idea: being able to detect cellular secretion not only as a function of time, but as a function of position from a single cell. This would require using multiple slot sensors in a very small area, and is the subject of the next section.

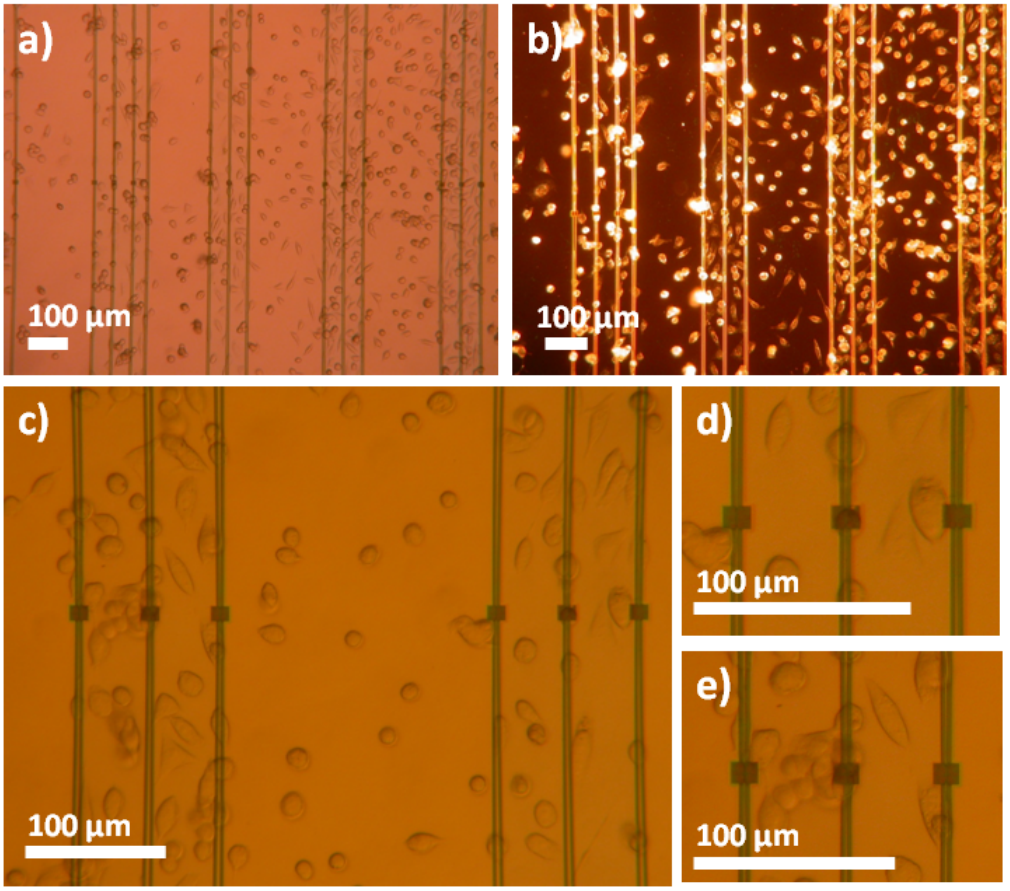

Figure 7.6: Chinese hamster ovary cells grown on silicon slotted photonic crystals. a) Bright field image before rinsing in medium. b) Dark field image before rinse. c)-e) Close-ups after rinsing in medium. Photonic crystals shown are approximately 10 µm long.

7.4 Spatial Array Sensing

7.4.1 Introduction

Whilst developing slotted photonic crystals for sensing exosomes, we proposed another interesting idea: the ability to detect where a cell secretes a substance using arrays of cavities. Whilst the devices in Chapter 6 and above use a single cavity, there is no reason to prevent us putting multiple cavities within a small area. We only have to ensure they are sufficiently spaced to prevent coupling between them, such that they are truly independent. The heterostructure cavity used in Chapter 6 is not so easy to densely integrate, thus I looked at other potential cavity designs. A single cell is typically 10-20 µm wide, which is comparable to the size of the slotted photonic crystal. The goal was to maximise the number of independent sensing elements that could be placed within such an area.

7.4.2 L3 – Like Slotted Cavity

Whilst the in-line coupling of Chapter 6 was successful, this is not as useful for multiple independent cavities within a small area. Side coupling allows denser integration as cavities can be fed along, and either side of, a bus waveguide. One simple design mentioned in the literature is an L3 – like slot cavity [14]. An L3 cavity in a standard photonic crystal involves the removal of three holes and the cavity can be optimised by altering the surrounding holes. In the slotted case, the three holes can be replaced by a slot. It should also be noted that a similar design has also been used to create a nanolaser based sensor by removing only a single hole [15]. These cavities were excited vertically. Instead, I looked at exciting them via side coupling.

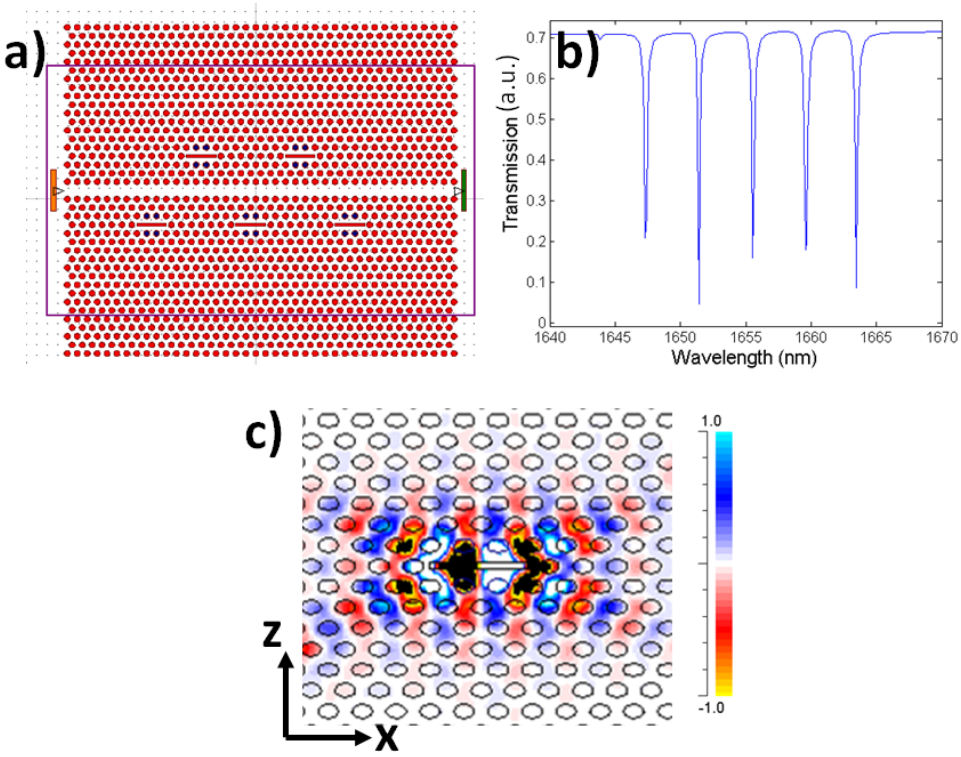

Figure 7.7: 'L3-like' slotted cavity. a) FDTD simulation area of 5 cavities. b) Corresponding transmission spectrum from FDTD. Each dip corresponds to one of the cavities. c) FDTD CW profile for single cavity on resonance. Ez component.

The cavity is formed from the slot itself. The lattice surrounding the slot behaves as a mirror. The W1 waveguide parallel to the cavity can feed it with the resonant wavelength, provided their two modes intersect in the dispersion diagram. Each cavity can be tuned to operate at a different wavelength by either altering the width of the slot, or by shifting the holes surrounding the slot. I performed the FDTD simulations in Fig 7.7. To test this type of cavity experimentally, I fabricated several designs using the protocols in Chapter 3. Figure 7.8 shows one of these devices which contains 10 cavities, and the corresponding transmission spectrum. The nice thing about this approach is that each dip in this single spectrum corresponds to an independent cavity, allowing the behaviour of each cavity to be extracted independently via the

wavelength. A similar principle has been demonstrated by Mandal [16], but the separation was much larger such that each could be independently functionalised with microfluidic channels. Whilst here it would be hard to functionalise each cavity with a different antibody (though perhaps it could be done with dip-pen nanolithography – see Chapter 2), they can of course be functionalised with the same antibody. Whilst this would not allow multiple antigens to be screened at the same time, it would allow a measure of the secretion of one particular antibody as a function of *position* on the cell. Since conceiving this idea, I came across a recent publication [17] using nanoantennas to probe cell secretion as a function of position. These antennas enhance fluorescence. Whilst the results are nice, the need of two antibodies for fluorescence, i.e. one to capture and another to fluoresce, prevents measurements being taken in real time and complicates the protocol. To test the idea of cell secretion, the cavities shown here will have to be designed to work in water, and near 1550 nm where we have a tuneable laser to confirm the dips seen in experiment are indeed the cavities, and such that they can be excited independently. This will be the subject of future work.

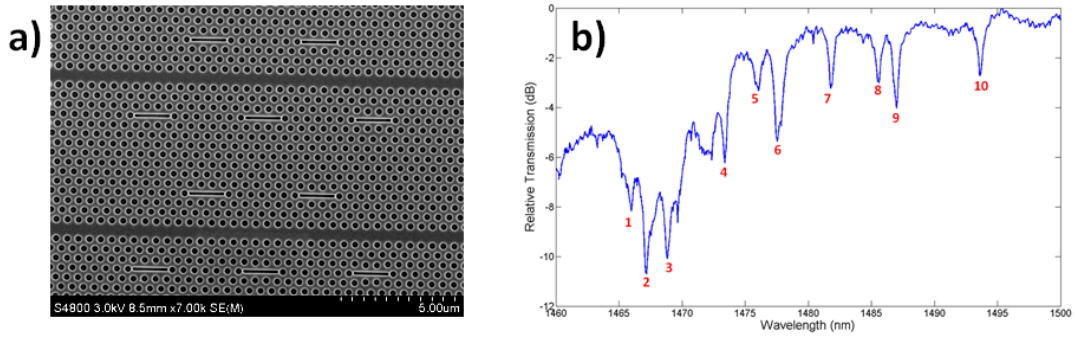

Figure 7.8: a) SEM image of 10 cavity design. b) Corresponding transmission spectrum. Each dip corresponds to one cavity, allowing spatial array sensing. Current design shown for air filled device.

7.5 On-Chip Slotted Photonic Crystal Spectrometer

7.5.1 Introduction

A major limitation of many types of optical biosensors, including the one presented in Chapter 6, is that whilst the sensor chips can be very small, they often need bulky sources and detectors to operate. Thus they are more 'chip-in-a-lab' than 'lab-on-a-chip'. In order to measure a shift in resonance, some form of spectrometer is required, for example the results in Chapter 6 were taken with an Advantest Optical Spectral Analyser (OSA). Whilst there is a general trend in the reduction of spectrometer size, such as the Ocean Optics spectrometers which can be as small as 50 mm square [18], it would be of benefit for small, disposable sensors if some form of spectrometry could be done on-chip using nano/micro photonic components, thus reducing size, weight, power and cost significantly. A number of solutions exist in the literature. Arrayed waveguide grating (AWG) spectrometers use differences in phase between several curved waveguides of different path length to perform wavelength division de/multiplexing. Whilst AWGs such as [19] have shown to operate with up to 50 channels, each of 0.15 nm bandwidth and 0.2 nm spacing, this device requires very high precision fabrication and has a free spectral

range of only 10 nm. Ring resonators can be used to selectively out-couple particular wavelengths from a bus waveguide, but these are also limited by low free spectral range. Photonic crystal based solutions include using arrays of different photonic crystals to out-couple specific wavelength bands [20], or the superprism effect [21] which uses diffraction within photonic crystals to separate out wavelengths; while these solutions offer a larger free spectral range, they do not tend to offer the same resolution and precision as an AWG.

Whilst investigating suitable coupling structures for slotted photonic crystals, as described in Chapter 4, I noticed that W1 photonic crystals coupled poorly to slotted photonic crystals. This is due to the mismatch in sign of the group index between the guided modes of the slotted and the regular structures. Early simulations showed that when placed in a directional coupler configuration, this difference in sign would result in light from a W1 coupling into a backwards propagating mode in the slotted photonic crystal. I later realised that this contra-directional coupling could be exploited for novel on-chip spectrometers and sensors. The advantages of this approach are its large free spectral range the fact that sensor and spectrometer can be made out of variants of one component (a slotted photonic crystal) in a planar configuration, and in the case of gas sensing, the slotted photonic crystals can simultaneously function as a sensor and as a spectrometer.

7.5.2 Contra-Directional Coupling with Slotted Photonic Crystals

Directional couplers in photonic crystals consist of two parallel defect waveguides separated by a number of rows of holes. Light can be periodically exchanged between these two waveguides. This exchange is described using coupled mode theory [22], where each waveguide mode is considered separately, before being considered as a perturbation to the other mode. Using coupled mode theory, it can be shown [22] that there is a total transfer of power between the two waveguides at every distance of l:

$$l = \frac{\pi}{2\kappa} \tag{7.1}$$

Where κ is the coupling coefficient determined by the orientation of the two waveguides. For *contra*-directional couplers, coupled mode theory shows that instead of a periodic power transfer between the two waveguides, there will be an exponential decay of power from the forward propagating mode of the incident waveguide into the backward propagating mode of the second waveguide [22]. As an exponential never reaches zero, making the waveguides longer only extracts more light from the incident waveguide, but never fully transfers. The waveguide length is therefore less critical than for co-directional couplers, as the periodic exchange of power is not observed. The waveguide only requires to be of sufficient length to gather the required power.

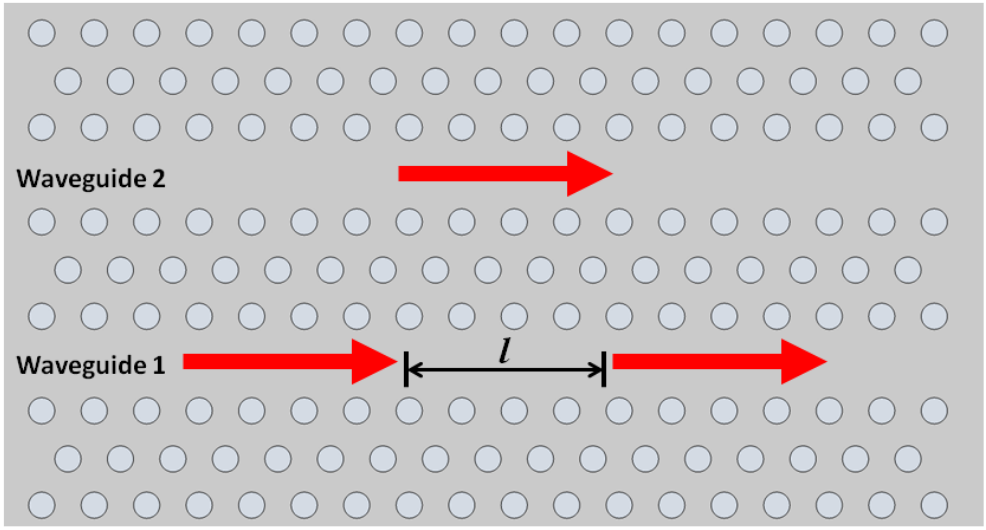

Figure 7.9: Sketch of photonic crystal co-directional coupler (not to scale). Power is periodically transferred between two photonic crystal waveguides at each distance of *l*.

Whilst contra-directional coupling has previously been shown between defect photonic crystal waveguides [23, 24], and between waveguides and photonic crystals [25, 26], I show here for the first time (to my knowledge) the contra-directional coupling between a W1 and a slotted photonic crystal waveguide. The great advantage of this approach is that the light extraction can be made wavelength-specific. This specificity not only allows light to be transferred between different media (from silicon into the slot), but the strong light matter interaction in the slotted architecture is also particularly attractive for sensing applications.

7.5.3 Simulations

When a slotted photonic crystal waveguide is placed parallel to a W1 waveguide, the coupling between them can be contra-directional due to the different signs of the group index of their guided modes. Light from the forward mode of the W1 couples into the backward travelling mode of the slotted photonic crystal waveguide. Simulations of the corresponding bandstructure of such a coupled system are shown in Fig 7.10, for a slot and W1, with 6 rows of holes in between. The guided modes of each structure create an anti-crossing point, separated by a mini stopband, as shown in Fig 7.10 a)-c). The width of this stopband determines the bandwidth of the transferred power, and is dependent on the separation between the slot and W1. Closer separation, as in Fig 7.10 d)-f), produces a larger perturbation, which in turn gives a wider stopband and hence larger bandwidth. Greater separation produces a narrower linewidth, but requires a longer interaction length to transfer the same level of peak power.

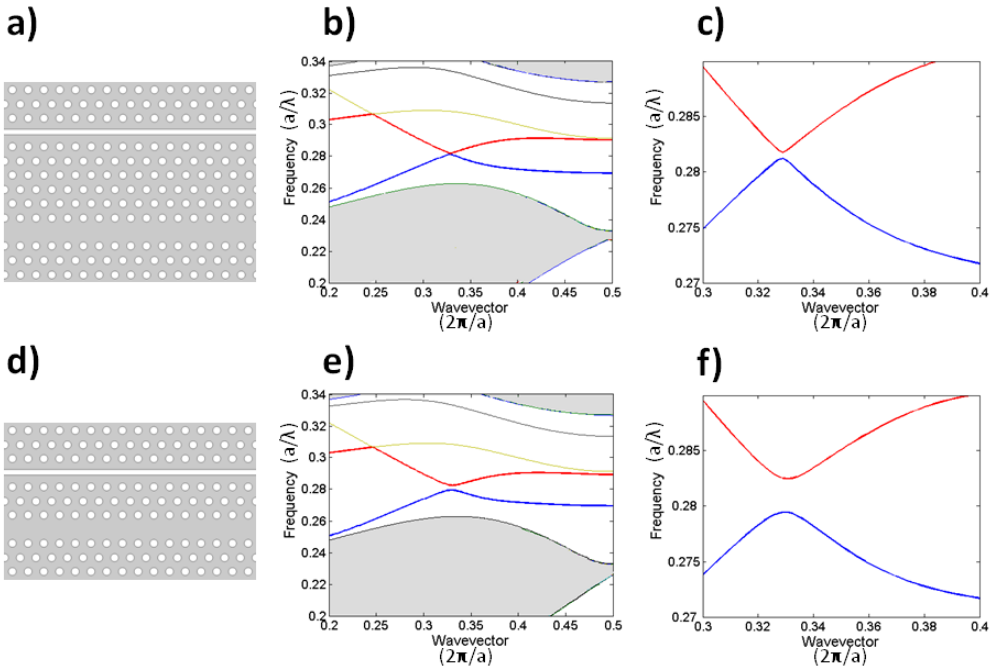

Figure 7.10: Slotted contra-directional coupler bandstructure. Intersection of **W1** and **slot** modes creates anti-crossing point, and associated mini stopband. Bandwidth dependent on waveguide separation. a) 6 rows of holes between waveguides and (b) corresponding bandstructure. c) Zoomed region of b). d) 3 rows of holes between waveguides and e) corresponding bandstructure. f) Zoomed region of e). All simulations carried out with slotwidth 0.27a, r=0.294a.

As a first test, I simulated different coupler designs using 2D FDTD methods. An 80 micron long crystal, of period 440 nm, slot width of 0.27a, radius 0.294a, effective index 2.7 and 6 rows of holes in between the w1 and slot was chosen. The results for CW and pulsed simulations are shown in Fig 7.11.

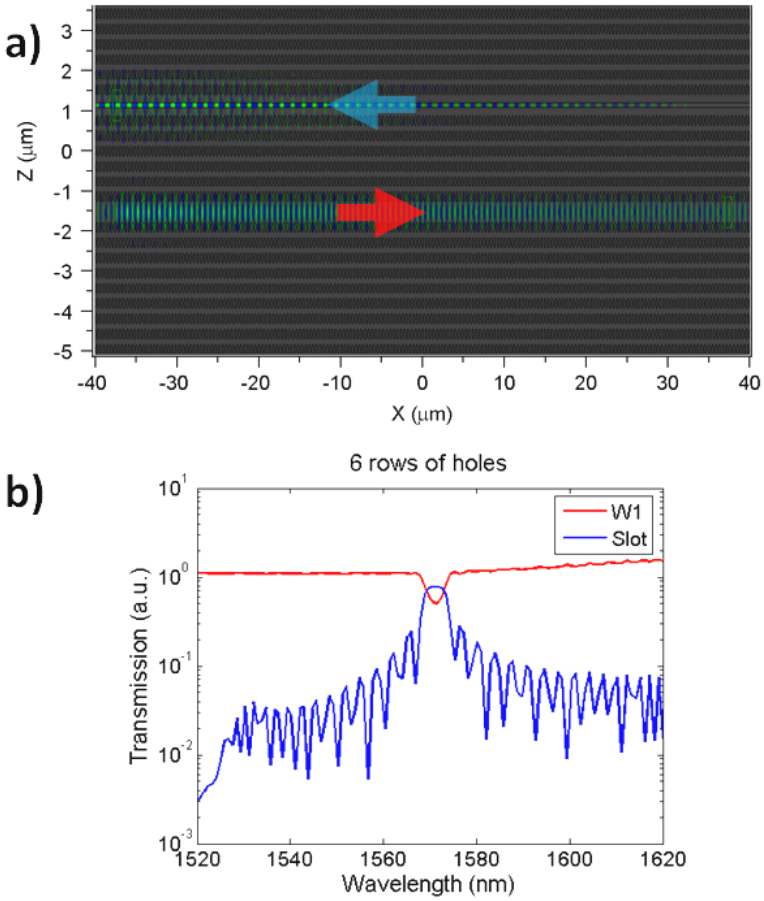

Figure 7.11: FDTD simulations of slotted contra-directional coupler. a) CW profile for Ez component at coupling wavelength. b) Computed transmission spectrum of **W1** and **slot** for pulse centred on 1550 nm.

7.5.4 Experimental Results

I fabricated and characterised contra-directional couplers using the methods detailed in Chapter 3. The contra-directional behaviour required looping the waveguides around so as to take the output to the back edge of the sample for characterisation, but this may not be required depending on the application. The waveguides providing the 180° turn are free-standing (Fig. 7.12), so in order to prevent a significant collapse during the under-etching of the photonic crystals, the waveguides were first taken more than 200 microns from the etching region, before looping around the crystal. To achieve coupling between the slotted photonic crystal ports and their corresponding waveguides, the resonant coupler structure from Chapter 4 was used. The experimental results are shown in Fig 7.12.

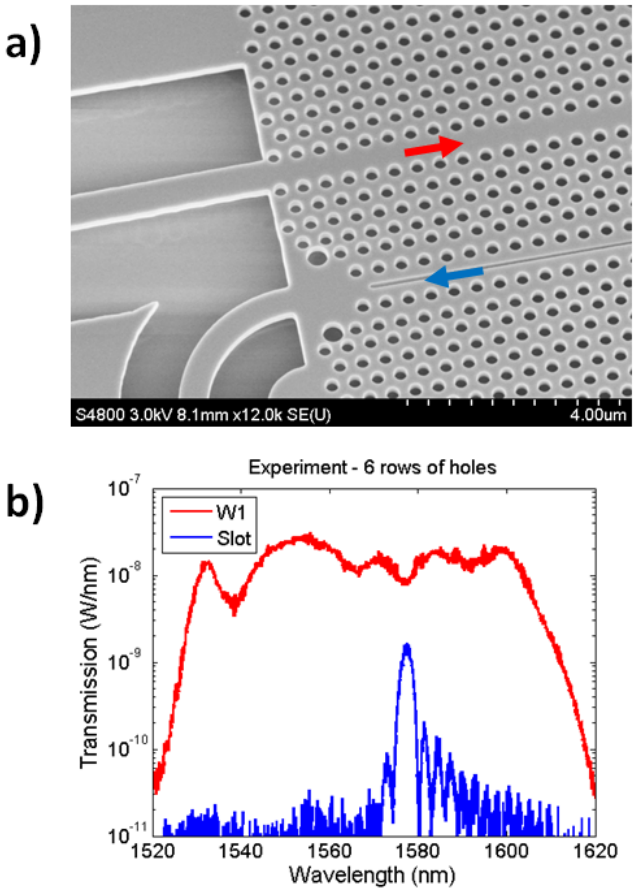

Figure 7.12: Slotted contra-directional coupler. a) SEM image of slotted contra-directional coupler. b) Experimental transmission (raw data) for **W1** and **slot** channels, of a 80 micron long crystal with 440 nm period, 100 nm slot width and 6 rows of holes separation.

The central wavelength and bandwidth closely match the expected values, but the coupled power is lower than that expected from simulations. A number of effects may be responsible for this discrepancy: additional interfaces, bend losses in the loop, and the fact that the simulation is 2D only. Making the crystals longer, or reducing the number of rows separating the waveguides would extract more light. Figure 7.13 shows the variation in transmission for devices with 3 rows of holes in between the waveguides, for different waveguide lengths, to highlight this effect.

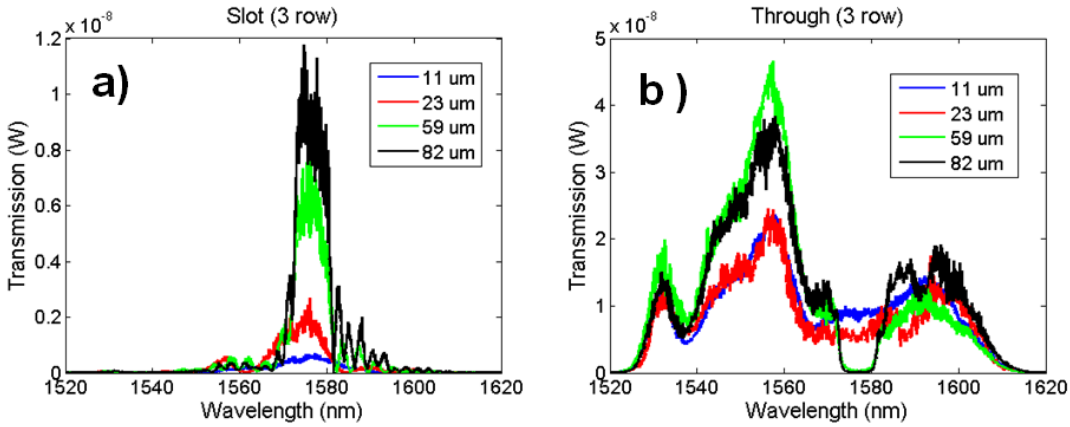

Figure 7.13: Experimental filter transmission as function of waveguide length for slot contra-directional couplers with three rows of holes between waveguides. a) Slot extracted transmission b) W1 transmission.

As the bandwidth and centre wavelength can be tuned by varying the waveguide separation and the slot width, respectively, then I soon realised that these structures have potential for sensors and on-chip spectrometers. Therefore, I connected a group of devices in series, the only difference between them being the width of the slot, and tuned through the dose to write it in the e-beam. Changing the slot width shifts the slot mode's dispersion curve, altering the position, and hence central wavelength, of the anti-crossing point. Each device therefore filters out a different wavelength from the W1 bus, the bandwidth of which is determined by the waveguide separation, with the output power being determined by the waveguide length. In the five filter designs shown experimentally in Fig 7.14 below, each slot extracts a different wavelength of light into its own separate channel. The spectrum of each port is designed to overlap, as this allows finer resolution and higher densities of channels to be realised. Greater levels of power could be transferred into the different slot extraction channels were the waveguides made longer. Here, a length of 80 microns was used to the limited writing area of the e-beam without stitching errors.

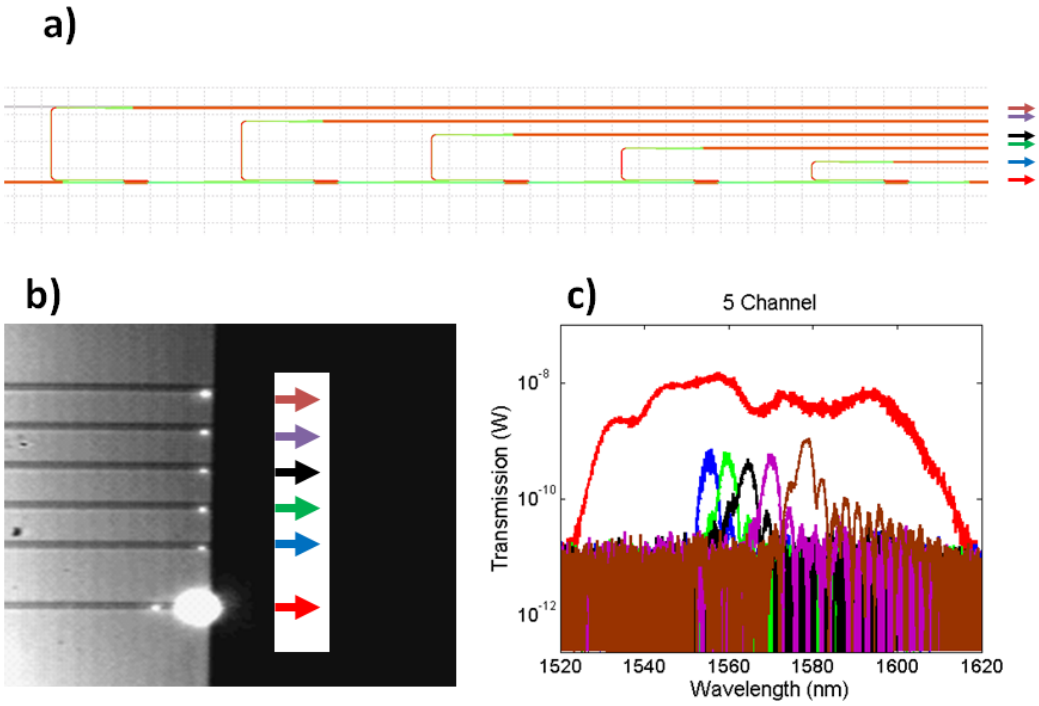

Figure 7.14: 5 filter design. a) GDS file of design. Each crystal has slightly different slot width, and thus extracts a different wavelength. b) Near-IR image of output. c) Measured output from each channel.

This device can function as an on-chip spectrometer, as each channel extracts a different wavelength of light. The filter wavelength and bandwidth can be engineered by adjusting the slot width and waveguide separation. The narrowest linewidth achieved in experiment was found to be around 3 nm at full-width-at-half-maximum. Increasing the separation between the W1 and slot would allow narrower lines to be realised, though requires making the waveguides longer to extract the same level of power. To function as a spectrometer all that is needed is a standard photodetector at each output to measure the intensity of each wavelength. The resolution is determined by the overlap and linewidth of each channel. Alternatively, and given that the channels overlap, a measure of the ratio of the intensities in each waveguide, compared to the calibrated measurement, could allow finer resolution to be achieved, as illustrated in Fig 7.15. In this case the resolution would be limited by the overlap of the channels, and the noise levels within the photodetectors. This could be used in conjunction with a slotted cavity to measure the shifts in wavelength as a result of antigen-antibody binding as in Chapter 6. The big advantage over other devices is the very large free-spectral range, in excess of 200 nm from simulations, compared with sub-10 nm of many ring resonators and AWGs. This device may also find use in other applications which require wavelength specific extraction of light from photonic crystals such as de-multiplexing or optical modulators, for example the slot could be infiltrated with an electro-optic polymer. The light confinement to air within the slot makes this device also very attractive for sensing applications. For example, if the exosomes are indeed being immobilized physically, rather than by antibodies, within the slot then this could be used as a way of measuring particle size. An array of different slot widths would have its own unique resonant wavelength. Observing which waveguides shift in resonance would allow detection of particles, and consequently their maximum size. My colleague, Abdul Shakoor, is also interested in making light sources in silicon using slotted photonic crystal cavities to

enhance emission, either through filling with erbium doped silica, or through creating defect states in the silicon through plasma treatment. It is therefore conceivable that in addition to a sensor and a spectrometer, slotted photonic crystals could also be used for a light source, further highlighting the versatility of the platform.

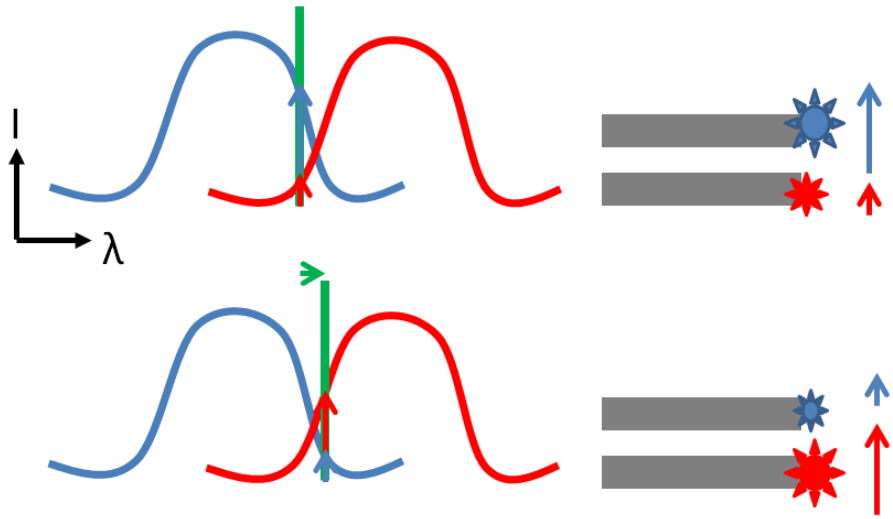

Figure 7.15: On-chip spectrometry strategy using two filters. Each contra-directional slot extracts a different wavelength from the W1 bus. If filters are overlapping, when a cavity wavelength is swept through the input of the bus, changes in intensity from each would result. Measuring the ratio of intensities would allow the wavelength of the cavity to be recovered. Resolution determined by the overlap, detector and noise.

All of these ideas use the device as a way of detecting a change in phase, however the device could also be used to detect a change in absorption, which would be useful in gas sensing. Whilst different gases can be inferred from the resonant wavelength, a major problem of the refractive index sensing approach is the lack of specificity. There is no antibody for gas, thus one needs prior knowledge of the gas composition to make such a sensor effective. Instead, it is better to look at absorption, rather than refractive index, when developing gas sensors, as many gases have unique absorption spectra in the infra-red. The unique distribution of narrow absorption lines can be used as a 'fingerprint' or 'barcode' to identify a particular gas. Remote gas sensing has useful applications in a diverse range of areas such as: monitoring gas leaks on oil platforms and within refineries, detecting pollutants (e.g. global warming), detecting volcanic emissions, and measuring gases on other planets. There is also a growing presence in medical applications, where over 30 biomarkers in human breath have been identified, such as acetone for diabetes, ammonia for asthma and butane for lung cancer [27]. When used in conjunction with an absorbing gas, this contra-directional design could function simultaneously as a sensor and spectrometer. The strong overlap of the light with the gas in the slot would maximise the absorption, whilst the absorption itself would cause a reduction of the intensity of the light extracted by the slot. As the slot extraction is wavelength specific, each slot could be optimised to a specific gas absorption line or be used as a blank reference. Using greater waveguide separations produces sharper spectra over a longer optical path length in the coupler: all of these properties are beneficial for gas detection. This way, a gas absorption spectrum could be taken on-chip simply by measuring the decrease in intensity in a channel

corresponding to a known line. This method will be subject to further investigation in future studies.

7.6 Marine Sensing

7.6.1 Introduction

It is often said that we know more about the surface of the Moon than we do about our oceans. Exploring the ocean depths can be just as challenging, if not more so, than exploring the outer space due to high pressures, marine creatures, currents, ice, volcanoes and other factors that have to be taken into consideration. Every ten metres depth of water generates an extra atmosphere of pressure, thus the engineering requirements can be huge. Whilst we have been fascinated by manned underwater exploration since the publication of the visionary *20,000 Leagues Under the Sea* and the real life adventures of Jacques Cousteau, like space exploration, ocean exploration is increasingly being done by machines. A science research vessel can cost up to $50,000 per day at sea, thus autonomous submersibles are being increasingly used [28]. It is not only significantly cheaper, and safer to send a probe, rather than a human being, into the ocean, but also perhaps more useful, as banks of sensors can relay many different measured parameters. One major issue is biofouling. A thimbleful of seawater contains approximately 1 million bacteria [28]. Microorganisms and other sea creatures can clog up or obscure sensors, rendering them useless. Whilst some strategies such as copper plating [29], nano-structuring of surfaces [30] and chemical paints [31] have been deployed, it is probably fair to say that no solution has proven to be universally effective. The constituents of the water are also very important in their own right. The sea contains many types of viruses and toxins. As I found out through many fruitful discussions with our collaborators at the Scottish Ocean Institute, several types of algae produce toxins that cannot only harm marine mammals, but also human beings. Detecting and understanding the production of these toxins is therefore an area of public importance. The detection of hydrocarbons is important for finding new oil wells and preventing pollution. Also of interest are the salinity, chlorophyll, dissolved gas and nutrient levels within the sea. These are not only important for marine life, but can also drive many vital global systems. Sensors to measure these quantities would therefore be of interest in many different areas of research.

7.6.2 Sea Mammal Research Unit

During this project we had a number of meetings with Dr Bernie McConnell and Dr Ailsa Hall at the Sea Mammal Research Unit (SMRU), within the Scottish Oceans Institute at St Andrews. We discussed problems relating to marine research, and what potential solutions photonics and microfluidics could offer. SMRU are particularly interested in the health and behaviour of seals, and have developed commercial remote data loggers that can be attached to the head of a seal using glue. This device detaches from the seal when its skin moults, allowing it to be recovered. Powered by batteries, they have been combined with GPS phone tags, temperature, depth, salinity and speed sensors [32]. Fluorescent probes have also been used within this device to study chlorophyll levels within the sea. Data can be relayed via satellite. The sensor is not only useful for studying seal behaviour, but also the environments to which they go, thus benefitting different areas of research. Our idea was to integrate our photonic sensors with these tags. The challenges involved are great, but there was strong enthusiasm from both sides, and

other marine researchers we involved to make this work. Particularly attractive to the marine biologists was the idea that we could incorporate tens or hundreds of independent sensors into a small chip. In theory, each sensor element could be kept sealed from the ocean, preventing biofouling. When a measurement was required, a single, fresh biosensor element could be opened through microvalve actuation. Later measurements could then be taken by opening further channels, thus every experiment is kept clean and independent. The large number of elements would allow many of these measurements to be made over a given period of time.

Three key quantities were initially identified as being of interest. These were:

1. **Detection of domoic acid**
2. **Detection of chlorophyll A**
3. **Salinity levels**

Later discussions also raised the possibilities of detecting dissolved gases such as oxygen and carbon dioxide.

7.6.3 Detection Strategies

Domoic Acid

Domoic acid is produced by red algae *Chondria* and diatoms of *Pseudo-nitschia* [34]. Humans can suffer from amnesiac shellfish poisoning (ASP), when consuming shellfish contaminated with domoic acid. This can cause severe food poisoning, loss of short term memory and can even induce a coma [33]. Domoic acid has been repeatedly detected in Scottish waters, forcing closure of large areas for shellfish harvesting [34]. Dr Ailsa Hall of SMRU is particularly interested in domoic acid due to its adverse effects on seals. Whilst developing the sensor shown in Chapter 6, we discussed the possibility of functionalising the device with domoic acid antibodies, rather than biotin. This would allow a small compact device to be constructed that is capable of detecting domoic acid in seawater in real time. In the past, domoic acid has been detected by injecting shellfish products into laboratory mice (mouse bioassay) [35]. If the mouse died, then the shellfish were contaminated. Lab-on-a-chip devices would provide more humane and quantifiable methods of detection. A few such devices have been demonstrated in the literature. References [36-38] have all detected domoic acid with surface plasmon based devices. With the aid of Dr Hall, we decided to look at functionalising the slotted photonic crystals with domoic acid antibodies in order to make a more compact and higher throughput device. Dr Hall provided us with antibodies she uses in her own tests of domoic acid, from an assay detection kit supplied by the company Biosense [39]. It was found that there were two major stumbling blocks. The first was that the antibodies cannot be used in unaltered seawater; filtration and dilution steps are required; the dream of in-situ measurements is therefore hard to realise. The second stumbling block was that the assay is competition (inhibition) based. In this type of assay the antigen (i.e. domoic acid) rather than the antibody is immobilized on a surface. To test for domoic acid, a calibration step must first be run where different known concentrations of laboratory-derived domoic acid are introduced in conjunction with domoic acid antibodies. The presence of known domoic acid solutions depletes the available domoic acid antibodies binding to immobilized domoic acid on the functionalized surface. In this case one looks for a *reduction* in the sensor response. Once the calibrated response is known, then this is repeated for the sample of domoic acid one actually wants to measure. This is more

complicated and time consuming to perform (even in the lab) than the direct assays used above, and has more scope for error. It is also much harder to do on-chip. In theory, we can use the chemical APTES, used to immobilize biotin in Chapter 6, to immobilize domoic acid such that they capture domoic acid antibodies, but we would prefer an assay where the domoic acid *antibodies* are immobilized to capture the domoic acid in seawater. Unable to resolve these issues, Dr Hall put us in touch with the Head of Microbial and Molecular Biology Department, Dr Keith Davidson, at the Scottish Association for Marine Science (SAMS), Oban, where we paid a visit. Whilst no viable solution could be found for domoic acid, other toxins were identified as points of interest. These could be the subject of future study if a suitable functionalization protocol can be identified. Whilst other sensors, such as the surface plasmon devices mentioned above, have demonstrated detection of domoic acid, the current need for a competition assay will ultimately put strong restrictions on them being used remotely.

Chlorophyll A

During the project, Dr Tim James of my research group developed an integrated fluorescent sensor capable of detecting chlorophyll [40]. Whilst this is not based on slotted photonic crystals, it is interesting to note briefly some of this work as many of the goals and challenges are the same, and I utilised some of my results from Chapter 5. The sensor consisted of an InGaN blue LED, covered by a thin film metal/dielectric excitation filter. Light from this filter is passed through a PDMS microchannel containing the analyte, exciting fluorescence in any chlorophyll present. Chlorophyll fluoresces around 662 nm. A second filter based on CdS is placed above the microchannel to cut out the excitation source (430 nm). Behind this is a silicon photodiode for measuring the intensity of the fluorescence. We decided to combine the microfluidic structures from Chapter 5 with Dr James' device to automate the entire device.

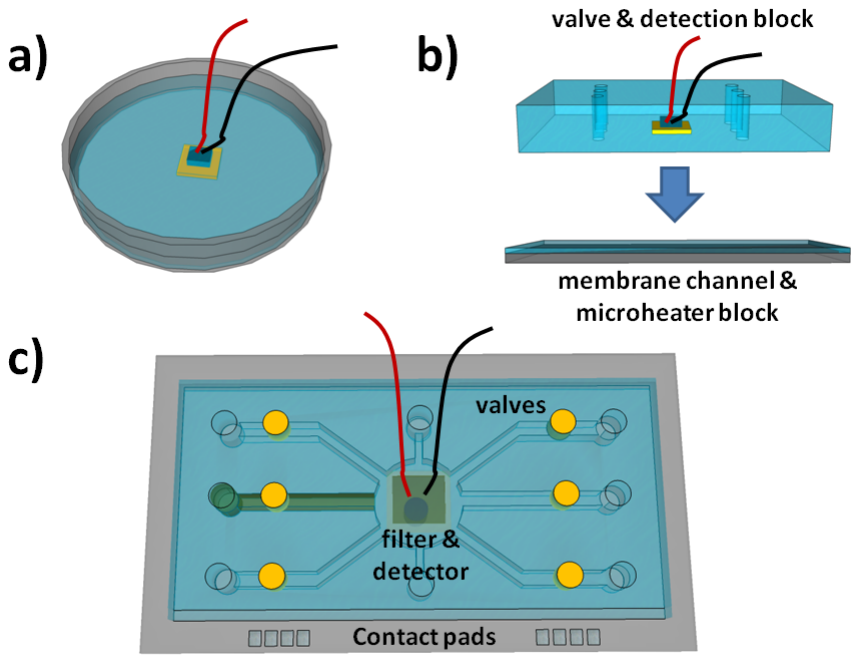

Figure 7.16: Integrated fluorescence detection system. a) CdS filter and detector placed in petri dish, and liquid PDMS poured over. b) Cured PDMS peeled and cut to size. Access holes punched for valve loading. Bonded to membrane channel section containing heaters as in Chapter 5. c) Final structure. Light from LED illuminates chamber from below.

The procedure is outlined in Fig 7.16. I first designed a new mould for the microfluidic circuitry using the method described in Chapter 5. The design consisted of 6 independent microchannels feeding a central reservoir. We decided to use the membrane wax valve approach to avoid contamination of the samples. A thin layer of PDMS was first spun and cured on top of this mould. In order to integrate the detector for the fluorescent device, a small, square membrane of PDMS was placed on the bottom of a petri dish. The CdS filter was glued to the detector using a drop of PDMS, and then placed face down on top of the membrane square. Liquid PDMS was then poured over this, making sure not to completely cover the electrical wires. This was cured in an oven for several hours. Once removed and cut to size, 2mm holes were punched at the corresponding valve locations. This large PDMS block was then aligned and bonded to the channel membrane layer on top of the mould. This was done such that the detector sat over the central reservoir, and each of the valve holes sat above a different microchannel. After bonding the two layers, they were peeled from mould and punched to give access hole for tubing. The device was then aligned and bonded onto a glass slide containing aluminium microheater arrays of similar dimensions as Chapter 5. The final result is shown in Fig 7.17. Microwax was then inserted into the valve holes as in Chapter 5.

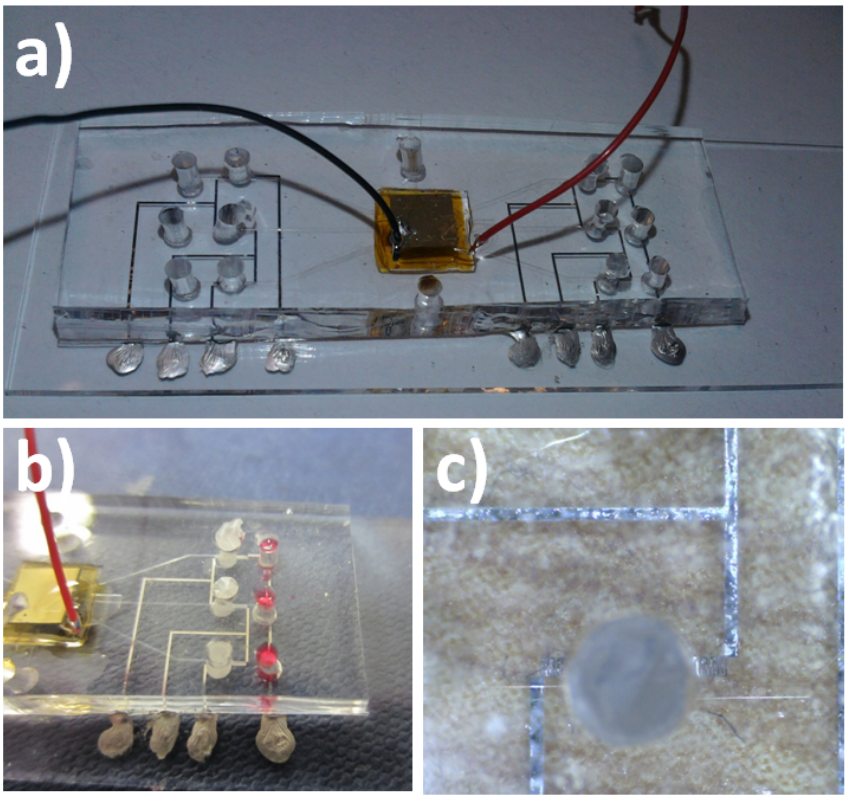

Figure 7.17: Fluorescence detection system. a) Full chip showing six channels feeding central reservoir above which sits the CdS filter and detector. b) Close up showing heater arrays. Different combinations can be actuated using contact pads. c) Single microheater controlled valve.

With this device Dr James was able to demonstrate the detection of chlorophyll in concentrations as low as 340 nM in ethanol. Given the simplicity of the device, this is a very good start; a detection limit nearer 1 nM is required for real applictions in seawater. We expect that better results can be obtained in the future by improved designs. Currently the detector sits in a direct line with the excitation source. Whilst appropriate filters are used to minimize false readings, the noise floor can be lowered by placing the source and detector at right angles or in the same plane such that they do not directly face each other.

Salinity/Density

On average, seawater has a salinity of 35 parts per thousand (3.5 %) [41]. Measuring salt levels is important for monitoring marine environments, not just for its inhabitants, but also to study its effects on global systems such as in climate change. Currently, many salinity measurements in the field are performed using electrical conductivity tests. These tests are not straightforward as they are influenced by temperature and pressure. They are also not specific. The presence of different ions in the water all impact on the conductivity. Currently, salinity is measured in Practical Salinity Units (PSU) on the Practical Salinity Scale (PSS) [42]. Such measurements themselves are based on electrical properties. Some researchers actually use salinity to estimate the density of seawater, but electrical tests do not take into account the presence of non-conducting material in the water. Optical sensors have an advantage here, as refractive index is more closely linked to density than electrical conductivity. If the sensor was to be used near potentially explosive environments (e.g. oil and gas platforms) it also better from as safety perspective to use optical rather than electrical methods.

Our group has previously shown detection of sugar concentrations using slotted photonic crystals, with a refractive index sensitivity of up to 1500 nm/RIU. The challenge is to measure very small changes in the salinity level. Salinity is related to refractive index by the approximate relation [43]:

$$\frac{\Delta n}{\Delta s} = 2e^{-4} \text{ RIU/PSU} \qquad (7.2)$$

Where n is the refractive index and s the salinity in PSU. Assuming the theoretical sensitivity of 500 nm/RIU obtained for the slotted photonic crystal, a 5 % change in salinity (50 PSU) would produce a shift of 5 nm, compared to the 0.06 nm shift of another photonic crystal based salinity sensor [44]. As seawater contains on average 3.5 % salt, and variations between seas can be smaller than 0.2 %, an order of magnitude improvement is needed over the device in [44] in order measure such changes. For our device, a 0.2% change in salinity would correspond to a shift of 0.2 nm. The final goal is to incorporate these sensors into the seal tags so that remote measurements of salinity can be made at a variety of depths and locations, but as mentioned above, the device needs an on-chip spectrometer. Using the contra-directional coupling scheme above may be an option in future, but in its current state would only be useful for coarse measurement of salt water vs. fresh water. Finer measurements could be realised using an optical spectral analyser, but these are too bulky for the seal to carry. A more realistic first test would be to fibre-couple the device and base the instrumentation on a ship or buoy, such that more bulky spectrometers could be accommodated. Following discussions with researchers at SAMS, Oban, we thought of creating a fibre based dip probe incorporating the photonic crystal.

Fibres could be coupled to the input and output waveguides of the SOI chip containing the slotted photonic crystal. This could be lowered into the sea from the ship or buoy. Light would be sent down the input fibre from a light source, and the signal then sent through the output fibre back up to a spectrometer, both of which are kept on board. Fibre ribbon would allow multiple fibres, and hence multiple sensors on the same chip, to be incorporated. The difficulty in this approach is achieving alignment between the fibre and the waveguides of the photonic crystal, which are only 220 nm thick. One solution we proposed was to use the UV curable glue (Norland) that was used for sealing the glass microfluidic chips in Chapter 5. A glue covered fibre could be butt-coupled aligned to the waveguide in the lab. Once alignment is achieved, then the glue could be cured with UV light locking the fibre in place. As the glue is solvent free, then the alignment should not change considerably during curing. To improve coupling, thick SU-8 waveguides, coupled to the photonic crystal access waveguides via inverse tapers, could be used. Bryan O'Regan of our group is currently trying to implement these ideas using custom made fibre holders, and fibre ribbon. Once achieved, this would allow field trials of the sensor to be performed from a boat. Salinity and other chemical levels may also find use in biomedical, or food and drink industries.

References – Chapter 7

[1] Simons, M., and Raposo, G., "Exosomes – vesicular carriers for intercellular communication," Current Opinion in Cell Biology 21, 575-581 (2009).

[2] Thery, C., Zitvogel, L., and Amigorena, S., "Exosomes: Composition, biogenesis and function," Nature Reviews Immunology 2, 569-579 (2002).

[3] Johnstone, R. M., "Exosomes biological significance: A concise review," Blood Cells, Molecules, and Diseases 36, 315-321 (2006).

[4] Simpson R. J., Jensen, S. S., and Lim, J. W. E., "Proteomic profiling of exosomes: Current perspectives," Proteomics 8, 4083-4099 (2008).

[5] Taylor, D. D., and Gercel-Taylor, C., "Tumour-derived exosomes and their role in cancer-associated T-cell signalling defects," British J. Cancer 92, 305-311 (2005).

[6] Lynch, S., Santos, S. G., Campbell, E. C., Nimmo, A. M. S., Botting, C., Prescott, A., Antoniou, A. N., and Powis, S. J., "Novel MHC class I structures on exosomes," J. Immunology 183, 1884-1891 (2009).

[7] Clayton, A., and Mason, M. D., "Exosomes in tumour immunity," Current Oncology 16, 46-49 (2009).

[8] Whiteside, T. L., "Tumour-derived exosomes or microvesicles: another mechanism of tumour escape from the host immune system?," British J. Cancer 92, 209-211 (2005).

[9] http://www.nanosight.com/, last visited on 20/09/2012.

[10] Soo, C. Y., Song, Y., Zheng, Y., Campbell, E. C., Riches, A. C., Gunn-Moore, F., and Powis, S. J., "Nanoparticle tracking analysis monitors microvesicle and exosome secretion from immune cells," Immunology 136, 192-197 (2012).

[11] Lidstone, E. A., Chaudhery, V., Kohl, A., Chan, V., Wolf-Jensen, T., Schook, L. B., Bashir, R. and Cunningham, B. T., "Label-free imaging of cell attachment with photonic crystal enhanced microscopy," Analyst 136, 3608-3615 (2011).

[12] Private communication with Dr Simon Powis, University of St Andrews, 8/12/11.

[13] Tsukakoshi, M., Kurata, S., Nomiya, Y., Ikawa, Y. and Kasuya, T., "A novel method of DNA transfection by laser microbeam cell surgery," Appl. Phys. B 35, 135-140 (1984).

[14] Gao, J., Yang, X., Wong, C. W., Green, W. M. J., Vlasov, Y., and Aseffa, S., "Demonstrations of an air-slot photonic crystal nanocavity with ultrasmall mode volumes for enhanced light-matter interactions," Conference on Lasers and Electro-Optics (CLEO), Baltimore, Maryland (2009).

[15] Kita, S., Hachuda, S., Otsuka, S., Endo, T., Imai, Y., Nishijima, Y., Misawa, H. and Baba, T., "Super-sensitivity in label-free protein sensing using a nanoslot nanolaser," Opt. Exp. 19, 17683-17690 (2011).

[16] Mandal, S., Goddard, J. M. and Erickson, D., "A multiplexed optofluidic biomolecular sensor for low mass detection," Lab Chip 9, 2924-2932 (2009).

[17] Wang, S., Ota, S., Guo, B., Ryu, J., Rhodes, C., Xiong, Y., Kalim, S., Zeng, L., Chen, Y., Teitell, M., and Zhang, X., "Subcellular resolution mapping of endogenous cytokine secretion by nano-plasmonic-resonator sensor array," Nano Lett. 11, 3431-3434 (2011).

[18] http://www.oceanoptics.com/Products/spectrometers.asp, last visited on 08/10/2012.

[19] Cheben, P., Scmid, J. H., Delage, A., Densomre, A., Janz, S., Lamontagne, B., Lapointe, J., Post, E., Waldron, P., and Xu, D. –X., "A high-resolution silicon-on-insulator arrayed waveguide grating microspectrometer with sub-micrometer aperture waveguides," Opt. Ex. 15, 2299-2306 (2007).

[20] Pervez, N. K., Cheng, W., Jia, Z., Cox, M. P., Edrees, H. M., and Kymissis, I., "Photonic crystal spectrometer," Opt. Ex. 18, 8277-8285 (2010).

[21] Momeni, B., Hosseini, E. S., Askari, M., Soltani, M., and Adibi, A., "Integrated photonic crystal spectrometers for sensing applications," Opt. Comm. 282, 3168-3171 (2009).

[22] Yariv, A., "Coupled-mode theory for guided-wave optics," IEEE J. Quant. Elect. 9, 919-933 (1973).

[23] Mao, X. –Y., Yao, D. –B., Zhao, L. –Y., Huang, Y. –D., Zhang, W., and Peng, J. –D., "An integrative biosensor based on contra-directional coupling between two-dimensional photonic crystal waveguides," Chin. Phys. Lett. 25, 141-143 (2008).

[24] Qiu, M., and Swillo, M., "Contra-directional coupling between two-dimensional photonic crystal waveguides," Photon. Nano. Fundam. Appl. 1, 23-30 (2003).

[25] Grande, M., O'Faolain, L., White, T. P., Spurny, M., D'Orazio, A., and Krauss, T. F., "Optical filter with very large stopband (≈300 nm) based on a photonic-crystal vertical-directional coupler," Opt. Lett. 34, 3292-3294 (2009).

[26] Shi, W., Wang, X., Zhang, W., Chrostowski, L., and Jaeger, N. A. F., "Contradirectional couplers in silicon-on-insulator rib waveguides," Opt. Lett. 36, 3999-4001 (2011).

[27] Wang, C., and Sahay, P., "Breath analysis using laser spectroscopic techniques: Breath biomarkers, spectral fingerprints, and detection limits," Sensors 9, 8230-8262 (2009).

[28] McLean, C. N., "Optical systems as an enabling technology for ocean and atmospheric sciences and how we understand our environment," Plenary Talk, European Optical Society Annual Meeting, Aberdeen (2012).

[29] Dormon, J. M., Cottrell, M., Allen, D. G., Ackerman, J. D., and Spelt, J. K., "Copper and copper-nickel alloys as zebra mussel antifoulants," J. Environmental Eng. 122, 276-283 (1996).

[30] Rosenhahn, A., Ederth, T., and Pettitt, M. E., "Advanced nanostructures for the control of biofouling: The FP6 EU integrated project AMBIO," Biointerphases 3, IR1-IR5 (2008).

[31] Yebra, D. M., Kiil, S., and Dam-Johansen, K., "Antifouling technology – past present and future steps towards efficient and environmentally friendly antifouling coatings," Progress in Organic Coatings 50, 75-104 (2004).

[32] http://www.smru.st-andrews.ac.uk/Instrumentation/Products/, last visited on 03/10/2012.

[33] Alexander, J., Benford, D., Boobis, A., Ceccatelli, S., Cravedi, J. –P., Di Domenico, A., Doerge, D., Dogliotti, E., Edler, L., Farmer, P., Filipic, M., Fink-Gremmels, J., Furst, P., Guerin, T., Knutsen, H. K., Livesey, C., Machala, M., Mutti, A., Schlatter, J., van Leeuwen, R., and Verger, P., "Marine biotoxins in shellfish – Domoic acid: Scientific opinion of the panel on contaminants in the food chain," European Food Safety Journal 1181, 1-61 (2009).

[34] Fehling, J., Green, D. H., Davidson, K., Bolch, C. J., and Bates, S. S., "Domoic acid production by *Pseudo-nitzschia Seriata* (bacillariophyceae) in Scottish waters," J. Phycol. 40, 622-630 (2004).

[35] Garthwaite, I., "Keeping shellfish safe to eat: a brief review of shellfish toxins, and methods for their detection," Trends in Food Science & Technology 11, 235-244 (2000).

[36] Yu, Q., Chen, S., Taylor, A. D., Homola, J., Hock, B., and Jiang, S., "Detection of low-molecular-weight domoic acid using surface plasmon resonance sensor," Sens. Act. B 107, 193-201 (2005).

[37] Stevens, R. C., Soelberg, S. D., Eberhart, B. –T. L., Spencer, S., Wekell, J. C., Chinowsky, T. M., Trainer, V. L., and Furlong, C. E., "Detection of the toxin domoic acid from clam extracts using a portable surface plasmon resonance biosensor," Harmful Algae 6, 166-174 (2007).

[38] Lotierzo, M., Henry, O. Y. F., Piletsky, S., Tothill, I., Cullen, D., Kania, M., Hock, B., and Turner, A. P. F., "Surface plasmon resonance sensor for domoic acid based on grafted imprinted polymer," Biosens. Bioelect. 20, 145-152 (2004).

[39] http://www.biosense.com/, last visited on 03/10/2012.

[40] James, T. D., Scullion, M. G., Ashok, P. C., Di Falco, A., Dholakia, K., and Krauss, T. F., "Valve controlled fluorescence detection system for remote sensing applications," Microfluid Nanofluid 5, 529-536 (2011).

[41] http://oceanservice.noaa.gov/facts/whysalty.html, last visited on 04/10/12.

[42] Unesco, "The Practical Salinity Scale 1978 and the International Equation of State of Seawater 1980," Tech. Pap. Mar. Sci. 36, (1981).

[43] Diaz-Herrera, N., Esteban, O., Navarrete, M. C., and Gonzalez-Cano, A., "Fiber-optic salinity probe," Second European Workshop on Optical Fibre Sensors, Proceedings of SPIE Vol. 5502, 455-458 (2004).

[44] Robinson, S., and Nakkeeran, R., "Photonic crystal based sensor for sensing the salinity of seawater," International Conference On Advances In Engineering, Science And Management (ICAESM -2012), (2012).

Chapter 8

General Discussion and Conclusions

8.1 Discussion

As shown in Figure 8.1 below, slotted photonic crystals form a complete and attractive platform for optical biosensing. This platform relies on the multiple branches of research that were carried out during this project. The results of each investigation, their limits, and suggestions for future work are all discussed in individual sections below.

8.1.1 Losses (Chp 4)

Chapter 4 showed that the losses of slotted photonic crystals, estimated using the cutback method, can be comparable to that of standard photonic crystals (of order 10 dB/cm) operating in the fast light regime. This is a little surprising as the surface roughness of the slot introduces another scattering object that standard photonic crystals do not posses, thus we would expect the losses to be much higher. However, slotted photonic crystals, in the fast light regime at least, sample less of the surrounding lattice than a W1 defect due to the strong spatial confinement of the slot waveguide effect. Provided the slot is wide enough, a large part of the field will not see the roughness of the slot walls or the holes of the crystal lattice. Smaller slots have a larger proportion of field near the slot walls, thus we expect a higher loss, as was observed by experiment in Chapter 4.

The unique optical properties of slotted photonic crystals can be challenging to work with, due to their often opposite behaviour to standard photonic crystals, requiring new solutions. The resonant defect coupler demonstrated by simulation and experiment in Chapter 4 allows more light to be injected into the air slot; and performs better over a wider wavelength range, whilst also being more robust than other solutions presented in the literature. Losses of 1.5 dB per interface were obtained over a bandwidth of 78 nm. With careful design, the losses of the device, both propagation losses and coupling losses, can be reduced to a minimum. For a single device we do not care too much if the loss is 10 dB/cm or 40 dB/cm in air, but when using multiple cavities or waveguides in a row (e.g. slotted spectrometer), long crystals or slow light effects, then these losses can start to become significant. It is important to remember that these values were obtained for air filled structures; when water is used, propagation losses due to material absorption also have to be considered. Future work could look at shifting the operational wavelength of the devices to shorter wavelengths, where water absorption is lower. In practice only the 1300 nm window could realistically be used, as silicon absorbs strongly below 1000 nm. Changing to a different material could help here, but will lead to the sacrifice of the high index contrast provided by silicon for the slot waveguide effect.

8.1.2 Microfluidics (Chp 5)

Chapter 5 showed that provided the right chemicals are used, slotted photonic crystals can be integrated with microfluidic channels fabricated in PDMS. The oxygen plasma bonding of PDMS allowed alignment to the photonic crystals to be achieved cleanly and relatively easily, whilst the soft lithography moulding process allows multiple chips to fabricated rapidly, cheaply and repeatably, traits which are favourable for mass production. The functionalization problems

encountered with organic solvents such as toluene highlighted the weaknesses of PDMS. In some cases it may prove hard to find a recipe that doesn't degrade the channels, though my own experience has shown that there are several options for solvents for functionalization protocols, and it is a good idea to explore these options beforehand.

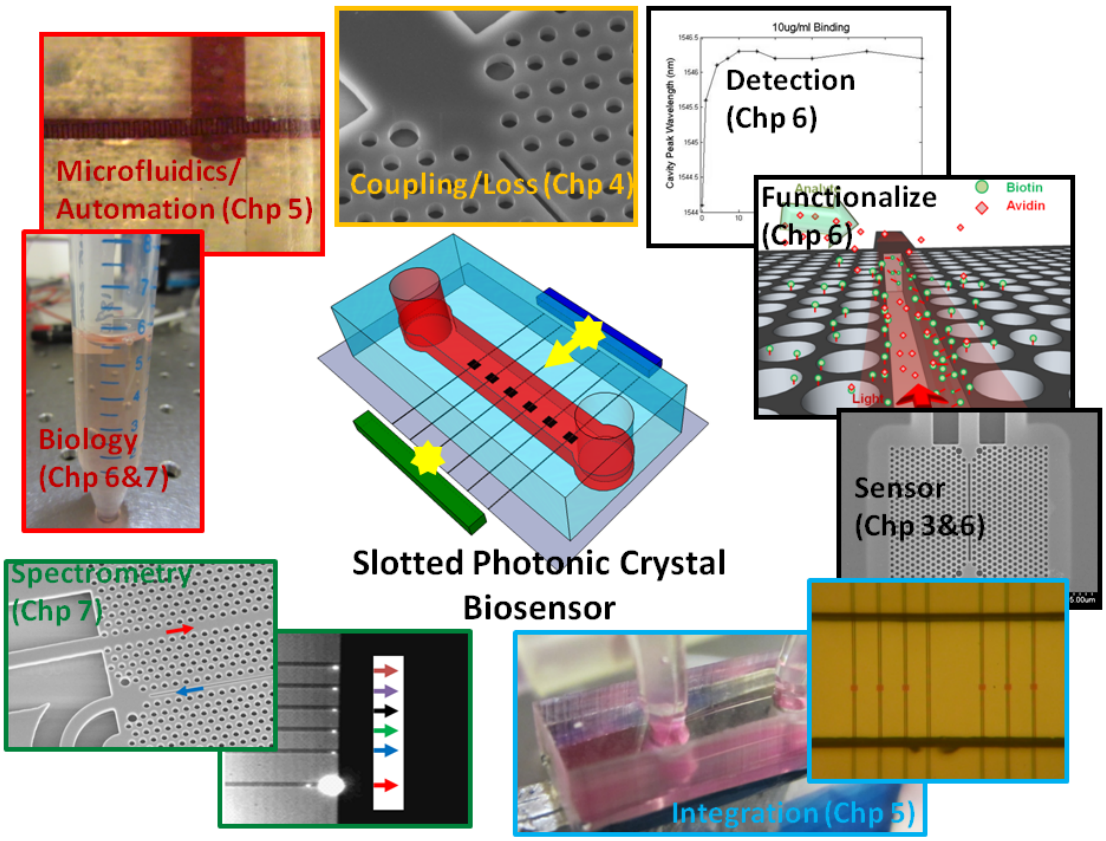

Figure 8.1: Slotted photonic crystal biosensor platform established in this project. Combining all of these elements makes for a promising lab-on-a-chip device. Slotted photonic crystals are versatile as they can function as sensor and spectrometer, and can be functionalized with many different antibodies. The small size and high sensitivity make them suitable for multiplexing and multifunctionality.

Here a simple straight channel was used to feed all of the photonic crystals. This prevented evaporation and minimised the amount of analyte required for measurement. Typically the devices I have shown here contained 50 sensors inside a sample chamber of only 0.1 µL in volume, though larger densities could possibly be realised. Using multiple small sensors in a microchannel would minimise the volume of expensive chemicals used in the drug screening, or blood taken from a patient in disease diagnostics. Not only would the cost be lower as a result of smaller samples, but also in terms of cost per test and time. Much of the cost for medical tests comes from the fact that one needs to pay a specialist to spend time processing multiple samples in a lab. Automation and multiplexing would not only allow faster processing, but also generate more repeatable results as some element of human error could be eliminated. If this device could be made cheaply and sufficiently small, it could also be made disposable.

Disposability would allow the device to be kept sterile prior to use, preventing the risk of cross-contamination.

Automation of the device is a great challenge in itself, but here PDMS shows strength. Whilst some applications may require glass channels (also fabricated in Chapter 5) for chemical resistance or mechanical strength, PDMS has the advantage that is flexible. This flexibility lends itself well to useful microfluidic components such as pumps and valves. Such membrane valves have been demonstrated before in very high densities, but require a pressurised gas source to work fully, and thus are more 'chip-in-a-lab'. The wax microvalves presented here, whilst not being multi-use, can be actuated electrically on-chip with energies of less than 1 J. If we care about having a sterile and disposable sensor, we may only wish to use it once anyway. It is true, however, that multi-use valves would allow more complex chemistry or biology to be performed on-chip, hence future work could look at some of the shape memory alloy designs briefly explored here.

Microfluidics may also help improve the performance of the sensor itself. Ideally we want to deliver as much of target molecules to the sensor region. Delivery to other places is ultimately wasted; not a problem in higher concentrations, but limiting when the signal is small. Almost all of the devices presented in Chapter 2, and the devices presented within this thesis, rely on binding of antigens that diffuse in solution to immobilized antibodies on the sensor surface. Diffusion is a relatively slow process, and the target molecules may never reach the antibodies on a reasonable timescale. Sedimentation may help, but may not always be prevalent. A simple way to improve performance would be to use as small microchannels as a possible way to deliver fluid only to the sensor region. Here a 200 micron wide channel was used, but this could be easily reduced to the same width of the photonic crystal, though alignment to the crystals would be more difficult. Other interesting avenues would be to look at configurable hydrophilic properties or other electrical ways of attracting the sample to the desired area. Having a micropump to continually recycle the analyte over the sensor would also create a higher probability of a target molecule being captured.

8.1.3 Avidin Detection (Chp 6)

In Chapter 6, the vitamin biotin was immobilized on a slotted photonic crystal sensor inside a microfluidic channel. Using these devices the protein avidin was detected with a lowest limit of 15 nM. This value is impressive considering that the sensing area is only 2.2 μm^2, and yet has sensitivities similar to much larger structures in Chapter 2. This sensitivity comes from the combination of strong spatial confinement of light within the slot, and temporal confinement of the photonic crystal cavity. Whilst the detection of avidin has regularly been done before, and is not of extreme importance in itself, the main benefit of this demonstration is its compatibility with other antibodies. Biotin and avidin are often used as a linker system to immobilize many types of antibody due to their high affinity, thus this protocol could easily be adapted for different targets.

As mentioned above, the performance of such devices is limited by diffusion. The results in Chapter 6 also highlight the two different ways of operating the device. At each injection point, dips were noticed in the signal due to dissociation of weakly bound material. An estimate of the bound material can be made by reading off the resonant wavelength of the cavity at these points. Another way to use the device is to use the slope of the observed diffusion curve to predict where the response will saturate, making the overall experiment shorter. The sample was only injected and left to sit within the microchannel; introduction of drift should increase the response time and improve the lowest limit of detection. Ideally, we wish all of the target molecules to be delivered to the sensor area. Whilst microfluidics may help, another problem is

the patterning of the functionalised molecules. In the devices presented in Chapter 6, the whole length of the microchannel is effectively functionalised. This could be a problem in low concentrations as the analyte can be depleted of target molecules whilst travelling along the channel, before it even reaches the sensor. One of the patterning techniques, or some other approach, could be used in the future to functionalise only the slotted photonic crystal. This would still be more than is needed, as most of the light at resonance is confined within the slot cavity, an area only 2.2 μm^2. There is therefore much room for improvement. Also mentioned before is the problem of water absorption, which lowers the quality factor of the cavity. This is one of the weaknesses of the slotted system, as whilst the analyte sees more of the light than a standard waveguide, if this medium is absorbing then this has detrimental effects on the quality factor of the cavity and the strength of the signal. Standard ring resonators can achieve much higher quality factors as most of the light is not guided in water. A trade-off therefore has to be made. The results in Chapter 6 show, however, that a reasonable quality factor of 3-4000 can still be obtained for slotted photonic crystal cavities in water, and that the wavelength shift is much larger than non-slotted devices for the same concentration of target molecules, thus there is a net gain to be made by using the slot.

8.1.4 Exosomes (Chp 7)

Initial groundwork with exosomes from the Jurkat and CEM lines have shown that they can be detected using the slotted photonic crystal platform presented in this thesis. Some of the results suggest that the exosomes may be immobilized physically by the slot, rather than by antibodies, due to their similarity in size. As mentioned in Chapter 7, if true, this could allow exosomes to be detected without antibodies, or based on their adhesive properties. This area is exciting given the interest of exosomes for diagnosing and treating diseases such as cancer. Slots may also allow some novel experiments to be conducted such as measuring direct secretion of exosomes from a living cell. This could be done with or without a stimulus. As much about them is unknown, this could also have impact in fundamental biology.

8.1.5 Slotted Spectrometer (Chp 7)

A point often neglected in optical biosensors is the need for an optical spectrum analyser. Like the gas source for pneumatic microvalves, the OSA results in a situation that is more ‘chip-in-a-lab’ than ‘lab-on-a-chip’. Initial work shown here to tackle this problem suggests that slotted photonic crystals can help. As was shown in Chapter 7, when a slotted photonic crystal is placed parallel to a W1 waveguide, coupling between the two waveguides can occur at specific wavelengths, and is contra-directional in nature. This was demonstrated via simulation and experiment. This system can therefore be used to create a variety of filters, as both the bandwidth and central wavelength can be engineered relatively easily. The contra-directional behaviour also ensures that light is extracted from one waveguide into the other, and is not periodically exchanged between them like in co-directional couplers, and gives over 200 nm of free-spectral range.

A bank of five such filters in a row was presented experimentally as a potential on-chip spectrometer. The idea being that by measuring the ratio of intensities between each extraction channel, the spectrum of a cavity could be recovered on-chip. The presence of the slot also makes this system attractive for sensing itself, in particular for gases. Light travelling through the slots at specific wavelengths will experience absorption from the presence of a gas. By observing the drops in intensities within extraction channels corresponding to absorption lines would allow specific gas sensing to be done on-chip. To test this idea experimentally, future work will have to re-design the crystals to work at the required absorption wavelengths, and would require a gas chamber to calibrate the sensor. This device may also find use in other

applications, such as optical modulators, or where light is desired to be transferred between different materials at specific wavelengths. This work demonstrates the versatility of the slotted photonic crystal platform: it can function as a sensor element, a spectrometer and perhaps even a light source or modulator.

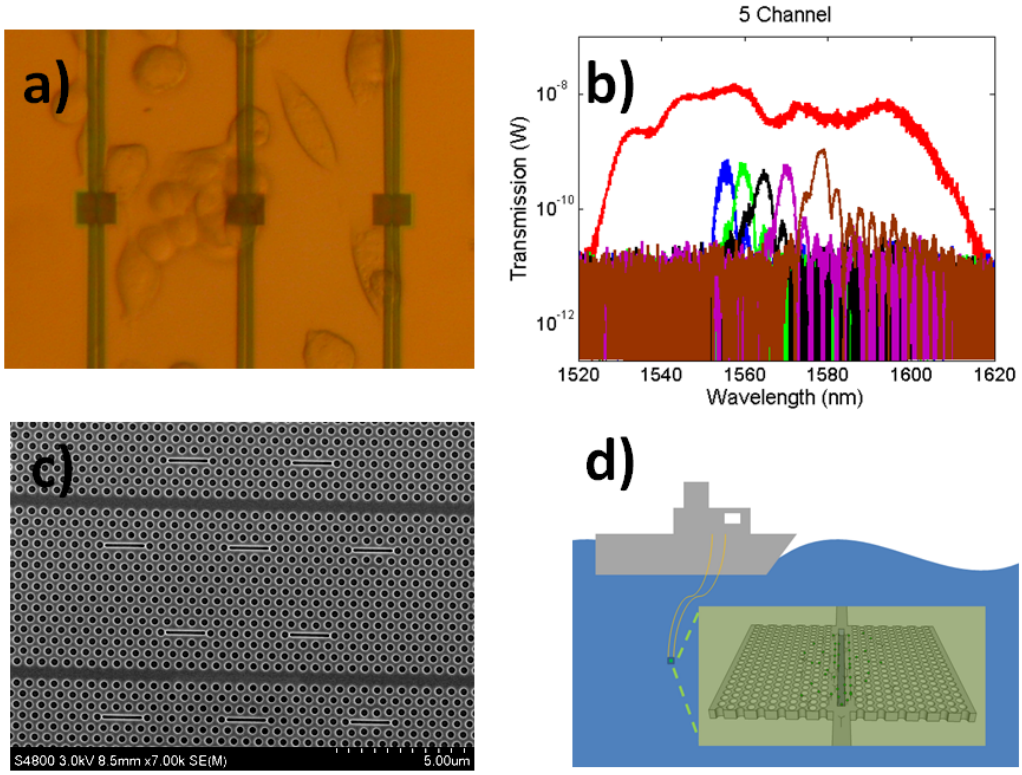

Figure 8.2: Potential future work. Slotted photonic crystals could be used to measure a) Cellular secretion, b) On-chip specific gas detection, c) Spatial arrays, d) Density of seawater with fibre probe.

8.1.6 Other Future Work and Applications (Chp 7)

The refractive index sensing capabilities of the slotted photonic crystal have previously been established to be excellent, with up to 1500 nm/RIU sensitivity. In future, the sensor could perhaps be used to measure salinity or density of seawater, a tricky problem for electrical sensors. Work is under way to connect the devices presented here to fibre ribbon so as to make a dip-probe for this purpose. Coating the sensor with toxin antibodies would allow dangerous algae blooms to be detected. This will require further engagement with marine biologists, yet the basic sensor is already there. Further work with microvalves could allow remote sampling to be achieved. Initial tests have also shown the feasibility of growing cells on top of slotted photonic crystals. An exciting experiment for future work would be to measure direct secretion from a single cell on top of the sensor. Using a multi-cavity design like the one introduced in Chapter 7 would provide spatial resolution and allow the point of secretion on the cell to be determined. Specific gas sensing on-chip may be possible with the slotted spectrometer design. A further idea could be to use the cavities to trap sub-hundred nanometre particles. This has

been done before with slot waveguides, but the small cavities offered by photonic crystals would allow more localized confinement. Improvements in functionalization patterning and microfluidics may allow lower limits of detection.

8.2 Learning Points

On entering the PhD program, I knew very little about photonic crystals, fabrication or biology. Through this project I have very much enjoyed gaining experience in all three. I was constantly fascinated by discussions with biologists of the amazing functions and abilities of biological systems, and have been inspired to learn more. It is also very motivating to believe that there is even a slight chance that my work could help make a difference to people's lives. Key things that stood out during the project were the difference in 'language' and outlook between the physicist and biologist. I soon realised that the biologists care less about how clever the physics is; their main concern is: does it work for their application and is it ready now? On the other hand, physicists want to find some immediate application for their new device, and want the biologists to give them 'something interesting' to measure. The problem is the biologist is not fully aware of the limitations and performance of the device, whilst the physicist doesn't know what to measure or which direction to take. I therefore see the great value of speaking to the biologists as often and as early as possible to identify genuine common ground, and thus help to solve important problems. Demonstrating proof-of-principle should be the beginning, not the end, of photonic biosensors. Where the different sciences meet is, for me, the most fascinating part and I loved the interdisciplinary nature of this project. The diversity within the physics itself was also interesting, sometimes working with light, other times electricity, fluids or gases; whilst there is a great sense of satisfaction and ownership of simulating, designing, fabricating and testing a new device.

If I were allowed to go back and do things differently I would probably have spent less time on trying to adapt the PDMS to the protocol of another photonic sensor, and spent a little more time reading up on the biology and chemistry so as to better understand the problems. My group's more focused look on communications, rather than biology, made reading up all the more important. I would also have fixed more on the medical applications, rather than others such as marine biology, as these have a larger market, less engineering constraints and are closer to becoming a reality; though I can't help still being drawn by the challenges and complete differences of these fields with the comfort and familiarity of the lab. Problem solving is one of my most favourite aspects of the PhD, and there is much to be learned from something that is hard to do than from something that is easy.

This thesis contributes to the literature in that it demonstrates the slotted photonic crystal as a realistic and versatile platform for biosensing. Yes, much work and many challenges still remain for making the device a final product within a lab, but the basic groundwork and feasibility have been established here. Fundamental coupling problems have been overcome, functionalization, sensitivity and biosensing demonstrated, solutions to integration presented, and real applications and collaborations begun. For me, the biggest advantage of the slotted photonic crystal is that it allows us to put the light where we want it most. In the case of biosensors, this means the light is in full contact with an analyte. This feature allows us to make very small and very sensitive devices, which I see as crucial to any scheme attempting to realise the dream of a protein microarray where 100s or thousands of tests are required. The slotted photonic crystal can be used for many different functions, and still has to reach its full potential, thus the work shown here should be the starting point for their future development.

8.3 Conclusions

This project has shown the development of slotted photonic crystals towards a realistic and promising platform for lab-on-a-chip style biosensors. The great advantage over many other photonic devices is the strong confinement of light, not only spatially, but also temporally due to combination of slot waveguide and photonic crystal effects. To better understand the limitations of the system and to maximise the amount of light within the slot, studies were performed on the losses. The propagation losses were found to be comparable to standard photonic crystals in the fast regime as a result of the slot waveguide effect. Coupling losses were reduced to 1.5 dB per interface over a large bandwidth of 78 nm using a resonant coupler designed and fabricated within this work. This allowed full advantage of the slotted photonic crystal light confinement in air to be taken. The sensitivity of this system was shown in proof-of-principle experiments where the protein avidin was detected, at a lowest concentration of 15 nM, and where bigger shifts in resonant wavelength were observed for the same concentration as many larger photonic biosensors. The functionalization protocol used could be adapted to other antibody systems, as was shown with CD45. When combined with the very small size of the device, this makes them attractive for the high throughputs, multiplexing and multifunctionality required by protein microarrays. This work also showed that slotted photonic crystals can be integrated with microfluidic circuits. Two microvalve designs, which do not require on-chip gas, and require less than 1J to actuate were demonstrated, and could find use in automating the device.

In addition, initial groundwork on applications and full on-chip integration was performed. Experiments with slotted photonic crystals showed that they can be used to detect tiny cellular packets of material known as exosomes. This could have huge impact, given the growing importance of exosomes in fundamental and applied biology. Future work could develop this further, helping to explore some of the mysteries of exosomes. A proposal for a novel on-chip spectrometer based on contra-directional slotted photonic crystals was also demonstrated. The great advantages over other solutions are much larger free spectral range (>200 nm), no periodic exchange between the two waveguides, the ability to tailor the central wavelength and bandwidth of the filter region easily, and the potential for measuring not only phase shifts but also gas absorption on-chip as a result of the wavelength specific light confinement within air. Cells were also successfully grown on top of the device paving the way for unique experiments to measure direct secretion of cellular material, and initial work for creating a multi-sensor pad for measuring the point of secretion from a single cell.

Slotted photonic crystals therefore provide an entirely new platform for optical biosensing, allowing higher sensitivities in smaller structures, and great potential for on-chip spectrometry. Whilst it will take at timeframe of 5-10 years and more resources and engineering to make this a commercial reality, the basis of design, performance, detection, proof-of-principle and application have all been demonstrated within this body of work. Many other exciting and novel ideas have been generated and await future work to explore fully. Slotted photonic crystals therefore still have much more to give, and have strong potential for true ‘lab-on-a-chip’ devices. My hope is that with this foundation they will shine new light on many of the mysteries of biology in years to come.